NOVA SCHOOL OF SCIENCE & TECHNOLOGY

DEPARTMENT OF MECHANICAL AND INDUSTRIAL ENGINEERING

# Design and production of tools for the automotive industry using Directed Energy Deposition-Arc

João Paulo dos Santos Figueiredo

BSc in Mechanical Engineering Science

MECHANICAL ENGINEERING INTEGRATED MASTER

NOVA University Lisbon

September, 2024

NOVA SCHOOL OF SCIENCE & TECHNOLOGY

DEPARTMENT OF MECHANICAL AND INDUSTRIAL ENGINEERING

# Design and production of tools for the automotive industry using Directed Energy Deposition-Arc

**João Paulo dos Santos Figueiredo**

BSc in Mechanical Engineering Science

**Adviser:** Telmo Jorge Gomes de Santos
*Full Professor, NOVA University Lisbon*

**Co-advisers:** Rui Fernando dos Santos Pereira Martins
*Associate Professor, NOVA University Lisbon*

MECHANICAL ENGINEERING INTEGRATED MASTER

NOVA University Lisbon
September, 2024

**Design and production of tools for the automotive industry using Directed Energy Deposition-Arc**

# ACKNOWLEDGMENTS

I would like to express my most gratitude for my Adviser Professor Telmo Santos for the guidance and for sharing his profound knowledge about the technologies applied in this work. I am also most grateful for the constant help, availability and expertise over all the tests used in this work of my Co-adviser Professor Rui Martins. I would also like to thank for all the suggestions and help in the re-designing of the part.

My sincere thanks to PhD candidate Rui Gonçalves for always being available to help and for the help with the use of the CNC machine.

This gratefulness extends to Mr. António Campos, Mr. Paulo Magalhães and PhD candidate Pedro Fonseca. These excellent technicians and PhD student helped me through all my experimental work, gave me worthful practical advice and knowledge I will take for my professional career. For that and for giving me company throughout this long months, I express my deepest thank you.

To the all the friends that shared with me the work of this thesis, thank you for giving me a hand and for sharing / listening the challenges involved this work.

To my dearest friend, one of the people I most like, João Carvalho. Thank you for all these 5 years we shared together full of moments to remember. No matter what you were always there. Thank you, my friend. I hope we still share some moments in the next years to come.

To my girlfriend Sara Correia, my best friend, my partner in life, thank you for all the support in everything but specially during this last months. Thank you for all the " you got this " that help me keep pushing into this work. Without you it would have been impossible to accomplish this integrated master's degree in 5 years.

To my parents, thank you for all the sacrifices you did to make this possible. This degree is also yours and I will always be grateful for giving me the chance to proceed to university and search for a better life. To my brother Rodrigo Figueiredo, thank you for all the company you gave me, it's much easier to have you by my side every day and have someone I can talk to.

Thank you all.

This work was developed under the project "Agenda Drivolution - Transição para a fábrica do futuro" (C644913740-00000022) - Aviso 2021-C05i01-01 PRR, funded by IAPMEI - Agência para a Competitividade e Inovação, I. P., within the scope of the Portuguese "Plano de Recuperação e Resiliência (PRR)" / União Europeia - NextGenerationEU.

# ABSTRACT

The rapid replacement of tools, in the automotive industry, is crucial, yet maintaining stocks of these tools is not ideal. The adoption of Directed Energy Deposition-Arc (DED-arc) technology would address the issue because it enables the production of large and complex parts with a significant material, cost and time saving. However, there are still limited application examples of DED-arc in the manufacture of stamping, cutting and forging tools.

This study addresses the testing and optimization of deposition strategies for the 3D printing of parts produced by DED-arc (for the material ER70S-6), along with testing different overlaps between welding beads to this purpose. After the testing of process parameters, the production of a part with application in the automotive industry was successfully fabricated by DED-arc and cutting operations.

It was concluded that the use of the suggested deposition strategy combined with the tested overlap values resulted in a non-defective specimen with 496.1 MPa of Ultimate Tensile Strength which represents 92.2 % of the technical specifications of the material ER70S-6. It also resulted in specimens that surpassed the technical specifications of nominal elongation of 24 % with values of 25.4 %. The microhardness tests resulted in values of 188.8 HV, which represents 68 % of the maximum calculated value of Vickers hardness.

This study also concludes that, combined with adjusted settings and inputs presented in this work, the Prusa slicer software is a suitable tool for generating G-codes for the production of parts by DED-arc with simple features (linear welding beads). For curved features some future work should be performed to ensure the infill of the part.

**Keywords:** Additive manufacturing, welding, DED-arc, low carbon steel.

# RESUMO

A rápida substituição de ferramentas na indústria automóvel é crucial, no entanto, manter stocks destas ferramentas não é ideal. A adoção da tecnologia *Directed Energy Deposition-Arc* (DED-arc) contribuiria para a resolução do problema uma vez que permite a produção de peças de grande dimensão e complexidade com uma gestão significativa de material, custo e tempo. No entanto, ainda existem exemplos limitados de aplicação de DED-arc na fabricação de ferramentas de estampagem, corte e forjamento.

Este estudo aborda a otimização e teste de estratégias de deposição para impressão 3D de peças por DED-arc (para o material ER70S-6), além de testar diferentes sobreposições entre cordões de soldadura para esse fim. Após os testes dos parâmetros do processo, a produção de uma peça com aplicação na indústria automóvel foi fabricada com sucesso através de DED-arc e operações de fresagem.

Concluiu-se que a utilização da estratégia de deposição sugerida aliada aos valores de sobreposição testados resultou em provetes sem defeitos com tensão de rotura de 496,1 MPa o que representa 92,2 % das especificações técnicas do material ER70S-6. Resultou também em provetes que superaram as especificações técnicas de extensão nominal de 24 % com valores de 25,4 %. Os ensaios de microdureza resultaram em valores de 188,8 HV, o que representa 68 % do valor máximo calculado de dureza Vickers.

Também se concluiu que, juntamente com as definições e parâmetros ajustados utilizados neste trabalho, o *software Prusa Slicer* é uma ferramenta adequada para geração de códigos G para produção de peças por DED-arc com características simples (cordões de soldadura lineares). Para características curvas, algum trabalho futuro deverá ser realizado para garantir o preenchimento da peça.

**Palavras-chave:** Manufatura aditiva, soldadura, soldadura por arco elétrico, aço carbono de baixa composição.

# CONTENTS

# LIST OF FIGURES

# LIST OF TABLES

# ACRONYMS

| | |
|---|---|
| **3D** | Three-dimensional |
| **AM** | Additive Manufacturing |
| **CAD** | Computer-Aided Design |
| $\boldsymbol{D_{i/i}}$ | Distance between infill welding beads |
| $\boldsymbol{D_{i/p}}$ | Distance between infill and perimeter welding beads |
| **DED-arc** | Directed Energy Deposition-Arc |
| **GMAW** | Gas Metal Arc Welding |
| **GTAW** | Gas Tungsten Arc Welding |
| **HI** | Heat Input |
| **HV** | Hardness Vickers |
| **L-DED** | Laser directed energy deposition |
| **PAW** | Plasma Arc Welding |
| **PBF** | Powder Bed Fusion |
| **UTS** | Ultimate Tensile Strength |
| **WAAM** | Wire Arc Additive Manufacturing |

# SYMBOLS

| | |
|---|---|
| **V** | Voltage [V] |
| **I** | Current Intensity [A] |
| **TS** | Travel Speed [mm / s] |
| ***w*** | Width of the welding bead [mm] |
| **WFS** | Wire Feed Speed [m / min] |

# 1 INTRODUCTION

## 1.1 Motivation

In the automotive industry, the fast substitution of tools in manufacturing is essential, yet maintaining stocks of these tools is undesirable. A solution to this matter is to implement Directed Energy Deposition-Arc (DED-arc) technology because it enables the production of large and complex parts with a significant material, cost and time saving. With a high deposition rate and low cost compared with other Additive Manufacturing (AM) technologies, DED-arc suits in various industry applications. Despite its potential, there are still limited application examples of DED-arc in the manufacture of stamping, cutting and forging tools.

## 1.2 Objectives

This dissertation aims to accelerate the implementation of DED-arc in the automotive industry with practical examples of how this technology can be used in this industry. With this in mind, the objectives of this thesis are to identify a tool, within the automotive industry, that can be manufactured by DED-arc and afterwards manufacture a prototype of it, selecting the adequate process parameters. Additionally, the process should require the redesigning of the tool such as varying the geometry and material with the use of CAD modelling and numerical simulation.

## 1.3 Document Structure

This document is organized in five chapters that are summarized as follows:

- Chapter 1 – Introduction: Describes the motivation in the current days to study the application of DED-arc in the automotive industry, the objectives of this thesis and the document structure;

- Chapter 2 – State of the Art: Explores the recent advancements of DED-arc technology, along with a search study of the applications and examples of DED-arc in the industry, with special attention to the automotive industry, dies and punches;
- Chapter 3 – Experimental procedures: Describes the experimental procedures in this thesis which involve: Materials and welding consumables, equipment, the process of overcoming problems with the DED-arc machine, testing of different deposition strategies and overlaps, and the process of fabrication of a part by DED-arc and cutting operations;
- Chapter 4 – Results and Discussion: This chapter is divided into two sections: the results and discussion of the overlap testing and the fabrication of a part with application in the automotive industry. The results of visual inspections, uniaxial tensile testing and microhardness testing are displayed and discussed for these two sections.
- Chapter 5 – Conclusion and Future work: It resumes the conclusions of the previous chapter while also suggesting future work to accelerate the implementation of DED-arc in the industry, in specific the automotive industry.

# 2 STATE OF THE ART

## 2.1 Additive Manufacturing

According to ISO/ASTM 52900:2021 standard [1], Additive Manufacturing (AM) is defined as the process of joining materials to create parts from three-dimensional models, typically layer by layer. This definition is quite broad, therefore, ASTM categorizes additive manufacturing into 7 categories, as represented in Figure 2.1.

The process addressed in this work was Directed Energy Deposition-Arc (DED-arc), also known as Wire Arc Additive Manufacturing (WAAM). DED-arc falls under the category of Directed Energy Deposition since, in this process, thermal energy is used to melt material as it is deposited. Given that WAAM is now a patented name, it is in the transition of changing its name to DED-arc, in this work it was referred as DED-arc.

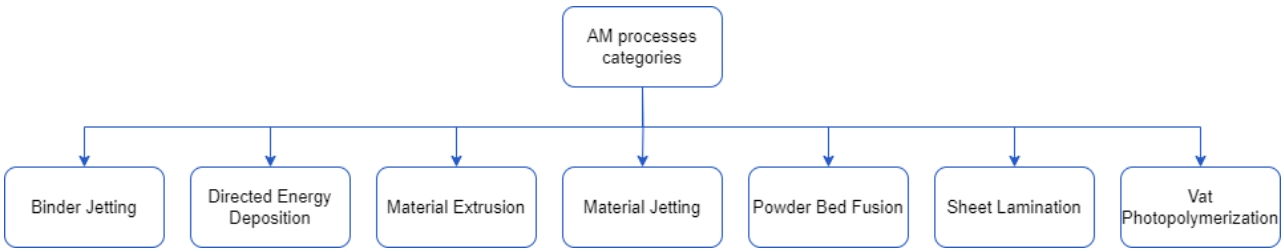


Figure 2.1 - Different AM processes categories.

The DED-arc concept initially emerged in 1925 when Ralph Baker decided to use an electric arc to melt metal wires, with the aim of creating an ornament [2]. Since then, several advancements have been made in technology, particularly in the last 15 years. Some variants of the process have been developed to obtain materials with improved mechanical properties. However, DED-arc has not yet reached its full potential in terms of industrial commercialization. The high complexity of the process planning and the need for post-processing contributes to its hard implementation in the industry. Therefore, the development of a more automated method of process planning and more techniques to decrease the need for post-processing would facilitate its application in industry.

## 2.2 Physical Principles

In the DED-arc process, the concepts of arc welding are combined with a system of feeding metal wire. An electric arc is used as a heat source to process the metal wire, which, after melting, is deposited layer by layer continuously until the desired geometry is achieved, as observed in Figure 2.2.

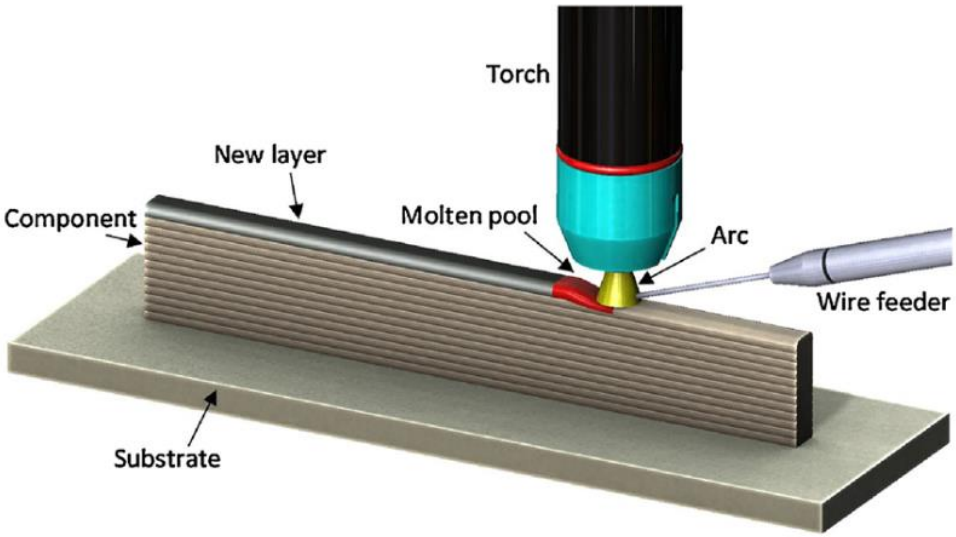


Figure 2.2 - Illustration of DED-arc process [3].

This process is heavily reliant on welding concepts, as the fusion of the additive material is also achieved through an electric arc. In DED-arc, various automated welding processes are used: GTAW (Gas Tungsten Arc Welding), GMAW (Gas Metal Arc Welding), and PAW (Plasma Arc Welding). The selection of the welding process depends on its specific application, as each process will have a different deposition rate, heat input, precision, among other process characteristics. Consequently, these welding processes will have different production times for the same part.

The most used among these processes is GMAW due to its higher deposition rate and, hence, shorter production times. This is a welding process produced by an electric arc between the filler metal and the substrate. The weld bead is obtained through the melting of the filler material, and inert or active shielding gas is used to protect the molten pool as well as the already deposited material. Deposition rates can vary between 15 and 160 g/min [3], depending on process parameters and desired properties, making the process ideal for manufacturing large-sized components.

The GMAW process has 4 transfer modes: short-circuit, globular, spray, and pulsed. These modes are influenced by:

- Type of shielding gas;
- Type and diameter of filler material;

- Current intensity;
- Voltage.

These transfer modes result in different deposition rates and, naturally, different surface finishes. Thus, there is a connection between the process parameters and the quality of the piece. GMAW based DED-arc, compared to other welding technologies, has the highest deposition rate, better material utilization, and low production costs [4].

The other welding processes used in DED-arc are GTAW and PAW. These welding processes utilize a non-consumable tungsten electrode under inert gas protection. In both processes, for material deposition, a separate material feeding system is required, distinct from the tungsten electrode. GTAW is a high-precision process with few defects since the arc is quite stable.

Regarding PAW, the tungsten electrode is enclosed within a torch, with a cooling water nozzle, which constrain the electric arc, resulting in increased arc stability. PAW is a high-energy density process, leading to a narrow and thin heat-affected zone. This allows for better control of the bead geometry and, consequently, greater precision in material deposition. By varying process parameters such as plasma gas flow, torch orifice diameter, and current intensity, different operating modes can be achieved. One of these modes is the microplasma mode, with the advantage of producing thin parts with a minimum total wall thickness of 2 mm. However, it has a deposition rate of approximately 1.0 g/min. Another operating mode is the medium current mode, where the layer wall thickness ranges from 4 to 15 mm, and the deposition rate can reach up to 30 g/min [4].

## 2.3 Main Parameters of DED-arc

The use of DED-arc enables the manufacturing of a wide range of parts. For each part, the process parameters should be optimized to align with the project's objectives and requirements. In order to control process variables such as bead width, penetration, bead height, and deposition speed, it is necessary to adjust parameters. The parameters Voltage, V [Volts], welding current, I [A], travel speed, TS [mm/min], and thermal efficiency, η, have a direct impact on heat input of the welding process, as shown in equation (2.1), that influences greatly the bead geometry. The typical thermal efficiency for GMAW is 0.8.

$$\text{Heat input} = \eta \times \frac{\text{V} \times \text{I} \times 60}{TS} \left(\frac{\text{J}}{\text{mm}}\right) \tag{2.1}$$

The desired weld attributes may vary within each project, for that it is necessary to adjust the welding parameters. Their influence on the weld attributes are presented in Table 2.1 [5]. To achieve a

good quality of produced parts, it is crucial to use optimized process parameters for each material and for each project objective.

Table 2.1 - Welding parameters influence on weld attributes, adapted from [5].

| **Parameters** | **Bead width** | | **Penetration** | | **Bead height** | | **Deposition rate** | |
|---|---|---|---|---|---|---|---|---|
| | Increase | Decrease | Increase | Decrease | Increase | Decrease | Increase | Decrease |
| **Intensity current / Wire feed speed** | ↑ | ↓ | ↑ | ↓ | ↑ | ↓ | ↑ | ↓ |
| **Voltage** | ↑ | ↓ | No effect | No effect | Small effect | Small effect | Small effect | Small effect |
| **Travel speed** | ↓ | ↑ | ↓ | ↑ | ↓ | ↑ | Small effect | Small effect |
| **Electrode extension** | ↓ | ↑ | ↓ | ↑ | ↑ | ↓ | ↑ | ↓ |
| **Wire diameter** | Small effect | Small effect | ↓ | ↑ | Small effect | Small effect | ↓ | ↑ |
| **Shielding gas** | ↑ | ↓ | ↑ | ↓ | Small effect | Small effect | Small effect | Small effect |

## 2.4 Materials

During the DED-arc process, the deposited material undergoes a series of heating and cooling cycles (thermal cycles), which can result in a variety of grain structures along its length. The difference in grain boundary morphology, directly related to the mechanical properties of the material, demonstrates significant importance in material selection. Typically, parts developed by DED-arc have large columnar grains. These are created by the epitaxial growth from a substrate aligned along the normal direction to the solid/liquid interface, with a high temperature gradient [4].

Epitaxial growth leads to anisotropic material properties, which can be detrimental under multiaxial loads, potentially triggering fracture processes in the material. Therefore, if the grains exhibit

equiaxial growth, the material will be close to isotropic properties, providing better ductility and a reduced facture probability [4].

For a better response in consecutive heating/cooling processes, a common practice is the use of alloys with added materials that promote isotropic properties. Another option is the use of inoculants to reduce grain size, resulting in improved mechanical properties of the material [4]. Taking this into consideration, one of the most important parameters in DED-arc is the choice of the additive material, most used being steel alloys, aluminum, titanium, and nickel.

In Figure 2.3, it is possible to observe a correlation between the filler material used in the DED-arc process and typical defects in this process.

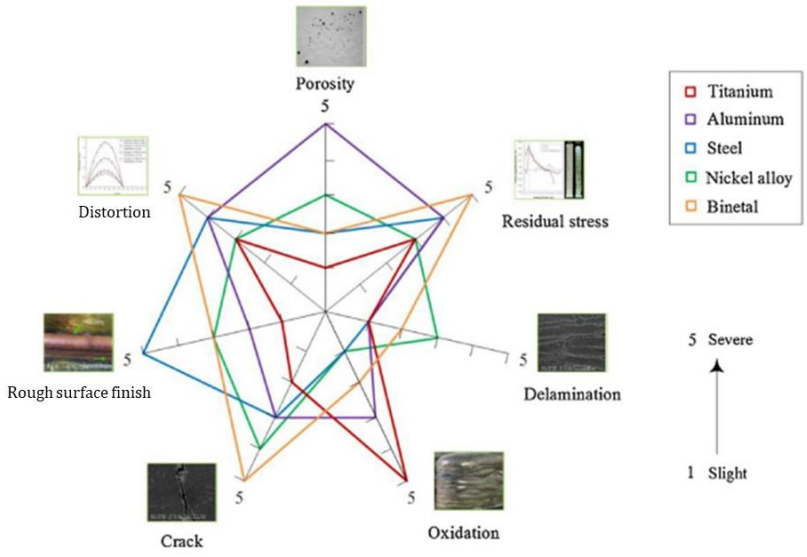


Figure 2.3 - Correlation between materials and defects in DED-arc processes, adapted from [6]

## 2.5 Undesirable phenomena and characteristics

Since the DED-arc process is based on welding technologies, its defects are very similar. The most common defects include hot cracking, cold cracking, porosity, delamination, inclusions, burn edges, and spatter. These can result from excessive heat input, poor toolpath planning, gas contamination, inadequate quality of filler material, among others. The following subsections aim to address typical defects and imperfections in the DED-arc process in more detail, along with their origins and suggestions for control.

The appearance of wavy surfaces with high roughness is common in parts produced by DED-arc. However, the selection of appropriate process parameters can contribute to a significant reduction in waviness and improvement in roughness, as demonstrated in the study by Xiong et al. [7]. In this study, it is concluded that a reduced wire feed speed combined with a reduced torch travel speed results in better surface quality.

Nevertheless, the occurrence of wavy surfaces with high roughness is an intrinsic characteristic of DED-arc. Therefore, post-processing of the part with a material removal operation, such as milling, is necessary to reduce the surface roughness of the piece. For instance, through a milling process applied to a DED-arc produced part, Lopes et al. [8] achieved a surface roughness (Ra) of 0.206 µm using a high cutting speed (v = 65 m/min) and a reduced feed per tooth (fz = 0.0115 mm/tooth).

Another undesirable aspect is the presence of distortions that contribute to non-compliance with geometric tolerances, as observed in Figure 2.4. Ley et al. [9] concluded that, for the same thermal input, a lower shielding gas flow rate and a shielding gas composition containing helium results in reduced welding distortion. Furthermore, residual stresses and distortions can be mitigated with the use of appropriate heat treatments, proper toolpath planning, and on-site cooling or heating mechanisms [4].

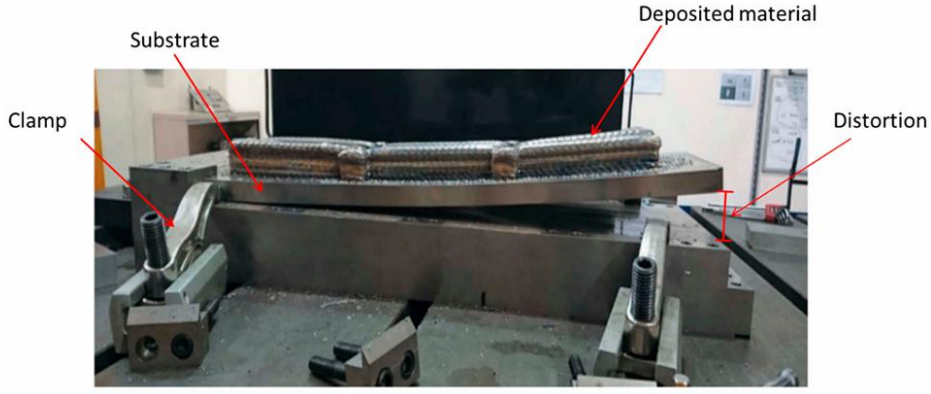


Figure 2.4 - Structural distortion of a piece produced by DED-arc [4,10].

Porosity is a common defect in parts produced by DED-arc, especially in aluminum alloys [11]. This can result from contamination by moisture, grease, other hydrocarbons present in the welding wire, poor toolpath planning or unstable material deposition.

Several techniques can be used for the prevention and removal of porosities, such as the use of high-quality shielding gas, as well as clean and high-quality welding wire. Additionally, effective toolpath planning and stable material deposition play crucial roles in minimizing porosity [12]. Other effective techniques for reducing porosity include the use of DED-arc variants like Cold Metal Transfer [13], Side Rolling, Machine hammer peening [14] and hot forging [15].

In general, parts produced by DED-arc can experience two types of cracks: grain boundary cracks and hot cracks [16]. According to TWI [17], hot cracking refers to the formation of contraction cracks during the solidification of the welded metal. Grain boundary cracking refers to the formation of cracks along the grain boundaries. Concerning delamination, bimetallic alloys are more susceptible due to differences in their solubility and chemical reactivity [11]. Both defects are not repairable through post-fabrication heat treatments. To control these defects, preheating of the substrate before the material deposition should be performed, along with reducing the cooling rate during material deposition [6].

As previously discussed, anisotropy is a common characteristic of DED-arc parts that results from a columnar grain structure aligned along the normal direction to the solid/liquid interface. Since the part tend to not be isotropic, the mechanical properties of the material aren't the same in every direction. For this matter, it is important to understand in what direction the material has the best mechanical properties to optimize the designing of the part. When designing a part, it is fundamental to consider the type and orientation of the loads that is going to have. To optimize the project, it is important to make the direction that corresponds to the best mechanical properties be the same as the direction of the applied load.

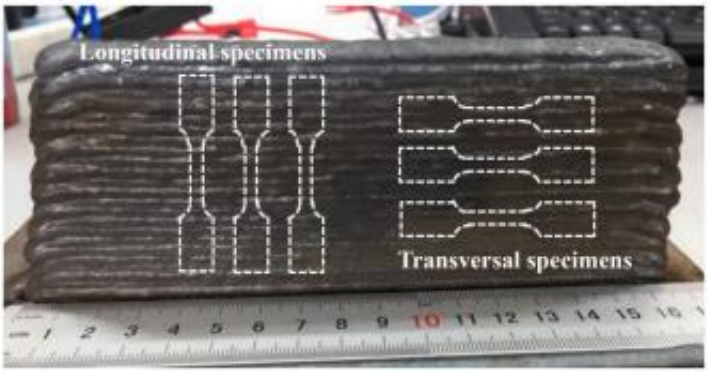


Figure 2.5 - A schematic diagram for the location of the tested specimens, which are longitudinal or transversal to the build-up direction [18].

In order to do that, Sun et al. [18] investigated the mechanical properties of a low carbon high-strength steel component fabricated by DED-arc. After performing tensile tests of machined longitudinal and transversal specimens it was concluded that the transversal specimen had better mechanical properties. The transversal specimen had 10.1 % more Yield strength, 4.2 % more ultimate strength and more 21.4 % elongation than the longitudinal specimen.

However, a similar study, conducted by Gordon et al. [19], investigated the mechanical properties of 304L stainless steel of longitudinal and transversal specimens and the results did not align with the previous presented. The transversal specimen had 5.01 % more ultimate strength and 3.4 % less Yield strength than the longitudinal.

For 304L austenitic stainless steel, Laghi et al. [20] observed different results. The transversal specimen had 8.0 % less ultimate strength and less 1.4 % Yield strength and 9.5 % more elongation than the longitudinal specimen. Additionally, the mechanical properties of a diagonal specimen (45 º) were also evaluated and concluded that a diagonal specimen had even better mechanical properties than the longitudinal with more 5.8 %, 13.2 % and 17.4 % of ultimate strength, Yield strength and elongation, respectively.

These varying outcomes, even with the same material, indicate the need for more studies addressing the anisotropy influence on mechanical properties for each material. Laghi et al. [20] and Gordon et al. [19] verified minimal differences of (1.4 % and 3.4 %, respectively) in Yield strength, these variations suggest that anisotropy may not be significant in all materials. This consideration should be integrated into the process planning of a DED-arc manufactured parts.

## 2.6 Process Planning

### 2.6.1 CAD and Slicing

The first step to produce a part by DED-arc is to make a 3D Computer-Aided Design (CAD) model, to after be converted into a STL file. The second is to slice the CAD model using an AM software. Typically, there are two types of slicing techniques, the unidirectional and the multi-directional [21]. The disadvantage of unidirectional slicing is that it needs more supports to create a complex part in comparison to the multi-directional slicing technique, as represented in Figure 2.6.

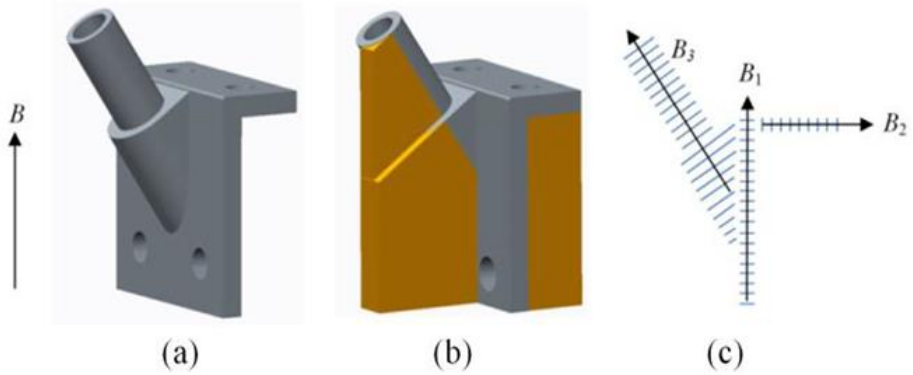


Figure 2.6 - (a) Component with basic build direction; (b) supports required (c) multi directional slicing with build direction B1, B2 and B3 [22].

Due to its simplicity, the unidirectional slicing technique is the most used in industry applications. The multi-directional approach can reduce the need for support structures which reduces post-process machining. Although the multi-directional approach has its advantages, in comparison with the unidirectional this technique demands a more complex process plan.

To facilitate the integration of multi-directional DED-arc system, Yuan et al. [23] created an automated process planning algorithm and integrated it with an automated robot offline programming engine and DED-arc hardware. The four main modules of the algorithm are related to robot motion planning, initial collision processing, layer sequence optimization and weld torch pose adjustment. The first step is generating the robot motions for the deposition of each layer using the automated robot offline programming engine. Then, these robot motions are used to create a collision matrix which will serve to further planning stages. The following phase is layer sequence optimization in order to eliminate collisions between the part and the robotic system. Adjustments are performed to the torch pose to prevent any remaining collisions if there are any. This algorithm was validated by producing a part with a complex geometry in the same paper [23].

### 2.6.2 Deposition Strategy

In terms of types of tool paths patterns, the main types are Raster, Zig-zag, Contour, Spiral and Hybrid. This tool path patterns are represented in Figure 2.7. The raster is regularly used in AM because of its simple implementation. The Zig-zag tool pattern compared with the raster has less arc interruptions as shown in Figure 2.7 b). These two patterns have a poor outer boundary accuracy because of its discretization mistakes on the edges. The contour tool path pattern prioritizes the boundaries which solves the previous problems with the outer boundaries. The spiral tool path pattern is an improvement of the Zig-zag method, but it can only be used in special geometrical models.

The previously presented tool path patterns resulted in the hybrid tool path pattern. This pattern can be a combination of multiple patterns such as the combination of the counter approach to make the

outer boundaries and the Zig-zag approach to fill the inside. In general cases, this hybrid tool path pattern is the most beneficial for DED-arc [21].

Another common inconvenience in parts produced by DED-arc is the unevenness between the beginning and end of each deposited layer when every layer has the same start and end. To reduce this effect, the zig-zag deposition method can be used. However, the zig-zag method can result in thermal accumulation at the wall boundaries [24]. Another simple method to mitigate this is by cutting the beginning and the end zones but results in more wasted material.

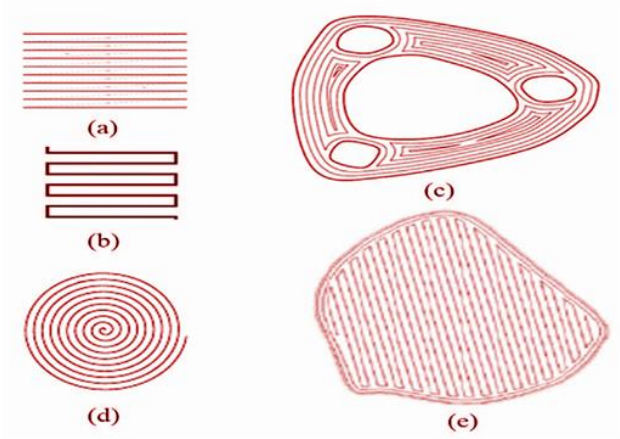


Figure 2.7 - Tool Path Patterns: (a) Raster, (b) Zig-Zag, (c) Contour, (d) Spiral, (e) Hybrid tool paths patterns [21].

The CMT based DED-arc also has this problem, so Wang et al. [25] presented an improved strategy that consists in adapting the travel speed and the tool path along the deposited layer. This technique consists in a reduction of the travel speed in the beginning of each layer and an additional return path, as illustrated in Figure 2.8. This study shows a reduction of the width and height displacement in the beginning, respectively from 5.81 % to 3.64 % and from 11.09 % to 5.06 %. In the end of the layer, there was also improvements of the displacements respectively from 4.20 % to 3.71 % and from 18.00 % to 4.89 %. This percentages represent the mean error between the stable width and height of the middle part and the width and height of the beginning/end of the part [25].

A path strategy for producing T-crossing features was developed by Venturini et al. [26] and is presented in Figure 2.9. The strategy consists of after the fourth usage of the first deposition strategy, the second deposition strategy must be applied. This study determined that using a fillet instead of a sharp corner led to a flued toolpath and stable deposition process and it must be taken into consideration while planning the toolpath.

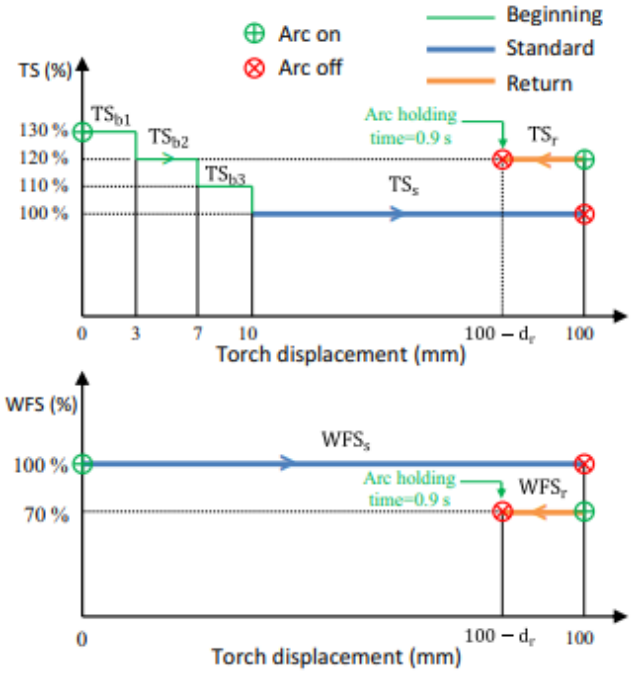


Figure 2.8 - Illustration of CMT based DED-arc improvement technique [25].

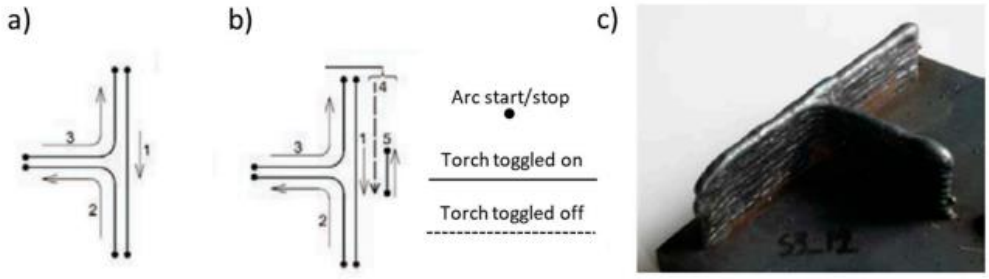


Figure 2.9 – (a) Deposition strategy to produce T-type structures (b) Improved deposition strategy to produce T-type structures; (c) part produced using deposition strategy detailed in (b), adapted from [4,26].

After the deposition of the material, post-process operations are carried out. Post-process heat treatments are substantial in DED-arc due to its capacity to reduce residual stress, improve mechanical properties, and regulate hardness. The selection of a proper heat treatment process depends on the material, AM process and desired properties of the material. An appropriate heat-treatment application is crucial to avoid increasing the risk of cracking [11]. In literature, an extensive study has been conducted for a variety of materials, such as aluminium alloys, nickel alloys, steel, and titanium alloys. Some examples of heat treatments can be seen summarized in Table A.1 on Annex A.

To achieve a near flat top surface after the deposition of a layer and to ensure that the infill of the part has no gaps, an optimal overlap between weld beads should be applied. In order to do that, Ding et al. [27] proposed an improved version of the traditional flat-top overlapping model – the tangent

overlapping model. Using this model, this paper concluded that the optimal distance between the center of two welding beads was 0.738 times the width of the welding bead.

## 2.7 DED-arc Applications

To understand the current status of DED-arc technology and applications, two research studies were conducted in this work. Given the name transition of WAAM to DED-arc, these research studies considered both names as explained further. The first research had the objective to understand if DED-arc technology is being developed and addressed in literature presently. From the Scopus database, the evolution over time of publications related to WAAM and DED-arc from 2016 to February 8, 2024, was exported. In Scopus search bar, the following line codes were used to conduct this research.

- TITLE-ABS-KEY (directed AND energy AND deposition AND arc ) AND PUBYEAR > 1976 AND PUBYEAR < Y[ i ]
- TITLE-ABS-KEY ( waam ) AND PUBYEAR > 1976 AND PUBYEAR < Y[ i ]

Where i is a natural number and varies from 1 to 8 (including), and Y is:

$$Y = \begin{bmatrix} 2017 \\ 2018 \\ 2019 \\ 2020 \\ 2021 \\ 2022 \\ 2023 \\ 2024 \end{bmatrix}$$

After the retrieving of this data, a graphic was made with the information summarized, as presented in Figure 2.10. The results reveal an increase in publications over the years, with 2158 documents associated with WAAM and 330 with DED-arc. This represents the continuous development of DED-arc and an increasing demand for its implementation in the industry.

Additional research was conducted to understand DED-arc applications regarding industry and tool manufacturing, such as cutting tools and stamping tools including punches and dies. This research included WAAM or DED-arc combined with several keywords, using the following line codes in Scopus search bar:

- TITLE-ABS-KEY ( directed AND energy AND deposition AND arc AND X[ j])

- TITLE-ABS-KEY ( waam AND X[ j ] )

Where j is a natural number and varies from 1 to 14 (including), and X is:

$$X = \begin{bmatrix} \text{Cutting} \\ \text{Cutting AND production} \\ \text{Cutting AND tool} \\ \text{Cutting AND tool AND production} \\ \text{Die} \\ \text{Die AND production} \\ \text{Industry} \\ \text{Industry AND aerospace} \\ \text{Industry AND applications} \\ \text{Industry AND Automotive} \\ \text{Industry AND shipbuilding} \\ \text{Punch} \\ \text{Punch AND production} \\ \text{Stamping} \end{bmatrix}$$

The results are presented in Figure 2.11, indicating that punch production via DED-arc is still to be investigated. Cutting tools and die production via DED-arc are addressed in literature but still with few articles. In terms of DED-arc applications in industry, the aerospace industry is the most explored for this process.

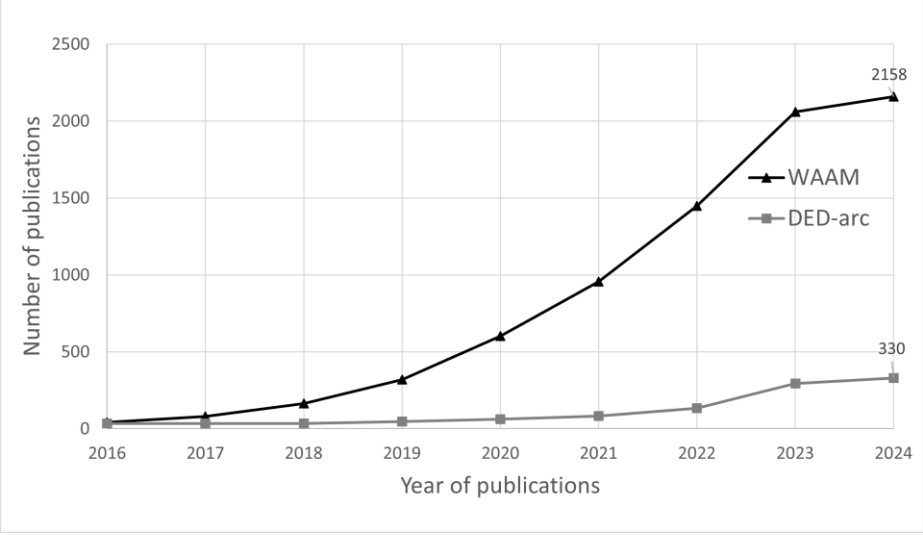


Figure 2.10 - Number of publications in Scopus with the keywords WAAM or DED-arc from the year 2016 to 8th of February 2024.

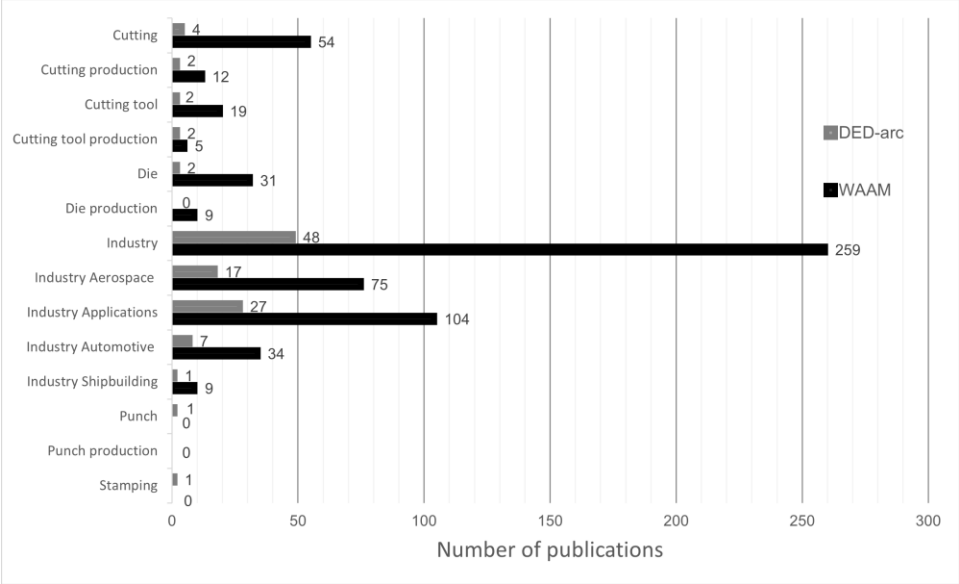


Figure 2.11 - Number of publications in Scopus with regards to WAAM and DED-arc and different keywords till 8th of February 2024.

In the aerospace and automotive industry, there is a persistent goal: producing lightweight parts with good mechanical properties. This goal can be achieved by optimizing structural design in order to use less material or by using lighter materials. These lighter materials can be expensive, so a secondary objective is to minimize wasted material. Which, in general, can be achieved by replacing traditional manufacturing processes to AM, and more specifically to DED-arc [28]. In comparison with other AM processes, like power bed fusion, DED-arc has a higher deposition rate, but worse precision in deposition. This makes DED-arc better suited to produce larger parts like tanks, trusses, chassis, and airframes [28].

STELIA Aerospace is a manufacturer company that is specialized in designing aluminium airframes and frame sections to Airbus aircrafts. In 2018, with the conclusion of the DEFACTO project in collaboration with other companies, STELIA Aerospace presented a 1 $m^2$ demonstrator for metallic self-reinforced fuselage panels manufactured by DED-arc as observed in Figure 2.12. In the future, this new technology could eliminate the need for added stiffeners in fuselage panels [29].

In 2019, a collaborative work of Thales Alenia Space, WAAM3D, Cranfield University and Glenalmond Tecnologies resulted in the manufacturing of the first full-scale prototype of a pressure vessel made of the titanium alloy Ti-6Al-4V deposited by DED-arc process. This piece has approximately 1 m in height, weights around 8.5 kg and it can be seen in Figure 2.13 a). Following its deposition by DED-arc, the piece underwent stress relief, laser-scanning, precision machining and through inspection by ultrasonic testing and computer tomography. This non-destructive testing techniques ensured that the piece met the mechanical requirements and specifications. This manufacturing method led into 80% material savings, 40% cost savings and 65% lead time savings

compared to traditional methods. In the future it is expected to be used in manned missions for space exploration [30].


Figure 2.12 - Demonstrator for metallic self-reinforced fuselage panels with 1 $m^2$, manufactured by DED-arc [29].

Another project involving the WAAM3D company is the manufacturing of an aluminium nose cone, presented in Figure 2.13 b), with 190 mm of diameter and 350 mm of length with the collaboration of Milton Keynes, Bedford and Aircraft Research Association Ltd. This component was produced in 2022 and led to 74% material saving in comparison with traditional manufacturing processes.

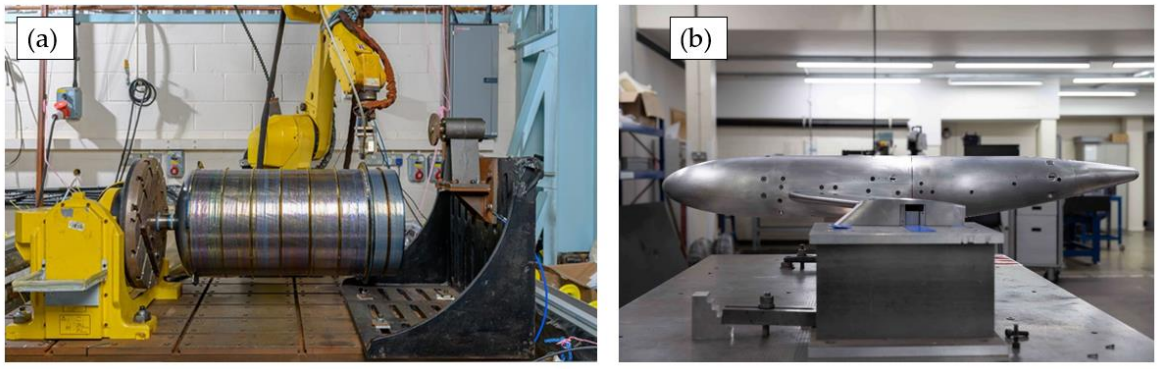


Figure 2.13 - Parts produced by DED-arc with application in the aerospace industry, a) full-scale prototype of a pressure vessel made of the titanium alloy Ti-6Al-4V (adapted from [30]), b) Nose cone made of the aluminium alloy Al 2319 (adapted from [31] ).

In 2023 Li et al. [32] addressed the challenge of developing a chassis within a constrained timeframe. Typically, the extended design and iteration cycles for automotive chassis extend over 2 to 3 years. In response, this study proposed a novel methodology that significantly compressed the design, optimization, and validation stages for automotive chassis through the application of DED-arc. Initially,

44 skeleton chassis were generated by a ground structure method and produced by DED-arc. Then, via OpenCV image processing, the researchers selected the chassis with minimum material occupancy, as illustrated in Figure 2.14. After, collision and modal simulation verifications were proceeded, the findings concluded that the optimized chassis exhibited minimal deformation of 0.1 mm within the project requirements. This study concluded that by adopting the presented methodology, the time invested in designing and iteration cycles can be 120 times lower. This conclusion demonstrates the potential of DED-arc in revolutionizing the testing of chassis in a designing phase.

Figure 2.14 - Skeleton chassis produced by DED-arc [32].

Another application of DED-arc in the automotive industry can be the reinforcement of critical body parts by adding local stiffening elements. In this study [33], orthogonal grids, made of G3Si1 steel, were deposited on uncoated steel sheets to increase the bending stiffness of the sheet, as presented in Figure 2.15. The implementation of this grid increased the bending stiffness at least 50 % and reaching a maximum of about 90 % increase [33].

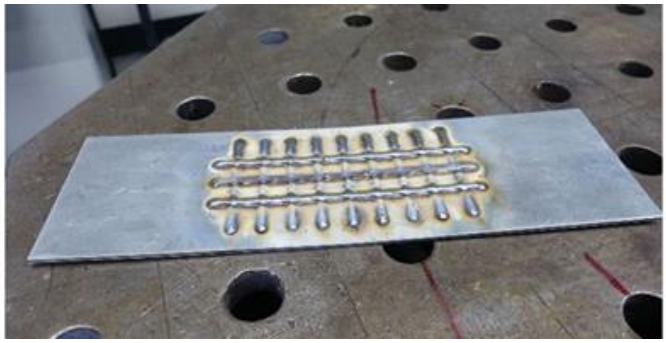

Figure 2.15 - Welding results of additive manufacturing a grid on zinc-coated steel sheets of 2 mm thickness [33].

Another potential application of AM is the production of sheet metal dies. Although literature is more focused in Laser directed energy deposition (L-DED) for this application, DED-arc can be used for high productivity production of sheet metal dies. The use of L-DED process for the manufacture of dies with cooling channels has been addressed in the literature. Cortina et al. [34] successfully used L-DED to close a cooling conduct with AISI 316L and AISI H13, presented in Figure 2.16. In this study, the deposition path was generated using the CAD model NX11 from Siemens Industry Software Ltd

and the zig-zag strategy was used. After the deposition, annealing process was applied in order to relieve residual stresses. Then the part was machined, and the mechanical performance and heat transfer capacity were evaluated to which the results were positive, since they met the project requirements.

Alimov et al. [35] developed and produced two types of hot-forming dies, optimized for AM, specifically one for DED-arc and another for laser powder bed fusion separately. After the third layer of the DED-arc process the piece stated to form slopes at the end areas which were compensated with additional deposition. The piece did not have any other defects, and the full process took about 3 hours. After the deposition of each process, heat treatment and machining were carried out, so the project mechanical properties were achieved and so the geometries met the tolerance requirements. The manufactured dies were under forging tests and an industrial screw press which proved the workability. The author stated that traditional die steels can be difficult to operate in AM because of its complex thermal loading. Other studies try to overcome this by substrate preheating [36]. In this study [35], the used material was 17-4PH steel (EN 1.4542) which showed no defects. Another suggested steels were MS1 (1.2709), CX and CM55 for the manufacture of dies.

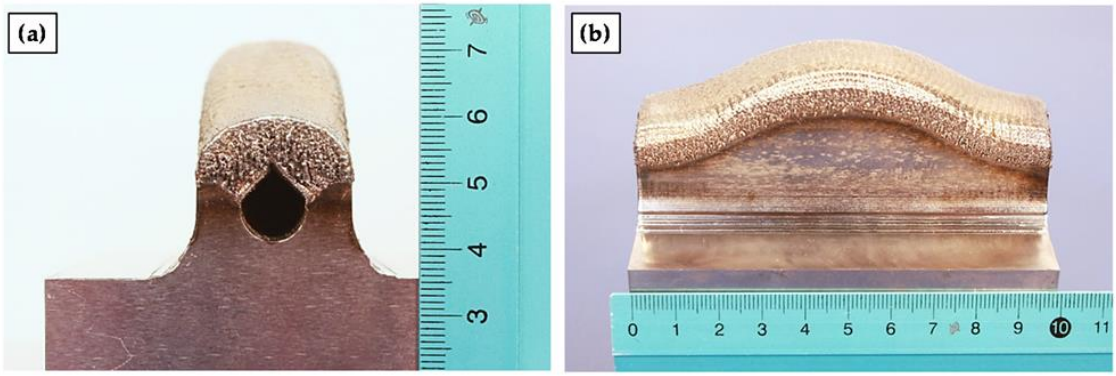


Figure 2.16 - Colling channel manufactured using L-DED [34], (a) Front view, (b) Lateral view.

Hot forging dies are subjected to thermal cycles and cyclical loads which leads to its failure. Consequently, the remanufacturing of this dies is needed in its life cycle. Ni et al. [37] successfully remanufactured a hot forging die by DED-arc incorporating multiple gradient materials. This hot forging die is used to produce a vehicle control arm. The process steps are demonstrated in Figure 2.17.

The implementation of multiple gradient materials aims to enhance the die's performance. Since the die undergoes varying working conditions along its geometry, it is essential to utilize materials with different strengths to specific temperatures ranges [38].

The failure zone of the original die was removed by carbon arc gouging. Subsequently, the deposition of 3 layers was performed, the transition layer, the intermediate layer and the strengthen layer. The transition, intermediate and strengthen layers are the result of the deposition of RM535, RM545 and RM650 welding wires. Following this, machining and polishing were carried out. The

remanufacturing of the forming die resulted in an increase of average life cycle of the die by 37.5%, from 4000 to 5500 expected pieces. To reduce the risk of cracking the substrate was preheated to 450 ºC for 2 h. The process parameters were obtained by using a programmable digital LORCH S8 welding supply and the used welding process was GMAW [37].

In a related study, Zhang et al. [39] also successfully remanufactured a hot forging die with similar process steps using DED-arc, employing three different layers to obtain a gradient structure. The surface material was deposited using DED-arc over the transition and base materials to remanufacture the die. This materials were, respectively, a Co-based material (deposited material), Fe-based material and 5GrNiMo. Their study also concluded that the service life cycle of a die manufactured by DED-arc with a gradient structure is greater than the conventional manufactured die. Additionally, the study proposed an innovative counter-parallel path generation strategy based on level set function, which was applied for the deposition path in remanufacturing the failed landing gear die.

Joghan et al. [40] manufactured the upper part of a punch and its cooling channels, using the tool steel powder Ferro 55, with L-DED. The study compared three punches: A conventional punch with two drilled cooling channels, an additively manufactured punch with a post-processed surface cooling channel by ball burnishing and another additively manufactured punch without a post-processed surface. After the performing hot stamping tests, the post-processed additively manufactured punch showed the best results with less 40 % temperature than the conventional punch. It was deduced that the non-post-processed punch does have less heat transfer that the conventional punch due to higher roughness surface of the cooling channels.

In the literature, the production of punches by powder bed fusion (PBF) has also been studied. Li et al. [41] produced a piercing punch using PBF with maraging steel M300 powder material. The punch underwent durability testing, demonstrating a good performance without damage and still meeting high practical requirements until 10000 stamping tests. These results are equivalent to non-additive manufactured punches. The M300 punch surpassed the reference toughness value of 39.0 J with 89.1 J.

Compared to DED-arc, both L-DED and PBF tend to have a better surface finish. This can be a drawback to the application of DED-arc in terms of the manufacturing of tools with cooling channels, as L-DED and PBF often do not need post-processing cutting operations in these channels, whereas DED-arc does. In this case post-processing ball burnishing can be applied in parts produced by DED-arc.

Three papers [35,37,39] of this research were relevant to identify an appropriate material for the production of tools in the automotive industry. Ni et al. [37] used RM535, RM545 and RM650 welding wires, which were co-developed by the author, thus, were not accessible to use in this work. Zhang et al. [39] employed a Co-based material to deposit onto a Fe-based material and a base material of

5GrNiMo. However, the Co-based material was not specified enough to identify the exact material, making it unsuitable for this work.

Finally, Alimov et al. [35] used 17-4PH steel (EN 1.4542) to manufacture a die and suggested the use of alternative materials such as MS1 (1.2709), CX and CM55. Although the mechanical properties of these alternative materials were worse than the material used in this paper. Therefore, based on this research, this work recommends the use of 17-4PH steel (EN 1.4542) also recognized as AWS A5.9 ER630 for the production of tools in the automotive industry.

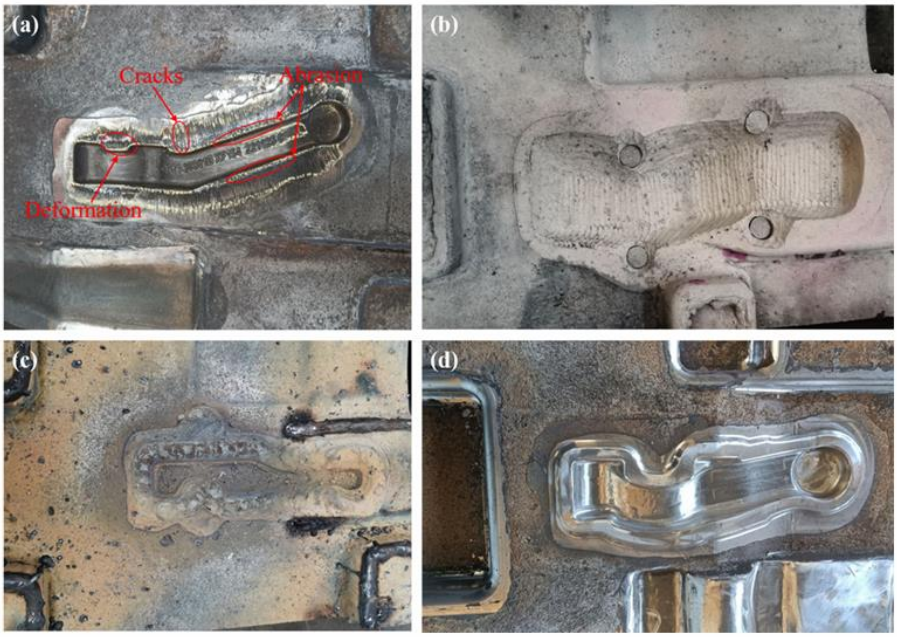


Figure 2.17 - Main steps of hot forging die remanufacturing: (a) failed forging die with defects, (b) removal of the failure zone, (c) DED-arc deposition with multiple materials, (d) post-processing by machining and polishing [37].

## 2.8 Conclusion Remarks

Presently, DED-arc is getting more involved in various industries with special interest in the aerospace industry. The implementation of DED-arc in industries enables the production of complex, large scale parts with a significant material, cost and time saving. In addition, it enables the production of a gradient structure that results in longer service life cycles of tools.

This ability is mainly important not only for prototyping and for stock reduction in the industry but also to enhance the durability of tools. While literature has explored the application of DED-arc in stamping tools production like dies have been studied, a lack of studies of punch production still remains. This work aims to access the feasibility of producing stamping, cutting and forging tools, that are applied in the automotive industry, using DED-arc technology. Subsequently, it aims for the design and production of these tools.

# 3

# EXPERIMENTAL PROCEDURES

This chapter describes the experimental procedures of this work, which involve materials and welding consumables, equipment, the process of overcoming problems with the DED-arc machine, testing of different deposition strategies and overlaps, and the process of fabrication of a part by DED-arc and cutting operations.

## 3.1 Materials and Welding Consumables

Throughout this study, the AWS A5.18 ER70S-6 mild steel solid wire with 1 mm diameter was used to experiment different deposition strategies and parameters. It was also used to deposit a part with application to the automotive industry.

The maximum Vickers hardness was calculated according to equation (3.1), from [5], for both used and suggest materials in order to access the applicability of the materials in the automotive industry. The substrate material used in this depositions was a structural steel plate with $100 \times 60 \times 10$ mm$^3$ and $200 \times 100 \times 10$ mm$^3$.

$$HV_{max} = 90 + 109\,C + 47\,Si + 75\,Mn + 30\,Ni + 31\,Cr \tag{3.1}$$

In Table 3.1 it is summarized the chemical composition of the materials used in this work and Table 3.2 presents its mechanical properties. Additionally, the chemical composition of the shielding gas used is specified in Table 3.3.

Table 3.1 - Chemical Composition of the deposited used material (wt.%) [42].

| | C | Mn | Si | Ni | Cr | Mo | V | Cu |
|---|---|---|---|---|---|---|---|---|
| ER70S-6 | 0.09 | 1.65 | 0.95 | <0.15 | <0.15 | <0.15 | <0.03 | 0.35 |

Table 3.2 - Mechanical properties of the deposited used material [42].

| | Yield Strength [MPa] | Tensile Strength [MPa] | Elongation [%] | $HV_{max}$ |
|---|---|---|---|---|
| ER70S-6 | 452 | 538 | 24 | 277 |

Table 3.3 - Shielding gas composition (wt.%).

| | Ar [%] | $CO_2$ [%] |
|---|---|---|
| Arcal Speed | 92 ± 0.8 | 8 ± 0.8 |

## 3.2 Motion and Welding Equipment

The DED-arc machine used, as it can be seen in Figure 3.1, is composed of a structure with a fixed substrate that has a travelling head driven by eight motors and eight linear motion guides that can move in three axis (x,y,z). In the travelling head there is a welding torch attached that is connected to the wire feeder and the control unit. The motion of the travelling head is controlled by the *Repetier Host* software that uses the programming language G-code. The welding machine used to deposit the material on the substrate was the model OERLIKON CITOWAVE III 520.

However, this machine presented a default fault when printing 3d parts, causing the printed parts to tilt. The resolution of this issue is addressed in § 4.1.


Figure 3.1 - DED-arc Machine.

## 3.3 Deposition strategy testing

Different welding parameters were tested for the ER70S-6 material. Parameters within the suggested by [43], presented in Table 3.4, were tested to obtain a stable arc and a welding bead without visible defects such as porosity. The tests were performed until the final parameters were completed, which resulted in a stable arc and a welding bead without visible defects.

Table 3.4 – Welding parameters of ER70S-6.

| | WFS [m/min] | Shielding Gas Flow [L/min] | I [A] | U [V] | TS [mm/min] |
|---|---|---|---|---|---|
| Proposed by [43] | 3.35-5.80 | - | 100-160 | 15-18 | - |
| Applied | 4.0 | 13 | 123 | 19 | 400 |

A single welding layer rectangle of 40 × 60 $mm^2$ was deposited, which was designed to start and end at the same point. The G-code involved in this test projected a synchronized start of the welding and the torch movement, using the parameters listed in Table 3.4, but without considering any

overlapping parameters. It was observed that the beginning of the layer and the end did not intercept which is not optimal for printing a part.

The strategies described in Table 3.5 were tested in order to develop an appropriate strategy to overcome this imperfection. Any percentages used in this table are related to the parameters of Table 3.4 and the width of the welding bead considered was $w = 5.45$ mm. All the performed strategies had different beginnings and end points separated by 0.75 mm as implemented automatically by Prusa Slicer. This distance is due to the consideration of the $w$ in the Prusa Slicer. The results of these strategies are specified in § 4.2.

Table 3.5 - Strategies to improve the deposition of the layers.

| Strategy | Beginning of the layer | End of the layer |
|---|---|---|
| 1 | Strategy of [25], described in Figure 3.2. | Strategy of [25], described in Figure 3.2. |
| 2 | Strategy of [25], described in Figure 3.2. with an extra welding time of 0.3 s before starting the movement on both the beginnings of welding. | Strategy of [25], described in Figure 3.2. |
| 3 | Strategy of [25], described in Figure 3.2. without the second welding. With an extra welding time of 0.3 s before starting the movement | Extra welding time of 0.9 s after the ending of the movement. |
| 4 | Extra welding time of 0.5 s before starting the movement | Extra welding time of 0.5 s after ending the movement |

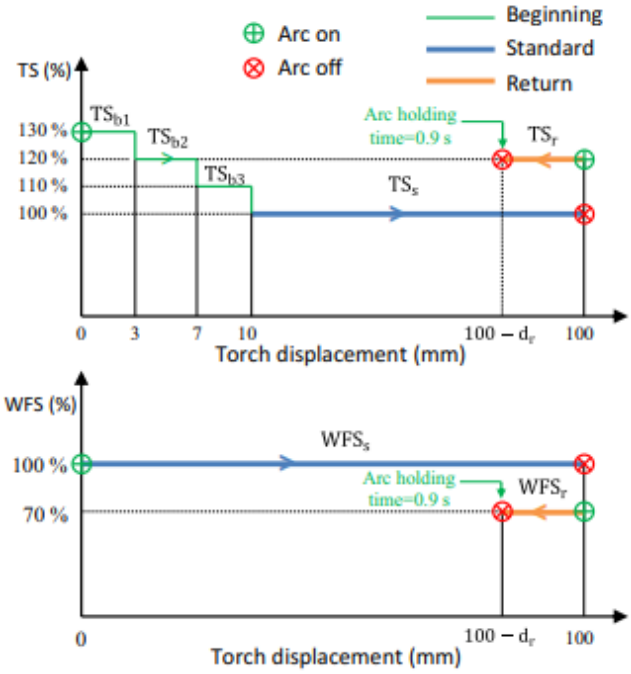


Figure 3.2 – Illustration of Strategy 1 [25].

## 3.4 G-code generation system for DED-arc

This section explains how the process of generating the G-code for the printing of metal parts were developed and implemented.

The slicer used to generate the G-code used was the Prusa Slicer (version 2.7.2) with several modifications in the printing, filament and printer settings. These adjustments adapted the software outcome from a standard Fusion Deposition Modelling process into the DED-arc process, as well as to adjust from printing Polylactic Acid to metal, specifically steel. The settings were refined from a previous work performed by Francisco Ferreira into more suited version to this dissertation. The final settings used, along with an explanation to the change of these settings, are presented in Appendix 1.

Although the Prusa slicer successfully generated the G-code for printing an entire piece, it was not optimized to be operated in the DED-arc machine used in this work. This G-code was a single file which means that the part had to be printed in one go, without the possibility to print layer by layer with a variable time between layers. Due to limitations of the machine software, to cancel the print it would require the operator to wait the original print time before starting another print. Even though it was possible to stop the print, if necessary, this approach is not optimal in an experimental setting, where defects and errors during deposition may happen, leading to time wastage.

To address this limitation, a solution is to have a G-code file for each layer. In this case, if an error occurs, only the time to complete the layer would be lost rather than the printing time of the rest of the part. In order to do this, a python script that would automatically create a G-code for each welding bead of each layer in the form of a text file was developed. The python script used can be found in Appendix 2 with a simple explanation of its functions.

## 3.5 Overlap model testing

An important parameter in DED-arc is the overlapping between welding beads, which is measured by the distance between two centers of parallel welding beads. To identify which overlapping was optimal to use in DED-arc, Ding et al. [27] concluded that the optimal distance between the center of two welding beads should be 0.738 times its width ($w$). In this dissertation, different overlapping were tested to understand which distances are optimal to this process and also confirm the work done by Ding et al. [27].

In order to test the overlapping between two welding beads, the $w$ of a single welding bead was measured using a *Leica* DMI 5000 M microscope. This welding bead was deposited with the welding parameters presented in Table 3.4 on row "Applied".

Initially, the bead was cut with a band saw, and then polished sequentially with the sandpapers: P80, P220, P320, P400, P600 and P1000. After polishing, the macroscopic observation took place and $w$ was measured. Figure 3.3 shows the macroscopic image used to measure the width, $w = 5.45$ mm.

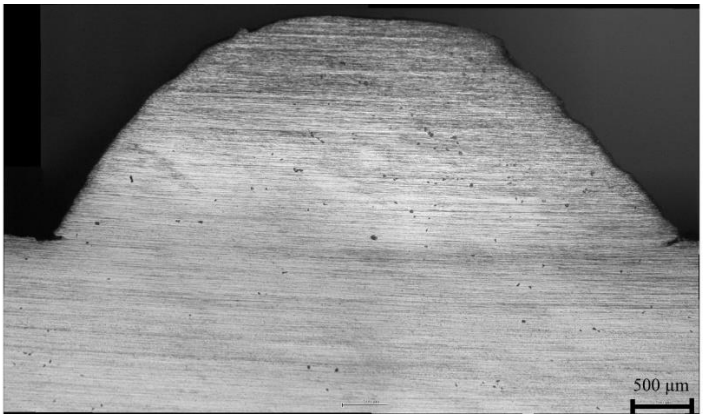


Figure 3.3 – Macroscopic view of one welding bead.

### 3.5.1 G-code generation system

To test the overlapping, four cuboids of $40 \times 60 \times 40$ mm$^3$ were printed with different distances between welding beads, in the infill and between the outer bead of the infill and the external perimeter bead. In this experiment, each layer had two welding beads: the perimeter bead and the infill bead, as seen in Figure 3.4, where the orange line represents the perimeter bead, and the red line represents the infill bead.

In this project, it was used a combination of the two deposition strategies, with the zig-zag approach being used to fill the inside and the counter approach to restrict the infill. This was performed since it is most beneficial for DED-arc in general cases [21].

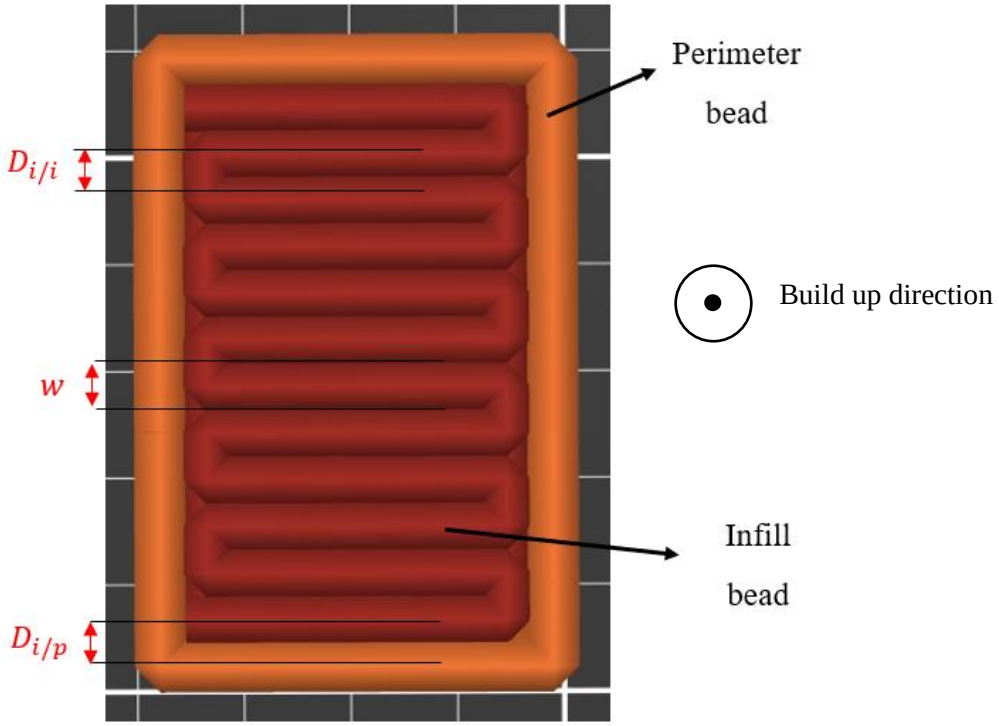


Figure 3.4 - Welding beads of each layer of the part.

This cuboid was first modeled in SolidWorks, saved as a *.STL file and opened in the Prusa Slicer. Afterwards, the settings on Appendix 1 were applied with a small difference. In the tab print settings, then in advanced tab and in extrusion width segment, the following settings were changed: Default extrusion width; First layer; Perimeters; External Perimeters and Infill. This settings dictated the *w* on different sections of the printing process. Since there is no setting on Prusa Slicer that controls the overlap between beads in the infill, an alternative width was inputted on this settings in order to achieve the chosen overlap. Considering that the inputted value for the *w* was 5.45 mm, it would lead to, theoretically, non-overlapping beads.

Since Ding et al. [27] concluded that the optimal distance between two welding beads should be 0.738 times its width, it was chosen to study distances between beads from 0.71 $w$ to 0.80 $w$ in the infill beads to evaluate if it would fill properly the part. These values did not differ greatly from the 0.738 $w$ since the main goal was to find an appropriate distance to fill the inside of the part.

To achieve these values, different inputs were tested on the parameters previously discussed: Default extrusion width; First layer; Perimeters; External Perimeters and Infill which resulted in different G-codes. The distance between beads in the infill, and between infill and perimeters beads, were then measured on the G-code for vertical and horizontal beads. The values of the distances between beads in the infill of the horizontal and vertical beads, $D_{i/i}$, were calculated. In addition, the values of the distance of the vertical and horizontal beads of the infill to the perimeter beads, $D_{i/p}$, were also calculated. Then these values were divided by $w$. The variables $D_{i/i}$ and $D_{i/p}$ are illustrated in Figure 3.4

The input results with the closest distance values, between horizontal and vertical beads in the infill section, to the intervals of 0.71 $w$ to 0.80 $w$ are presented on Table 3.6. These were used on this work.

Table 3.6 - Settings inputs on Prusa Slicer in mm, distances between beads that resulted from these settings inputs in mm and its values in fraction to w .

| Sample | Default extrusion width | First layer | Perimeters | External Perimeters | Infill | $D_{i/i}$ | $D_{i/p}$ | $\frac{D_{i/i}}{w}$ | $\frac{D_{i/p}}{w}$ |
|---|---|---|---|---|---|---|---|---|---|
| A | 4.2 | 4.2 | 4.4 | 4.4 | 4.2 | 3.881 | 3.948 | 0.7115 | 0.7237 |
| B | 4.4 | 4.4 | 4.6 | 4.6 | 4.4 | 4.385 | 4.3315 | 0.8038 | 0.7941 |
| C | 4.4 | 4.4 | 5.45 | 5.45 | 4.4 | 4.193 | 4.66 | 0.7687 | 0.8543 |
| D | 4.25 | 4.25 | 4.25 | 4.25 | 4.25 | 4.017 | 3.942 | 0.7364 | 0.7227 |

The corresponding G-codes of the samples A, B, C and D were then used to create multiple *.txt files, as explained in §3.4 that corresponds to each welding bead used. These G-codes used to print Sample A are presented in Appendix 3.

### 3.5.2 Deposition strategy and welding parameters

The *.txt files were used to deposit the 4 cuboids with the material ER70S-6, according to the processing parameters presented in Table 3.4. A zig-zag approach was used to fill the interior and the counter approach to constrain the infill as detailed in Figure 3.4.

During the deposition of these cuboids, an extra strategy was applied for specimens B, C and D, in addition to the preset strategy of Prusa slicer, as it is explained in Table 3.7. In contrast, specimen A was deposited without an extra strategy.

The welding parameters used in this work can be seen in the applied section of Table 3.4. During this experiment, the temperature of the welding beads was constantly measured using an infrared thermometer. Between the deposition of each welding beads, the part was cooled to a temperature below 300 ºC, which defined the dwell time. To decrease this dwell time, the part was first allowed to cool down naturally to around 400 ºC, and then compressed air was applied to the part until reaching a temperature of 300 ºC.

The natural cooling process to 400 ºC normally took over one minute. At this temperature and cooling time, the material surpassed the typical transition line in a steel TTT diagram and have a more stable microstructure that is less responsive to cooling rates. Thus, the application of compressed air does not affect greatly the microstructure of the deposited part and also accelerates the deposition process [44].

Table 3.7 - Extra deposition strategy used to deposit specimens B, C and D in addition to the preset strategy of Prusa Slicer.

| Strategy | Beginning of the layer | End of the layer | Result notes |
|---|---|---|---|
| 5 | Infill: Extra 0.5 s of welding time.<br>Perimeter: Extra 0.4s of welding time. | Perimeter: Extra 0.2 s of welding time. | It appeared to fill all the gaps while printing. |

## 3.6 Characterization techniques

### 3.6.1 Sample production

For each sample it was performed uniaxial tensile tests and microhardness measurements. In order to prepare the samples for characterization testing, the samples were sliced into three pieces using a band saw, as shown in Figure 3.5. The middle slice was used to conduct the uniaxial tensile tests and

one of the outer slices was chosen to perform the microhardness measurements. The outer slices codification were defined by sample's letter following "L1" or "L2". Hence, in the remaining of this work these outer slices were identified as: AL1, AL2, BL1, BL2, CL1, CL2, DL1 and DL2.


Figure 3.5 – Sample divided in three pieces.

To prepare the test specimens for the uniaxial tensile test, first the normalized subsize specimen for metallic parts in the ASTM standard E8 [45] was adapted to enable its production. Initially, the nominal dimensions were adapted to the values described in Table 3.8 as "Adapted subspecimen without scale factor". Following that, it was applied a scale factor of 0.5 which is specified at Table 3.8 with the identification "Adapted Subspecimen with scale 0.5". To reach the used tensile specimen dimensions the width, T, was adjusted from 2.5 mm to 2.6 mm to decrease its time of production, which is specified as "Adapted specimen used" in Table 3.8. The technical drawing of the used specimen can be seen at Appendix 4.

Table 3.8 – Adapted dimensions of the subsize specimen of ASTM standards E8 in mm.

| | W | T | R | L | A | B | C |
|---|---|---|---|---|---|---|---|
| ASTM subspecimen [45] | 6±0.1 | 6 (Upper limit) | 6 | 100 | 32 | 30 | 10 |
| Adapted Subspecimen without scale factor | 5 | 5 | 45 | 66 | 10.4 | 13 | 10 |
| Adapted Subspecimen with scale factor of 0.5 | 2.5±0.1 | 2.6±0.1 | 22.5 | 33 | 5.2 | 6.5 | 5 |
| Adapted specimen used | 2.5±0.1 | 2.6±0.1 | 22.5 | 33 | 5.2 | 6.5 | 5 |

To prepare these specimens, the central slice sides were cut using a milling machine in order to make two even surfaces with parallel sides of 2.7 mm of thickness. This operation was accomplished using an end mill shell cutter. Afterwards, it was surface finished by a grinding machine which resulted in a polished slice of 2.6 mm of thickness, as illustrated in Figure 3.6 a). The sheets were then machined in a 3 axis CNC machine from HAAS to a near-net shape of the final specimens, as it can be seen in Figure 3.6 b). The CNC operation was performed using an X-Coated Carbide end mill.

The end mill is illustrated in Annex 2 along with the cutting parameters used in the CNC operation. Then, each specimen was extracted from the waste metal with the usage of a manual saw and manually polished with a polishing paper of 1200.

The final specimen is illustrated in Figure 3.6 c). With this operation, 16 specimens for uniaxial traction testing were produced. Each of these 16 specimens were identified as sample's letter following a number from 1 to 4. Hence the identification of these 16 specimens were the designations A1, A2, A3, A4 that correspond to the specimens produced with sample A, the designations B1, B2, B3, B4 that correspond to the specimens produced with sample B, the designations C1, C2, C3, C4 that correspond to the specimens produced with sample C and the designations D1, D2, D3 and D4 that correspond to the specimens produced with sample D.

To prepare the samples for the microhardness measurements the method was similar to the presented prior to the slice represented in Figure 3.6 a), except the thickness of the slice was not reduced to 2.7 mm, it was maintained just enough to make the sample sides parallel and polished. The slice was machined with milling machine to level the surface and then polished with the grinding machine.

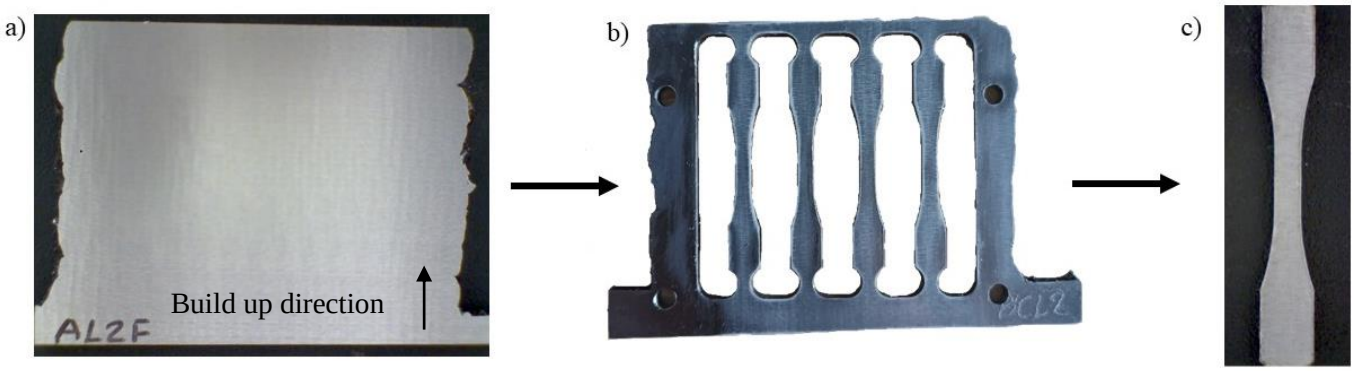


Figure 3.6 – Main steps of manufacturing a specimen for uniaxial tension test: a) Machined slice of the sample; b) Machined slice after milling in CNC machine; c) Final specimen

### 3.6.2 Microhardness measurements

Microhardness measurements were conducted on four outer slices identified as AL2, BL2 CL2 and DL2. Being one slice of each sample, they were properly machined and polished, as explained before.

This measurements were performed along 4 vertical lines with a distance of 0.5 mm between lines and between indentations. These lines length were centered in the full height of the piece and in width being spaced form the center of the piece from 0.5 mm to 1.5 mm in both directions, as illustrated in Figure 3.7. The lines have a total length of 25 mm which results in 50 indentation per line. With four lines of indentations, it totals 200 indentations for each sample. The distance between indentations, and from an indentation to an edge, used in this work was greater than the minimum of 2.5 times the Vickers diagonal specified in the ASTM standard E92-23 [46]. This experiment was conducted using a Mitutoyo HM-112 810-126D microhardness tester and by applying a load of 0.5 kgf for 20 seconds for each indentation.

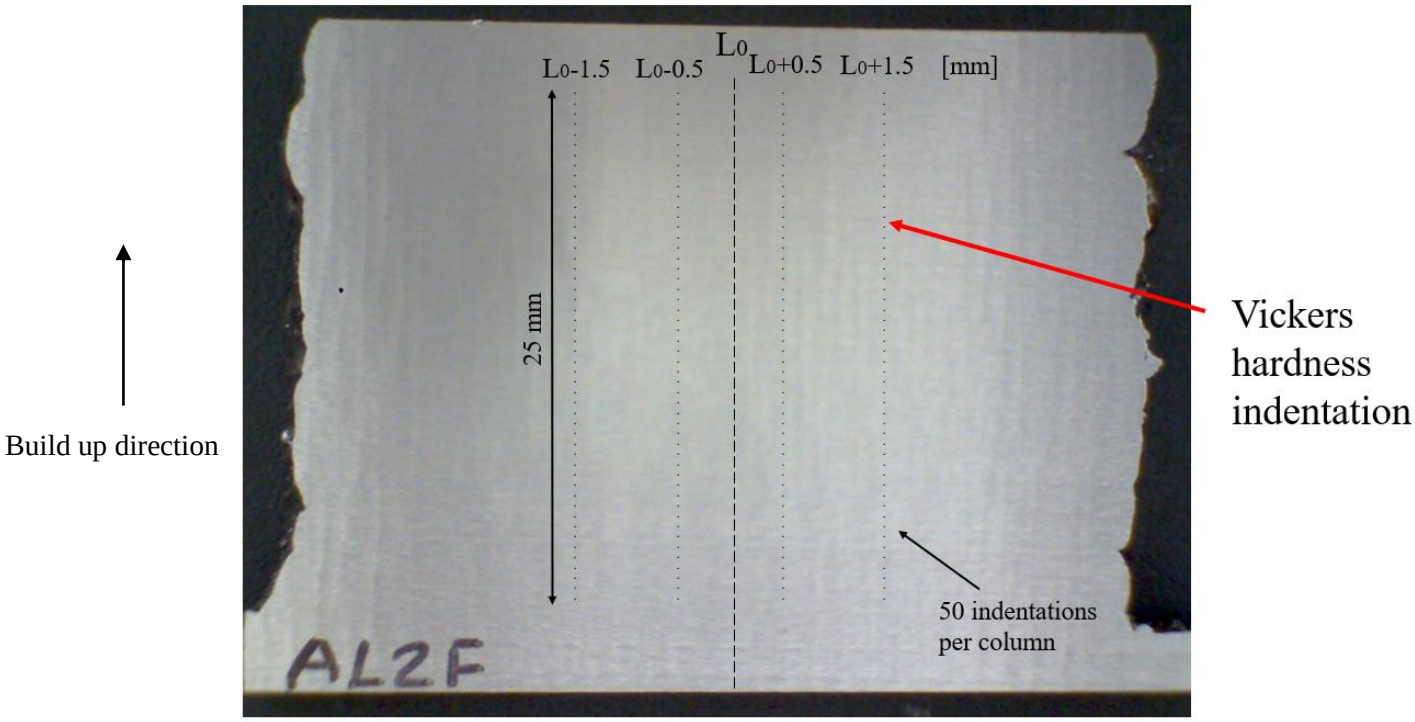


Figure 3.7 - Schematic representation of Vickers hardness indentations.

### 3.6.3 X-ray

In order to evaluate the existence of inner defects in the specimens to be used in the uniaxial tensile tests, an x-ray inspection system was applied to 16 specimens. The machine used was Kodak 2100, using a time of exposure of 1.0 s for each specimen.

### 3.6.4 Uniaxial Tensile Tests

The uniaxial tensile tests were performed on 16 tensile specimens identified from 1 to 4 for each sample. These tests were conducted in an electromechanical testing machine EA05 from STEP-Lab with a maximum static force of 10 kN with a speed test of 0.017 mm/s. Since the sample had limited dimensions, only four specimens per sample were uniaxial tensile tested which totalizes 16 tested specimens. Due to unfamiliarity with the machine, the tension / elongation relation was lost on two uniaxial tensile specimens of sample A, where only the elongation to fracture was able to be retrieved from the device. In addition, the elongation at fracture of specimen D4 was lost to. The information about the rest of uniaxial tensile specimens (13) was successfully retrieved from the machine.

## 3.7 Re-design and Fabrication of the part

### 3.7.1 Re-design of the part

The objective of this work was to fabricate a part that is applied in the automotive industry and possibly re-designing it to able its production by DED-arc. The part observed in Figure 3.8 a) was chosen to be studied, as it was suited to be produced by DED-arc since it has many complex features. In addition, the implementation of DED-arc to fabricate this part, in comparison to machining from a solid block of steel, would lead to a significant material saving.

This particular part experiences severe wear, while operation, on the edge of the wear zone illustrated in Figure 3.8 a). In practical cases, the wear in this specific zone originates the replacement of the hole part since it loses its feasibility. Thus, the original part was modeled in SolidWorks CAD and re-designed into being divided in two parts: the base part, and the part of interest, as illustrated in Figure 3.8 b). This enables the part of interest to be replaced instead of the whole part and lead to saving costs of manufacturing.

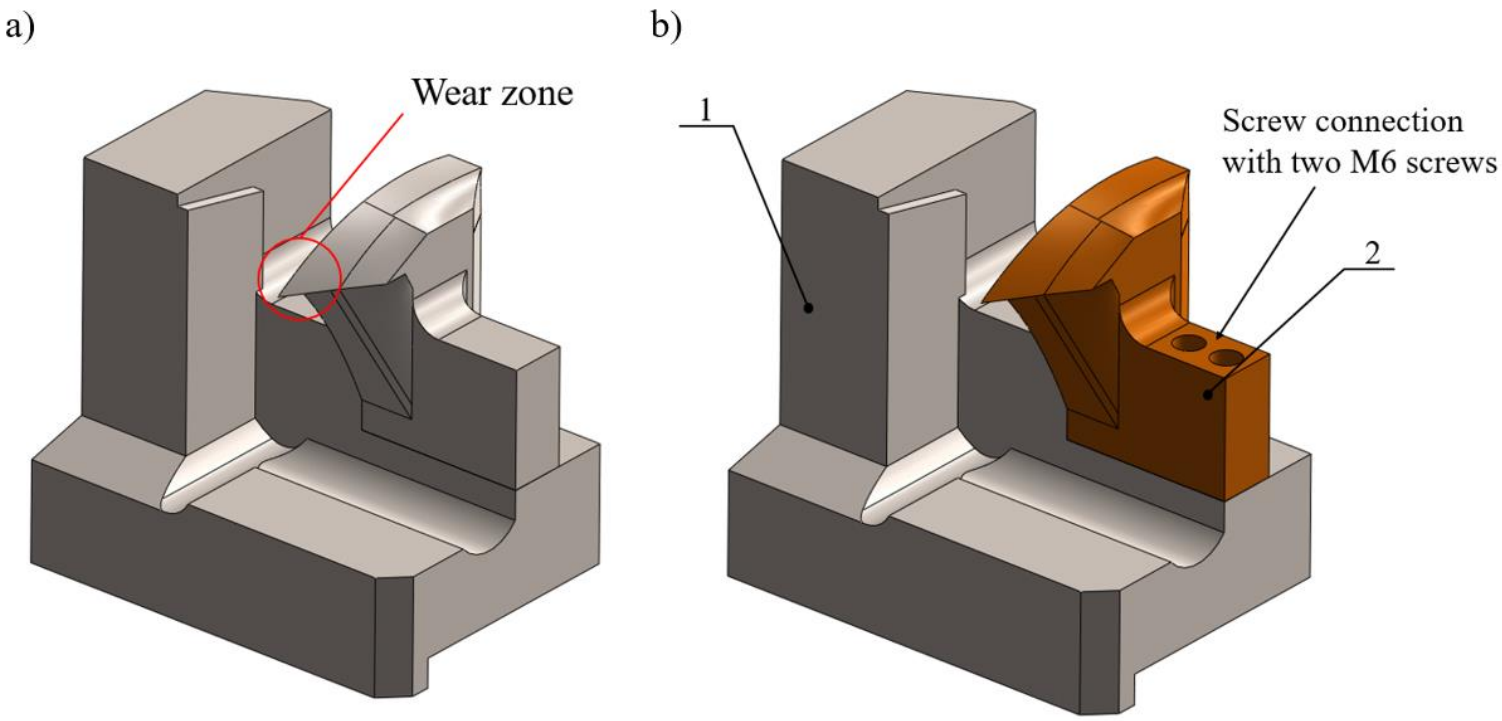


Figure 3.8 - Part to be produced by DED-arc: a) Original part; b) Re-designed part: 1) Base part; 2) Interest part.

To ensure that these two sections could be joined together, a screw connection solution was developed as it can be seen in Figure 3.8 b). The screw connection is composed by two M6 screws. The technical drawings of each part, along with its assembly are presented on the Appendix 5.

After the completion of the re-design, the part illustrated as 2 in Figure 3.8 b) was chosen to be produced by DED-arc.

### 3.7.2 Fabrication of the part

Similarly to the method explained in §3.5.1, the SolidWorks file of the part to be produced was converted into an *STL file. Once this file was on the slicer, a scale of 1.2 was applied to compensate the displacement movements of the X-axis that the machine generated and some possible distortion that may happen during its deposition. The configurations detailed on Appendix 1 were applied and a G-code was generated. The overlap settings used on Prusa Slicer were specified as specimen D of Table 3.6. Similarly to the strategy employed in the overlapping model testing, a zig-zag approach was used to fill the interior and the counter approach to constrain the infill.

After this, the g-code was copied to a *.txt file and the name changed to “g.txt”. Then this was moved to a folder with the python file mentioned in §3.4. After running the python file, a G-code in a *.txt format was created for each welding bead: Perimeter 1, Infill 1, Perimeter 2, Infill 2 and Gap infill. These welding beads are illustrated in Figure 3.9, which represents a generic layer of the first section of the part. The welding beads of the second section of the part are represented in Figure 3.10 as Perimeter 1 and Infill 1. The *.txt files of the G-codes used to print the part cannot be seen in this work due to its high space required.

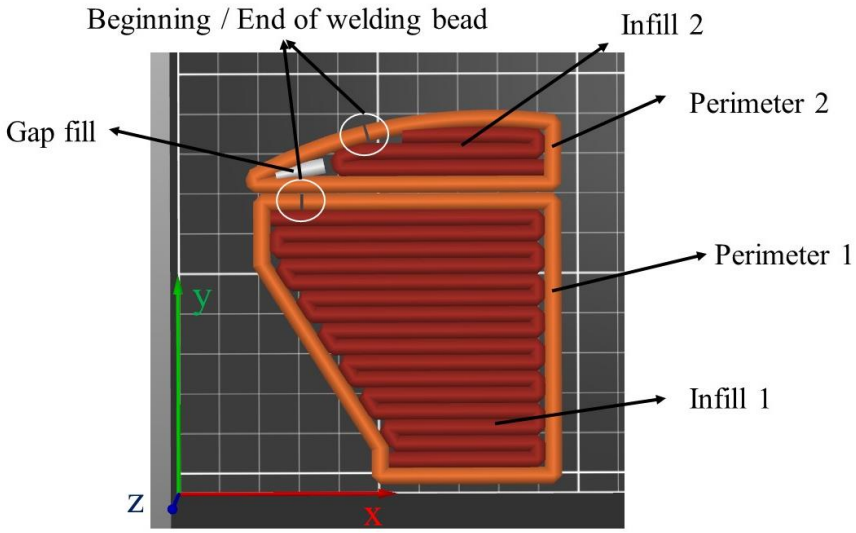


Figure 3.9 - Illustration of the first stage of the part's deposition.

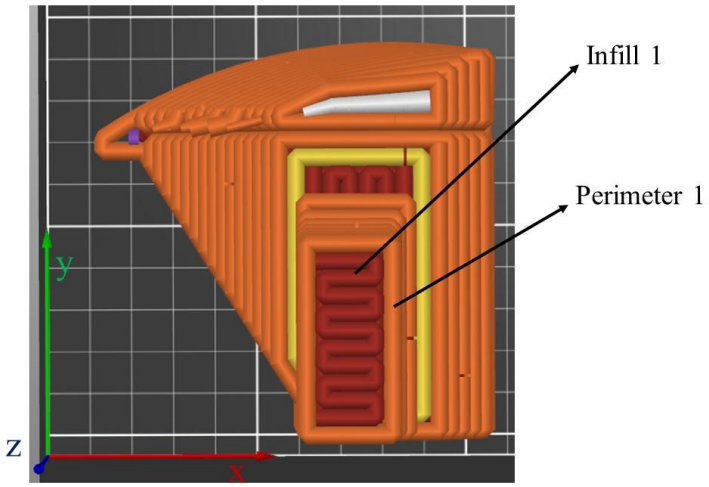


Figure 3.10 - Illustration of the second stage of the part's deposition.

To print the part, the G-code of each welding bead was implemented on the DED-arc machine. The welding parameters used in this experiment are specified in Table 3.4 in the row "Applied". The deposition strategy for this part was strategy 4, described in Table 4.1. The substrate used in the print was a $200 \times 200 \times 6$ mm$^3$ steel plate that was attached to the DED-arc machine. The part was then printed, where the dwell time between welding beads was dictated by the time that the part took to cool down to around 300ºC.

During the deposition of this part, at moments, the infill beads had an extra z dimension then the perimeter beads. To compensate this, some Infill welding beads were skipped: "layer 14", "layer 17", and "layer 36". The Prusa Slicer also included in the initial G-code, an extra welding beads that did not

match the wanted part along with some Gap fill that weren't needed, thus the following welding beads were nor deposited: "layer 37", "layer 42", "layer 57", "layer 78", "layer 79" and "layer 117".

Subsequent to the deposition of the welding bead "layer 51", pores were present due to the welding torch being clogged. As a result, the welding torch was cleaned and the print continued smoothly. To prevent this, the welding torch was cleaned again after the deposition of "layer 88" and "layer 138".

After the deposition of the welding beads "layer 138" to "layer 142", multiple pores were observed. Since the printed part's height overcame the overall height of the projected final part, it was decided to stop the print.

Following the deposition of the part, several cutting operations were performed. A section of the substrate that was not welded was removed using a band saw to allow its attachment to the CNC machine. Following this, a G-code to machine the part on the CNC machine was generated using SolidWorks CAM. The part was then machined using a CNC machine with an carbide end mill with 16 mm of diameter. This end mill is illustrated on Annex 3, along with the cutting parameters used in this operation.

In this CNC cutting operation, only an end mill was used which made it complex to produce some of the curve features of the part according with its technical drawing present on Appendix 5. To approximate the curved features, the part was machined in one set up, layer by layer, with a 2.5 mm of dept per layer, which caused a step effect on the part, as it can be seen in Figure 3.11. While choosing a smaller dept per layer would reduce the step effect, it would also increase operation time. Hence the value of 2.5 mm was chosen as a compromise.

A clear lacquer finish was then applied in the part to protect effectively the surface of the part from oxidation.

Figure 3.11 - Step effect on the machined part.

# 4
# RESULTS AND DISCUSSION

This chapter is divided into four sections: The method developed to solve the issues with the DED-arc machine, the results of multiple tested deposition strategies, the results and discussion of the overlap testing and the results and discussion of the fabrication of a part with application in the automotive industry. The results of visual inspections, uniaxial tensile testing and microhardness testing are displayed and discussed for these last two sections.

## 4.1 Overcoming problems with the DED-arc machine

Some problems were found during the printing of 3d objects. As illustrated in Figure 4.1, the parts were printed inclined, which did not match the G-code used. To find the source of the problem, a device was designed to trace the movements of the welding torch implemented by the G-code. This device attaches a pen to the welding torch, using a linear rail guide. The linear rail guide has a weight so the pen could ink the paper with different heights which simulates the printing of 3d parts. This device can be seen in Figure 4.2.

Subsequent to the development of this device, various G-codes files were tested to find out if the problems origin was related to specific G-codes commands. The results, illustrated in Figure 4.3, show that the pen lines did not overlap as expected, they deviated from each other which results in inclined parts.

After further testing, it was found that the source of this issue was not the G-code used, but rather the motors that controlled the X movement of the welding torch. These were misaligning with usage, which resulted in the observed inclination. After the alignment of the motors, the ink revealed consistent overlapping lines, as it can be seen in Figure 4.3 b), indicating that the machine was ready to print aligned parts.

Figure 4.1 – Tilted 3d part.

Figure 4.2 – Tracking system the movements of the welding torch.

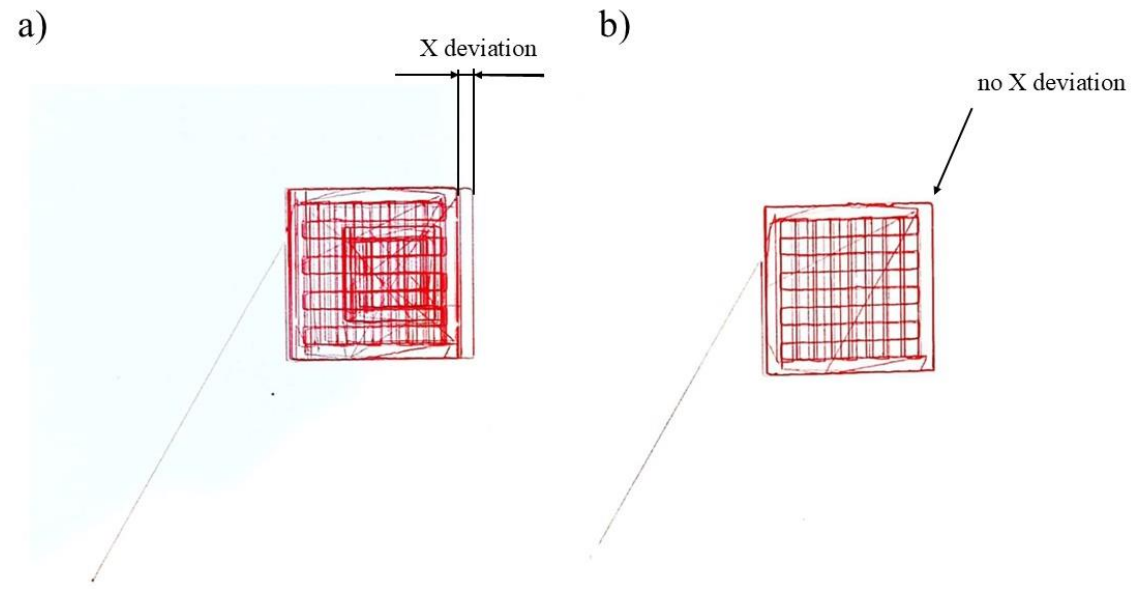


Figure 4.3 - Illustration of the results of the pen device: a) Before aligning both x motors; b) After aligning the x.

## 4.2 Deposition Strategies Results

The deposition strategies presented in § 3.3 showed diverse outcomes. Strategy 1 displayed good results in [25], but this did not replicate on this work, and it can be due to several factors. In this strategy, the movement of the torch and the wire feed begin simultaneously, but this does not represent that the welding and movement times are synchronized. The wire distance to the substrate before welding delays its contact, which delays the welding. Considering a wire distance to the substrate of 10 mm and a WFS of 4 m/min, the time for the wire to touch the substrate is 0.0025 min. Given a TS of 400 mm/min, this delay represents a distance of 1 mm. Adding the distance between end start and end points of each layer as assumed by the Prusa slicer (0.75 mm), the total distance is equal to 1.75 mm.

This distance contributes to the beginning and ending of the welding bead not intercepting. Thus strategies 1 and 2 do not intercept correctly the start and the end of the welding bead. However, strategies 3 and 4 pose a greater time of welding before moving the welding torch which contributes to the interception of the start and end of the welding bead.

The results of each strategy are detailed in Table 4.1 and illustrated in Table 4.2.

Table 4.1 – Results of tested strategies to improve the deposition of the layers.

| Strategy | Beginning of the layer | End of the layer | Result notes |
|---|---|---|---|
| 1 | Strategy of [25], described in Figure 3.2. | Strategy of [25], described in Figure 3.2. | The beginning and ending of the welding bead did not intercept. The extra welding did not cover the intercepting zone, but it leveled well the end of the layer with the beginning. |
| 2 | Strategy of [25], described in Figure 3.2. with an extra welding time of 0.3 s before starting the movement on both the beginnings of welding. | Strategy of [25], described in Figure 3.2. | The beginning and ending of the welding bead did intercept but barely. The extra welding did not cover the intercepting zone, but it leveled well the end of the layer with the beginning. |
| 3 | Strategy of [25], described in Figure 3.2. without the second welding. With an extra welding time of 0.3 s before starting the movement | Extra welding time of 0.9 s after the ending of the movement. | The beginning and ending of the welding bead did intercept correctly. The ending of the welding bead was slightly uneven with the begging. |
| 4 | Extra welding time of 0.5 s before starting the movement | Extra welding time of 0.5 s after ending the movement | The beginning and ending of the welding bead did intercept correctly. The ending of the welding bead was slightly uneven with the begging. |

Strategies 1,2 and 3 were tested by welding the rectangle $40 \times 60$ mm$^2$ described before, while strategy 4 was tested on other prints throughout this work. In this setting, although strategy 3 showed promising results, strategy 4 presented similar results with a lesser complexity of implementation. Due to its simplicity and good results, strategy 4 was chosen to the fabrication of the part, detailed on § 3.7.

Table 4.2 - Illustration of different deposition strategies tested.

| Strategy | Plant View | Side Elevation |
|---|---|---|
| 1 |  |  |
| 2 |  |  |
| 3 |  |  |
| 4 |  | - |

## 4.3 Overlap Model Testing Results

### 4.3.1 Visual Inspection

A visual inspection was conducted to the interior face of the outer slices for each sample. As explained in §3.6.1, each sample resulted in two outer slices that were identified as L1 and L2. The inspection displayed were frequent pores on the slices: AL1, CL1 and CL2. The remaining samples did not show relevant pores through the visual inspection as shown in Table 4.3.

The pores were located in the infill–perimeter intersection region rather than in the infill region (center) which indicates that all the sample's infill overlaps were successful in all samples. These pores can be originated from several factors:

- Lack of overlapping between the infill and perimeter welding beads;
- Inadequate deposition strategy in the beginning and ending of each welding bead;
- Inadequate Welding parameters.

Since none of the infill regions presented pores, the welding parameters were likely not the cause. To understand the cause to these pores, it is necessary to analyze the production of the samples and its G-code.

After the deposition of the samples, these were sliced into 3 pieces using a band saw. Which thickness was not controlled to be uniform. Meaning that the visual inspection done in these slices can only provide conclusions if there was a lack of overlap between the infill and the perimeters welding beads since it would appear across all the length of the samples. This inspection cannot evaluate if the deposition strategy applied was successful since it is not guaranteed that the slice surfaces cover the beginning and ending points of the welding beads.

Although the start of the infill welding bead was randomly decided by the Prusa slicer, in the deposition of the samples, it was observed that it started more often in 3 points on each sample. Figure 4.4 illustrates the 4 possible starting points of the infills welding bead. Table 4.4 presents the number of times that the infill welding bead starts on each of the four possible points for each sample print.

As explained in §3.5, sample A was not deposited using an enhanced strategy of deposition, as detailed at Table 3.7, unlike other samples. The origin of the pores in sample A was not the lack of overlap between infill and perimeter welding beads since it only showed one line of pores instead of four lines. This concludes that the absence of a deposition strategy results in lack of filling on three-dimension parts.

Table 4.3 – Visual Inspection of samples AL1, AL2, BL1, BL2, CL1, CL2, DL1 and DL2.

| | Slice L1 | Slice L2 |
|---|---|---|
| Sample A | 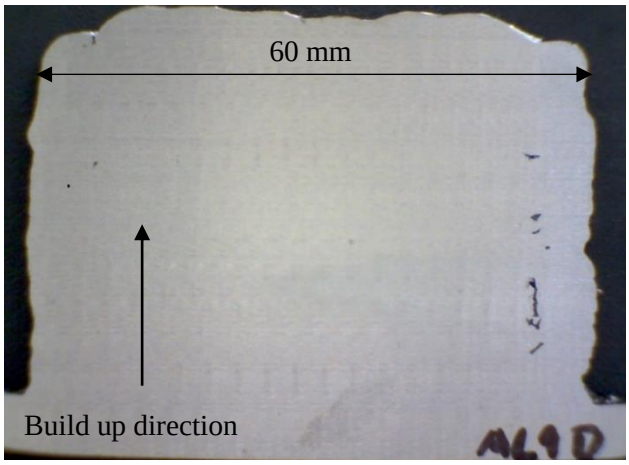 | 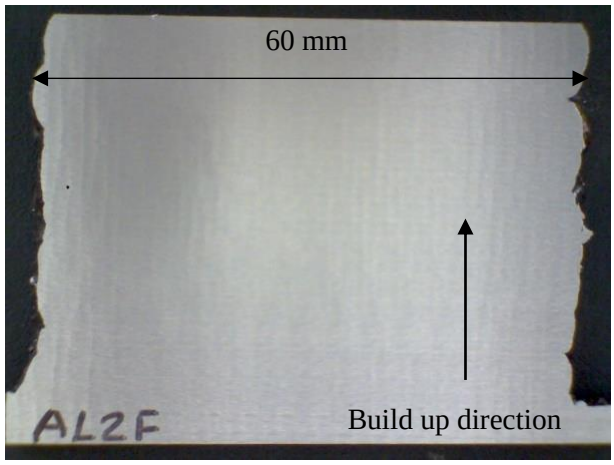 |
| Sample B | 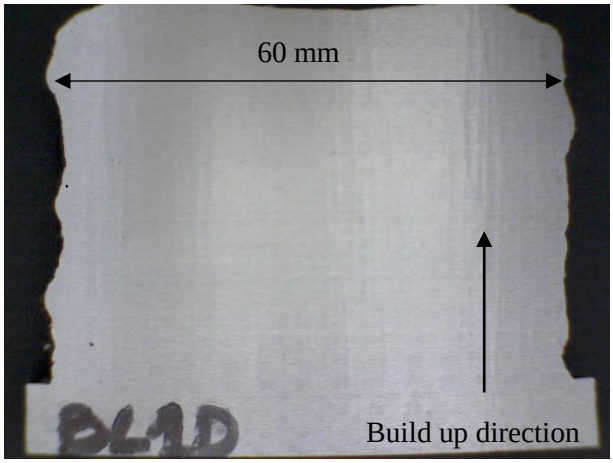 | 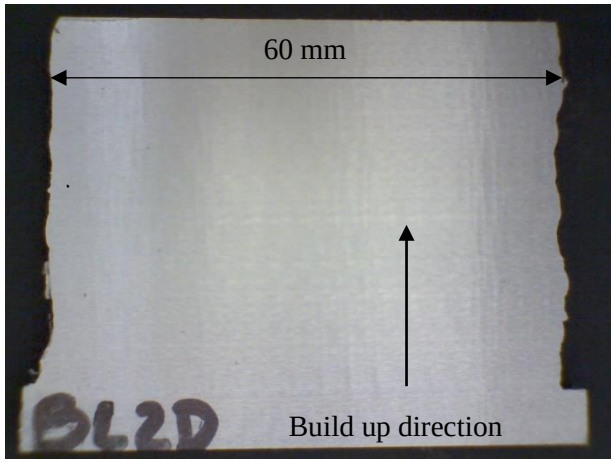 |
| Sample C | 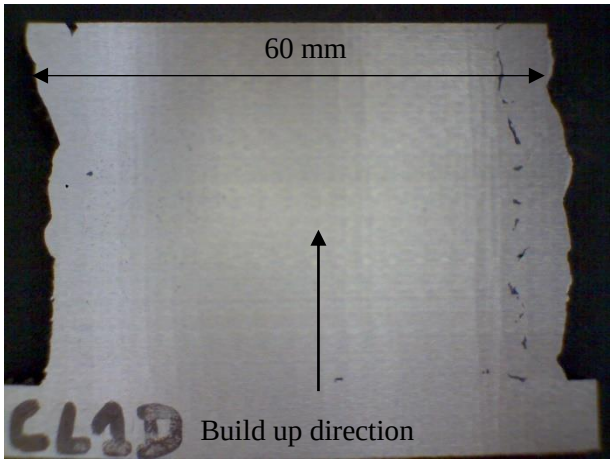 | 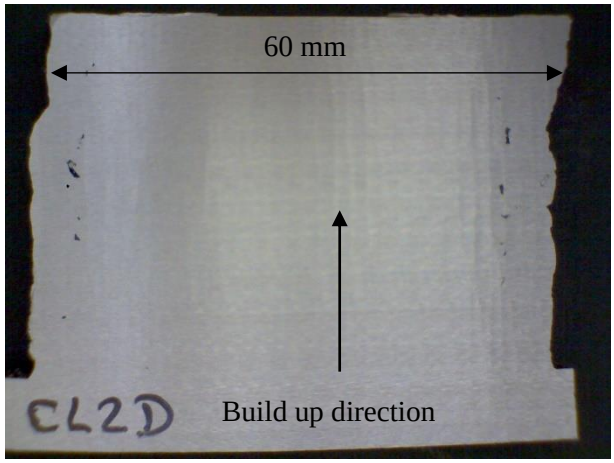 |

Sample D

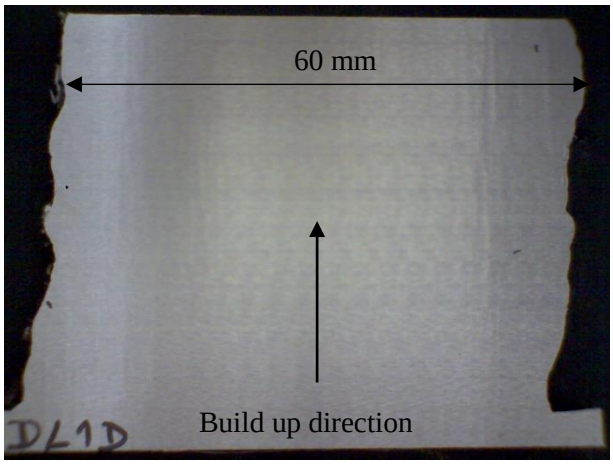


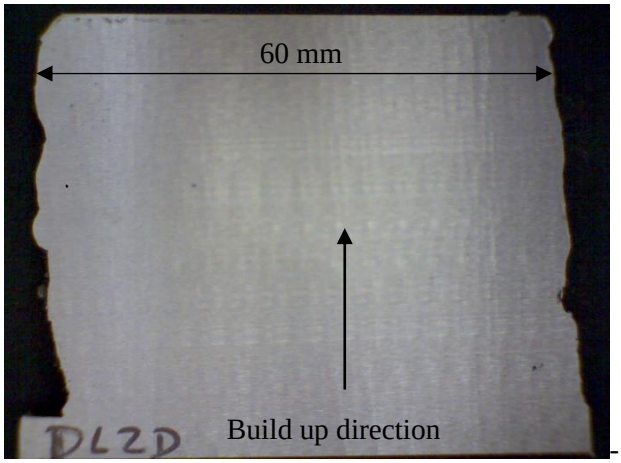


As explained in §3.5, sample A was not deposited using an enhanced strategy of deposition, as detailed at Table 3.7, unlike other samples. The origin to the pores in sample A was not the lack of overlap between infill and perimeter welding beads since it only showed one line of pores instead of four lines. This concludes that the absence of a deposition strategy results in lack of filling on three-dimension parts.

Sample C displayed three lines of pores in the infill-perimeter intersection zone. This could be due to the lower values of overlap between these two sections. In Sample C, the distance between the infill and the perimeter welding beads is 0.854 $w$ which is the highest value in this experiment. If this was the cause, the slices face would have displayed four lines of pores which indicates that the deposition strategy was not optimized to this overlap values. Although the other samples with a deposition strategy applied did not result in pores, it does not imply that it would fill the gaps completely, using the overlap of sample C. The overlap may compensate some of the gaps created by an inappropriate deposition strategy, and since sample C did have less overlap than the other samples, the results are conclusive.

Table 4.4 - Number of times that the infill welding bead started on each point, for all the printed samples.

| Sample Identification | Point 1 | Point 2 | Point 3 | Point 4 | Total of points |
|---|---|---|---|---|---|
| A | 10 | 8 | 5 | 0 | 23 |
| B | 7 | 5 | 10 | 0 | 22 |
| C | 6 | 3 | 17 | 0 | 26 |
| D | 11 | 7 | 0 | 8 | 26 |

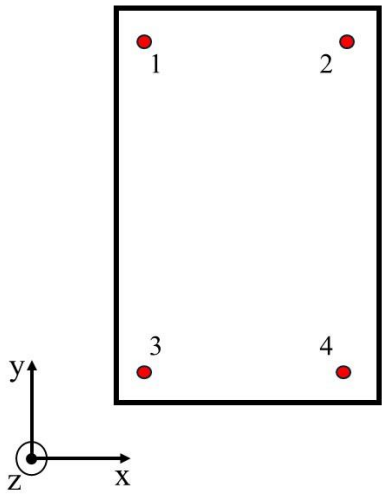


Figure 4.4 - Representative image of the starting points of deposition of the infill beads.

### 4.3.2 Uniaxial Tensile Tests

Before the uniaxial tensile tests were performed, all 16 specimens underwent an x-ray test to identify potential internal or superficial defects. The tests, combined with a visual inspection, indicate that none of the specimens exhibited macroscopic defects before the uniaxial tensile testing. Figure 4.5 shows a representative x-ray result for all the specimens.

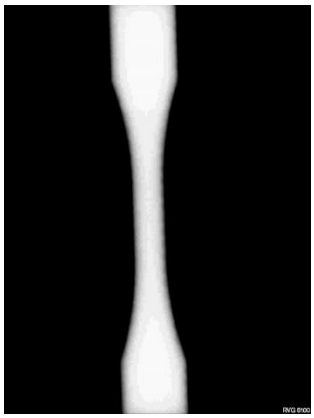

Figure 4.5 - X-ray result of a uniaxial tensile specimen.

All the specimens fractured in the central region, as illustrated in Figure 4.6. In this figure it is also possible to observe the identification of these 16 specimens as explained in §3.6.

Both the ultimate Tensile Strength and Elongation were calculated for each test and are presented in Figure 4.7 a) and Figure 4.8 a). The stress-strain curves of the uniaxial tensile specimen C1 is representative of the overall of the curves and is presented in Figure 4.9. The graphics of the remaining 15 uniaxial tensile specimens are presented in Appendix 6 along with Table A. 2 and Table A. 3 that presents the UTS of each specimen and its elongation to fracture. The average UTS and elongation to fracture of each specimen group are shown in Figure 4.7 b) and Figure 4.8 b).

Figure 4.6 - Uniaxial tensile specimens after testing.

Comparing the UTS and the elongation to fracture of the technical specified in , none of the specimens reach the 538 MPa of UTS with the highest value of 500 MPa in the specimen C1 and the lowest value of 489 MPa in the specimens D2 and D3. The maximum difference of UTS of the specimens were 11 MPa which is not significant. The group of specimens C had the maximum average value of UTS with 496 MPa, although it was not significantly greater than the rest of the group of specimens. All the samples presented similar values to each other and the average UTS of all the specimens was 494 MPa which represents 92 % of the technical specified in [42].

Considering the elongation to fracture, the results did surpass the technical specified of 24 % reaching a maximum value of 26.8 % of specimen B4. And the lowest value being 21.8 % from specimen C4.

a)

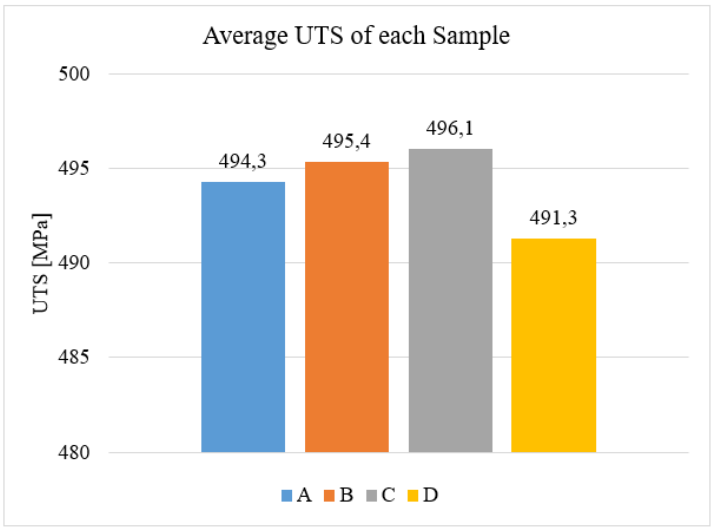


b)

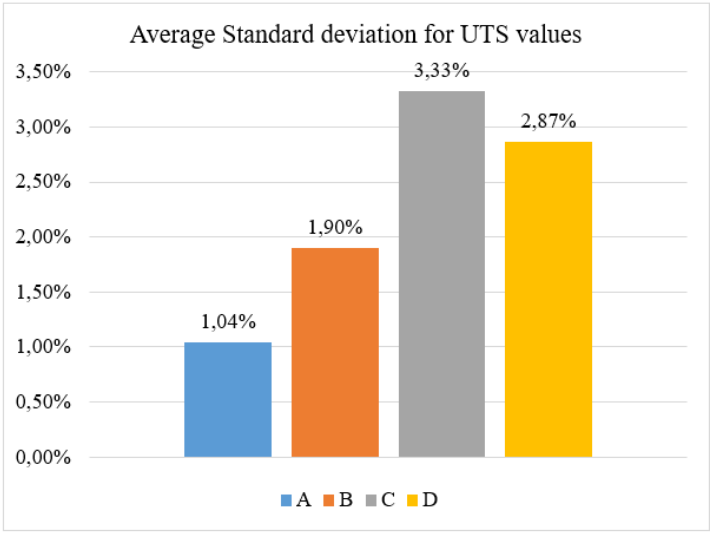


Figure 4.7 - UTS results of the Uniaxial tensile test.

a)

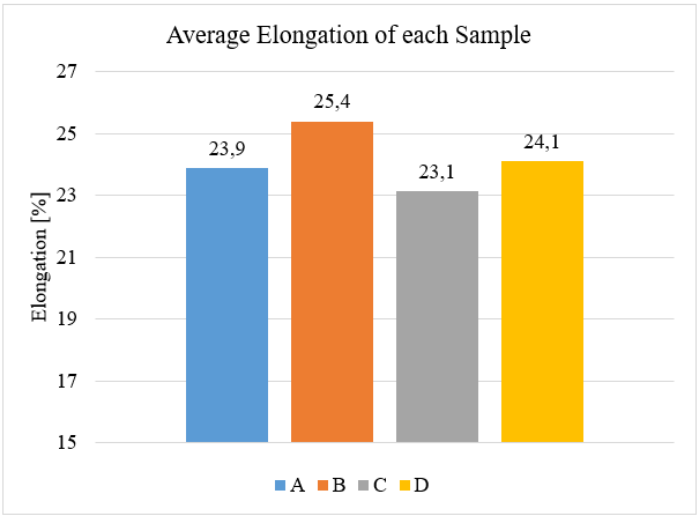


b)

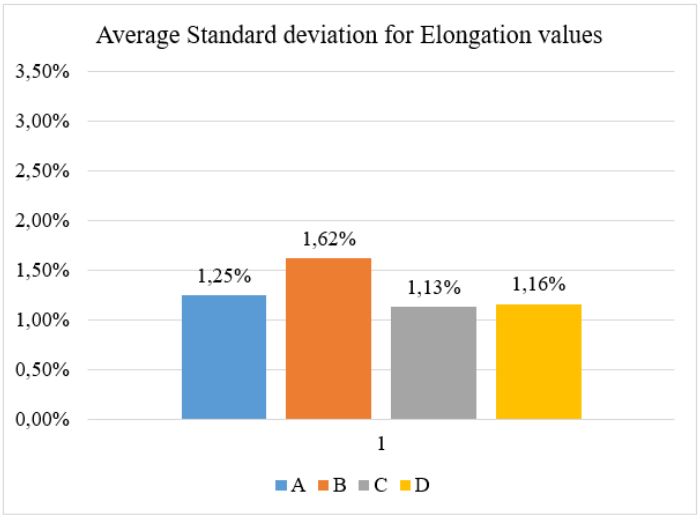


Figure 4.8 - Elongation results of the Uniaxial tensile test.

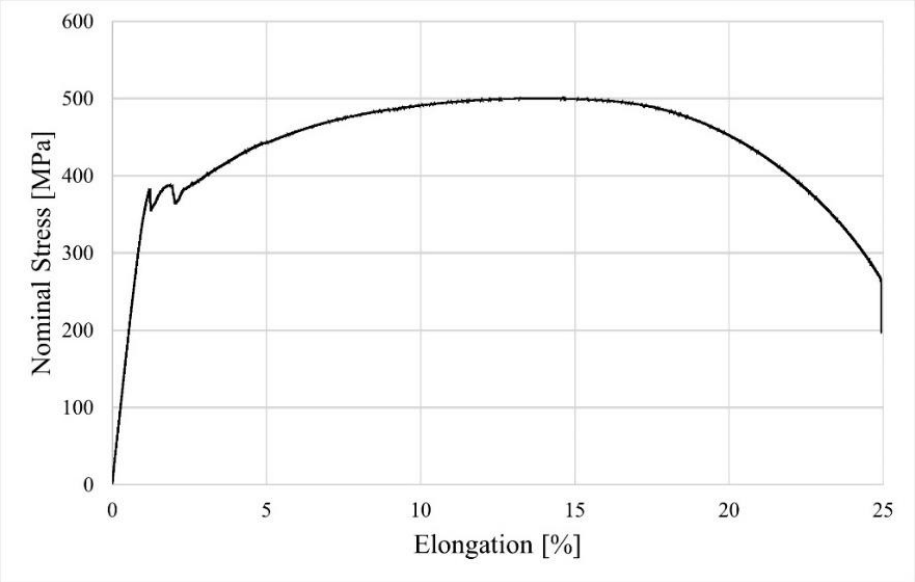


Figure 4.9 - Stress-strain curve of specimen C1.

### 4.3.3 Microhardness

The results presented in Figure 4.10 to Figure 4.13 are the microhardness values of each of four vertical columns per sample, from the column L0-1.5 mm to the column L0+1.5 mm, as explained in Figure 3.7. The figures also illustrate the tendency line of the microhardness in its distance. The mean values for all the points of the samples A,B,C and D are 188.8 HV, 183.7 HV, 181.9 HV and 186.7 HV, respectively. Its standard deviation are 14.3 HV, 21.5 HV, 8.9 HV and 11.3 HV, respectively. In Appendix 7 it is possible to observe the Vickers hardness of each sample displayed in heatmap graphics.

The maximum value of hardness registered in an indentation was 230 HV of sample A and the lowest value of was 74.5 HV of sample D. The samples did not reach the previous calculated maximum value of hardness of 277 HV, using (3.1). However, sample A had a mean value of 188.8 HV which represents 68 % of the calculated maximum.

All the samples presented similar values to each other, however, samples A and D reveal greater hardness in comparison to the others and lower values of standard deviation.

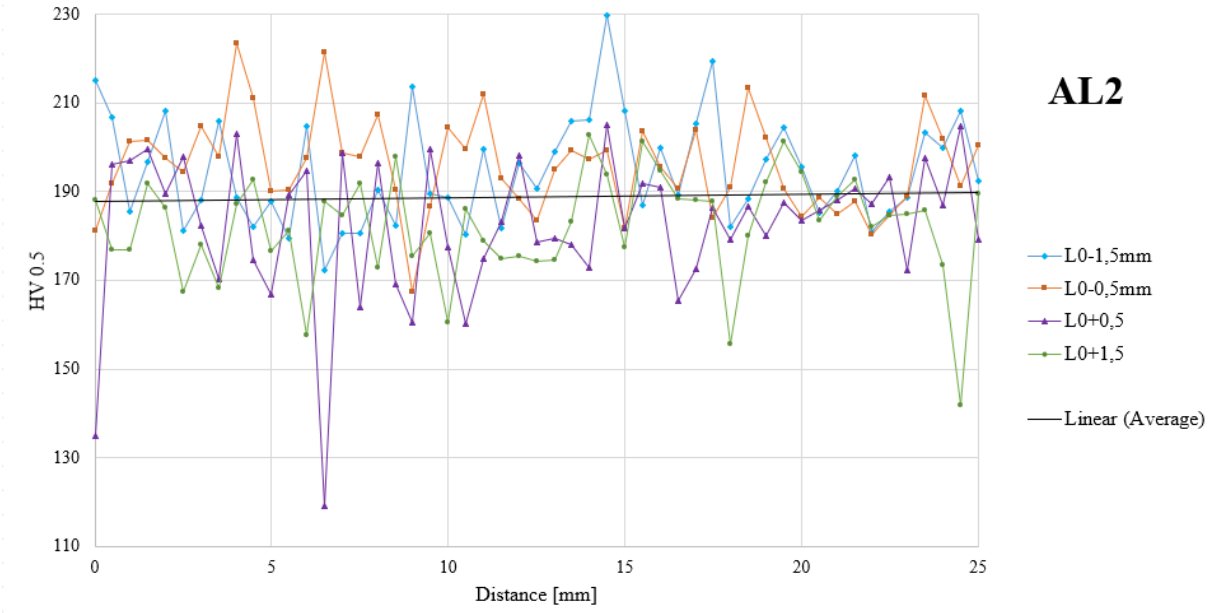


Figure 4.10 - Microhardness results for sample A, slice AL2.

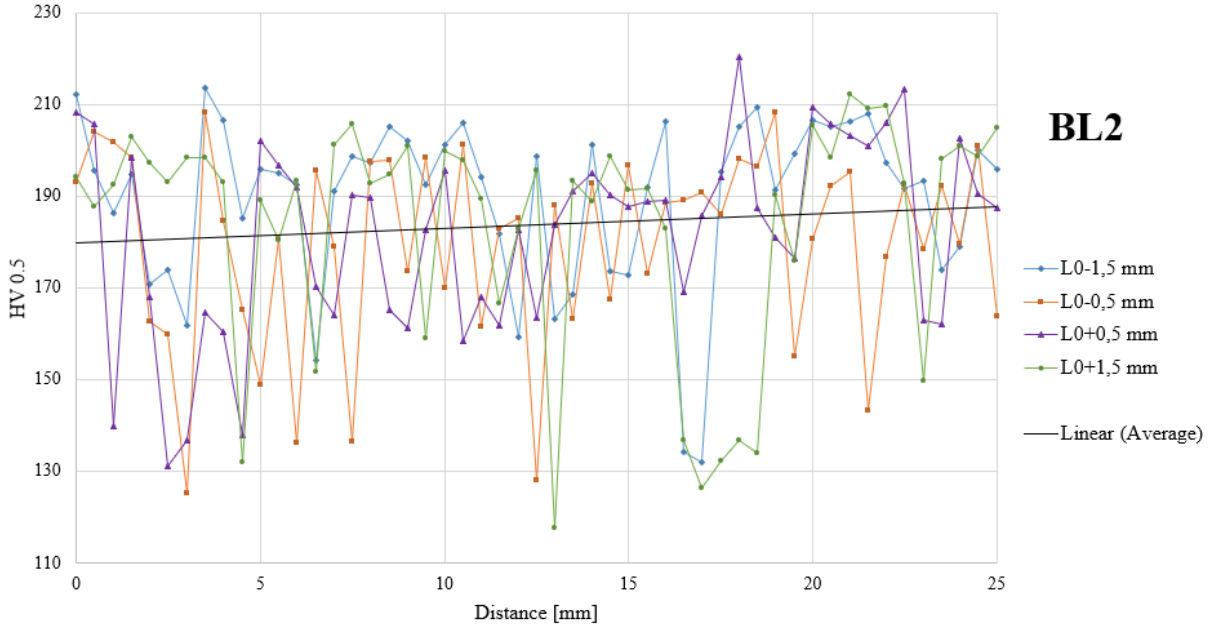


Figure 4.11 - Microhardness results for sample B, slice BL2.

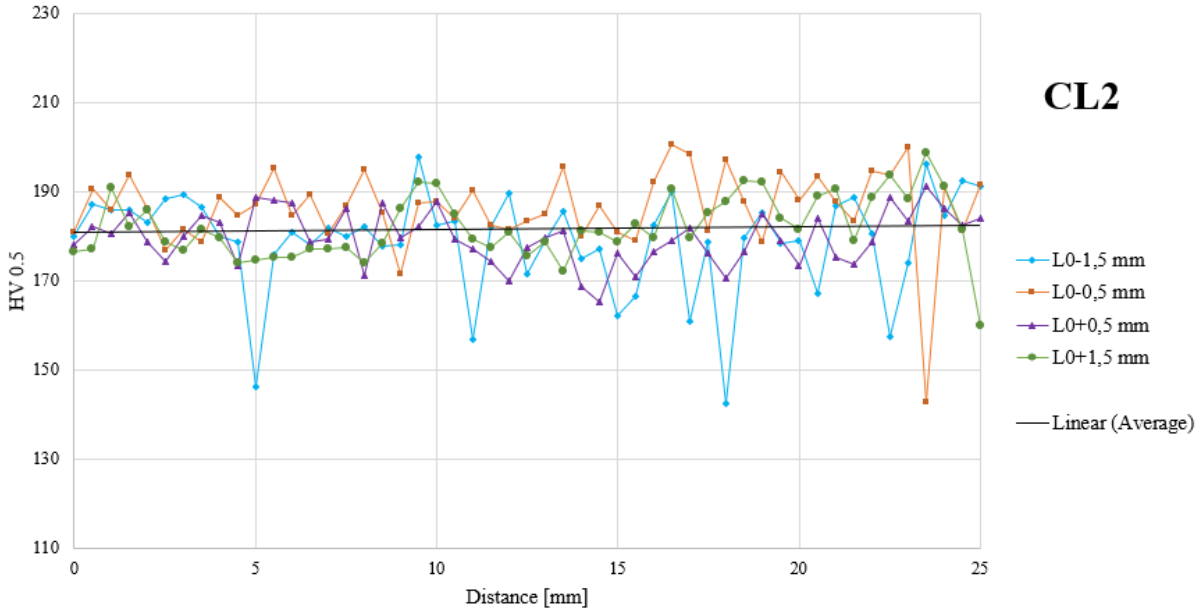


Figure 4.12 - Microhardness results for sample C, slice CL2.

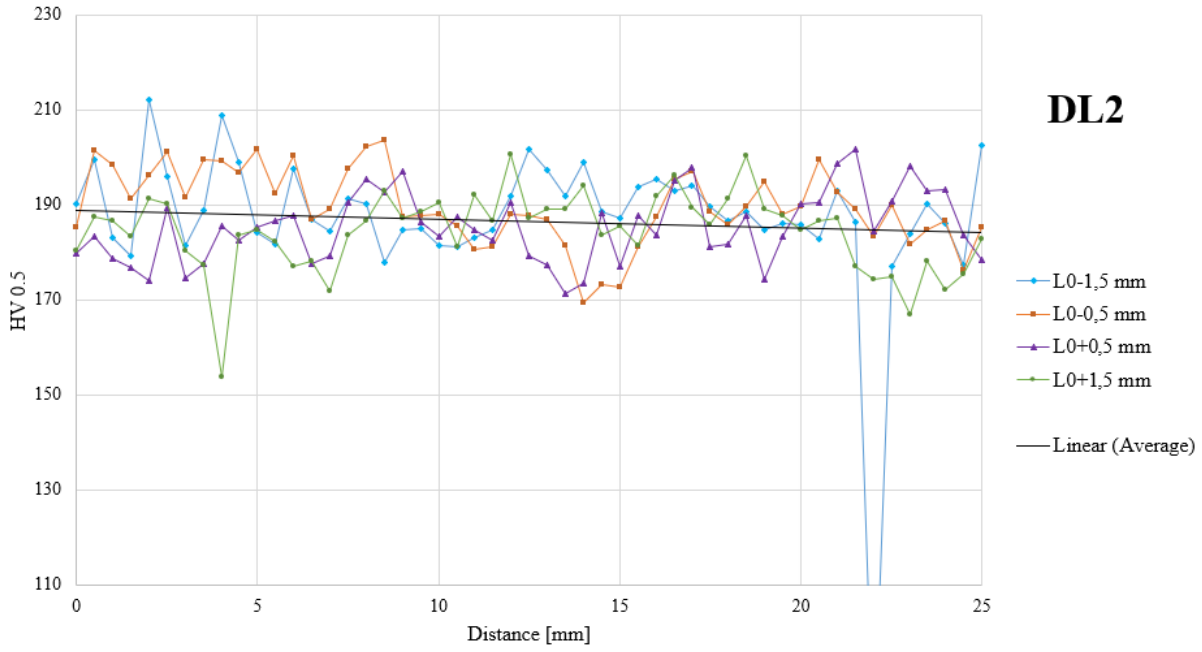


Figure 4.13 - Microhardness results for sample D, slice DL2.

## 4.4 Part produced by DED-arc

The outcome from the DED-arc operation to produce the part can be seen in Figure 4.14 and its undesired phenomena in Figure 4.15. As previously detailed in §3.7.2, some pores were present in the final deposited layers. These could result from the welding coil being almost out of wire, and the wire left being unclean. Which would restrict the wire feed and lead to the formation of pores. It could also be due to the welding torch being clogged but the pores continued to appear after its cleaning.

After the deposition, the part went through cutting operations and was successfully produced, nevertheless, some minor flaws were observed. Figure 4.16 shows the final result of the machined part.

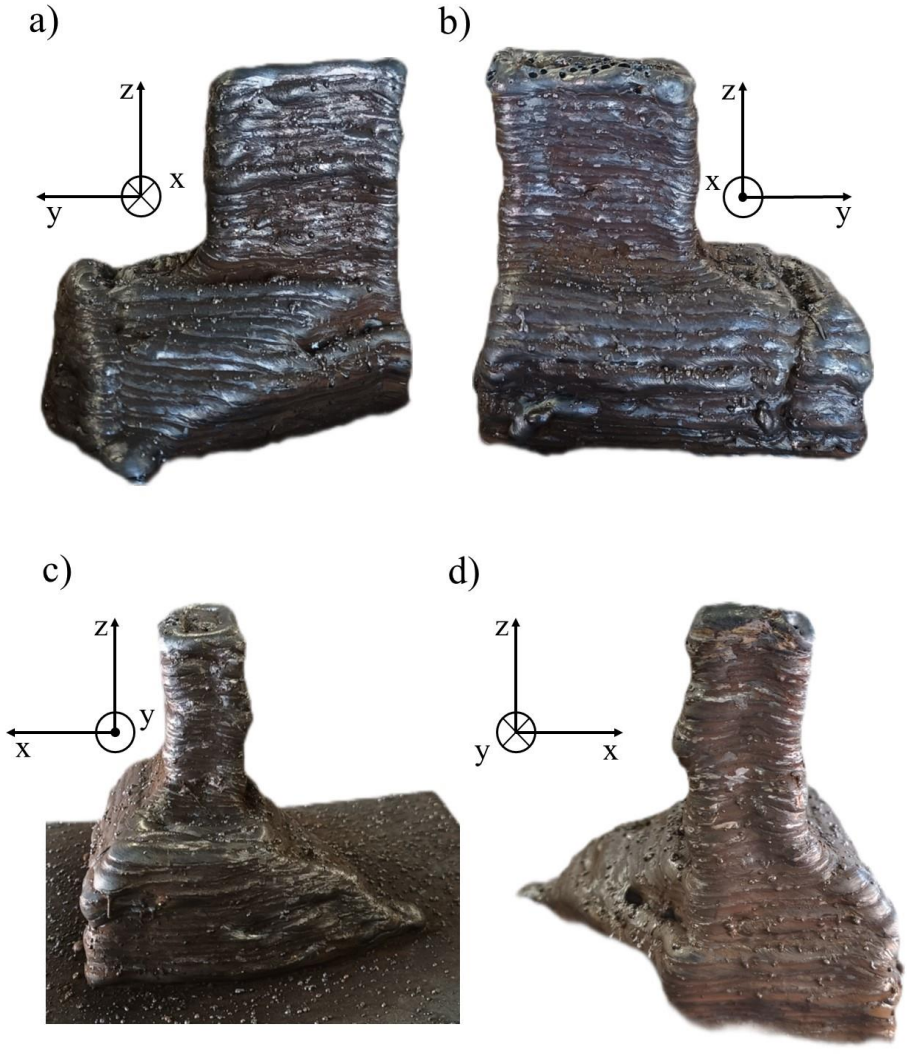


Figure 4.14 - Part after being deposited by DED-arc and its different perspectives.

As explained in §3.7, the deposited volume of the part was scaled 1.2 times the required volume to compensate for distortions and minor deviations in the X-axis. However, during the deposition of the rectangular section of the part, there was a greater deviation than predicted in the X-axis, which led to the scale not being enough to compensate for distortions. This resulted in the side region of the rectangular section of the part not being completely machined because there was not enough material. This feature of the part can be seen in Figure 4.17.

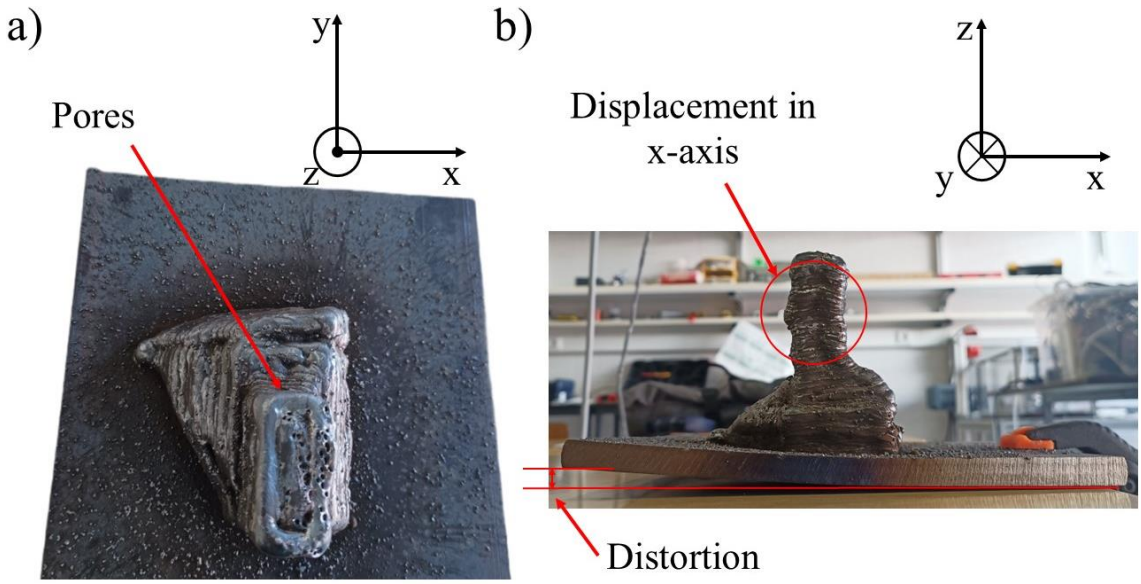


Figure 4.15 – Undesired phenomena of the part after DED-arc process.

The machined part also presented some minor pores as it can be seen in Figure 4.17. These pores could be due to using non-optimized welding parameters for curved features. However, sample D of the overlap model testing did not present any pores, the deposition of this sample did not involve curved features.

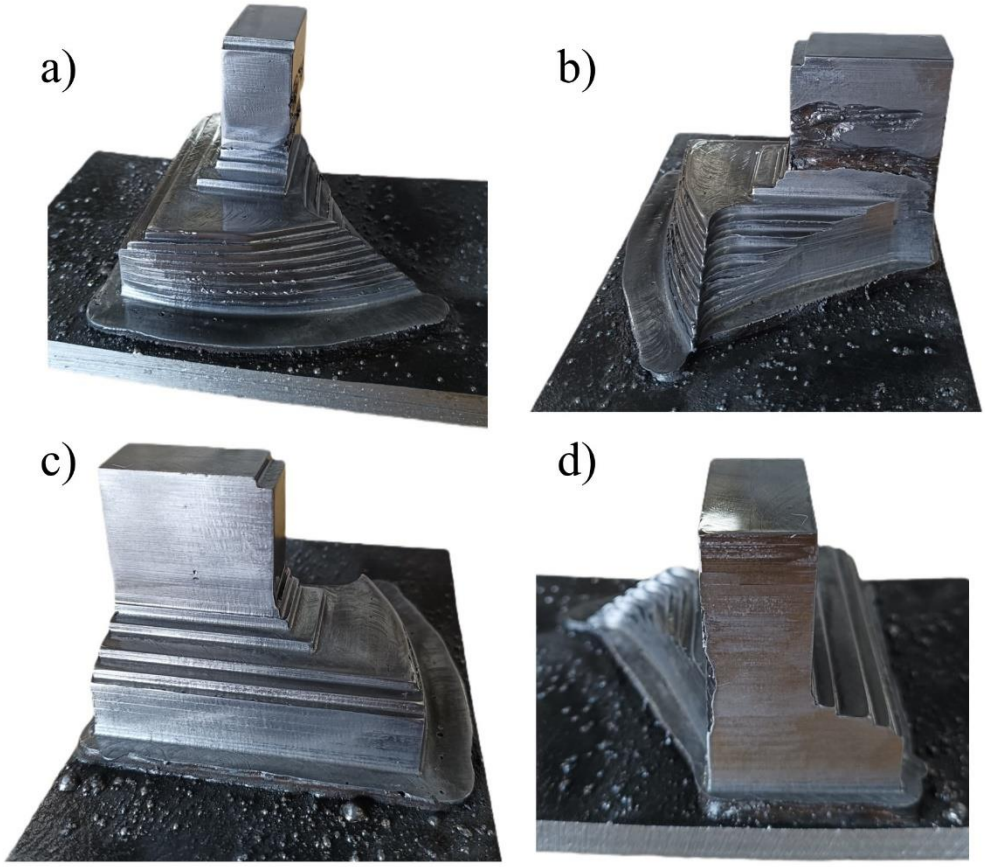


Figure 4.16 - Different perspectives of the machined part.

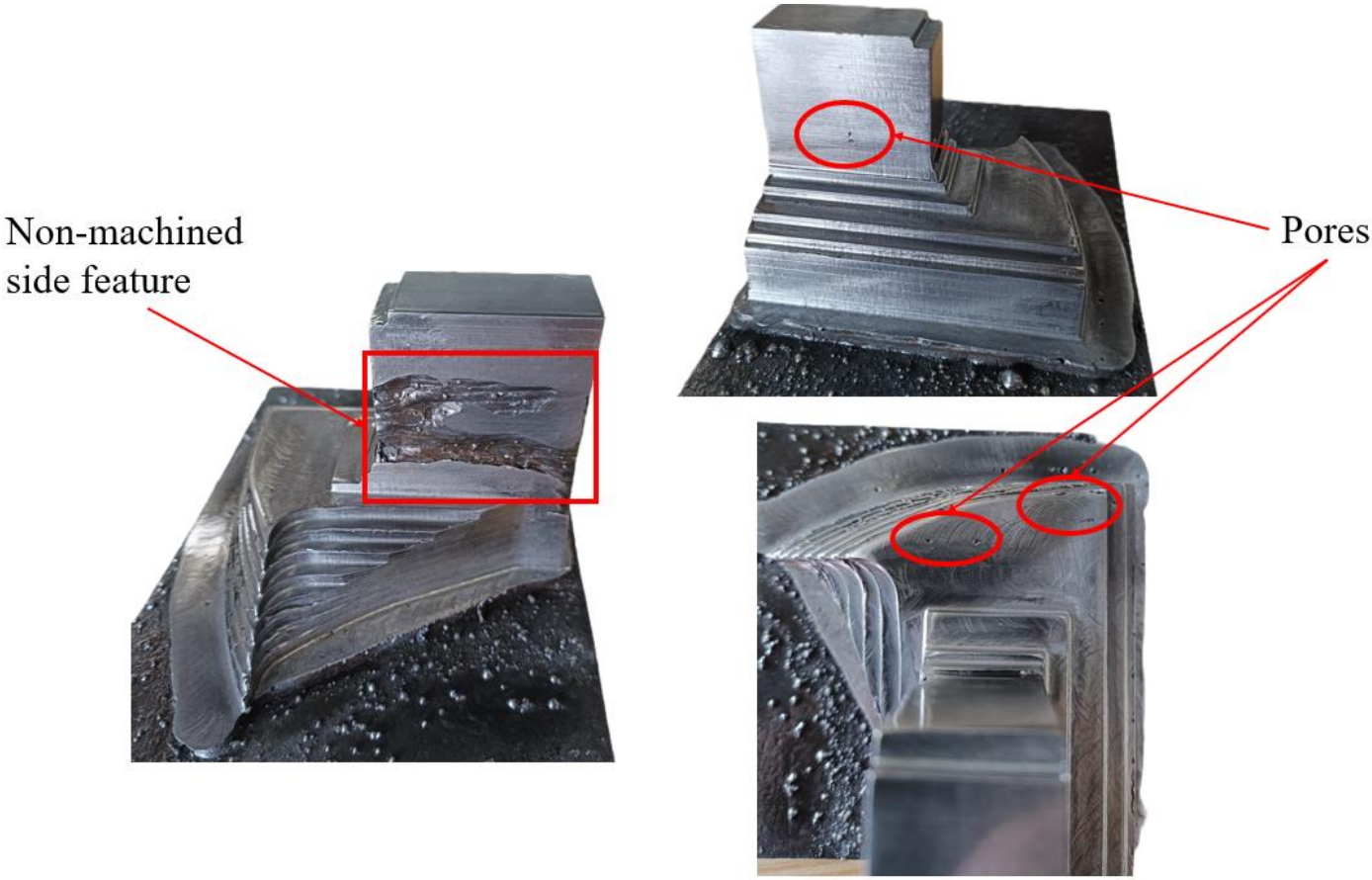


Figure 4.17 - Imperfections detected by visual inspection of the machined part.

# 5

# CONCLUSION AND FUTURE WORK

Various deposition strategies and overlap values for DED-arc were tested and validated in this study. In addition, a practical model for producing a part by DED-arc using an open-source slicer was developed and tested, specifically for the fabrication of a part with application in the automotive industry. Based in this study, the following can be concluded:

1. The welding parameters used to deposit the material ER70S-6, specified in Table 3.4, are applicable;
2. Deposition strategy 5 (Table 3.7), combined with the overlap values of Samples B ( $\frac{D_{i/i}}{w} = 0.7941$ and $\frac{D_{i/p}}{w} = 0.8038$ ) and D ( $\frac{D_{i/i}}{w} = 0.7364$ and $\frac{D_{i/p}}{w} = 0.7227$ ) is suitable for fabricating non-defective parts using DED-arc;
3. The adapted uniaxial tensile specimen used in this work is appropriate for tensile tests.
4. Prusa slicer is a suitable tool for generating G-codes for the production of parts by DED-arc with simple features (linear welding beads);
5. $\frac{D_{i/i}}{w}$ values of 0.7115, 0.8038, 0.7687 and 0.7364 are effective for achieving proper infill of the parts;
6. Sample C present the highest average value of UTS with 496.1 MPa which represents 92.2 % of the technical specifications. Sample A present highest average values of 188.8 HV, which represents 68 % of the maximum calculated hardness. Sample B presented the highest average values of nominal elongation in rupture of 25.4 %, which surpassed the 24 % of the technical specifications;
7. The application of a scale of 1.2 times is not sufficient, for the dimensions of the required part, to compensate for distortions and minor deviations in the X-axis of the machine.

Subsequently to promising results in this study, to introduce DED-arc in the automotive industry there are still future research and work to be conducted:

1. Develop an optimized deposition strategy for the DED-arc machine and the suggested material of application ER 630;
2. Adapt the original python file to implement automatically the enhanced deposition strategy.
3. Machine the part to approximate even further its geometry of the part to the required part. To achieve this, the use of a helical end mill or a 5 axis CNC machine may be required.
4. Develop deposition strategies for curved features using the Prusa slicer or an automatic model;
5. Make an economic model to determine the minimum material volume which producing parts by DED-arc becomes more cost-effective compared to apply cutting operations from a solid block to produce a part.

# BIBLIOGRAPHY


[1] ISO/ASTM 52900:2021(en), Additive manufacturing — General principles — Fundamentals and vocabulary 2021.

[2] Baker R. Method of making decorative articles, 1925.

[3] McAndrew AR, Alvarez Rosales M, Colegrove PA, Hönnige JR, Ho A, Fayolle R, et al. Interpass rolling of Ti-6Al-4V wire + arc additively manufactured features for microstructural refinement. Addit Manuf 2018;21:340–9. https://doi.org/10.1016/j.addma.2018.03.006.

[4] Rodrigues TA, Duarte V, Miranda RM, Santos TG, Oliveira JP. Current status and perspectives on wire and arc additive manufacturing (WAAM). Materials 2019;12. https://doi.org/10.3390/ma12071121.

[5] Rebelo Duarte V. Additive manufacturing of a high resistance steel by MIG/MAG. n.d.

[6] Wu B, Pan Z, Ding D, Cuiuri D, Li H, Xu J, et al. A review of the wire arc additive manufacturing of metals: properties, defects and quality improvement. J Manuf Process 2018;35:127–39. https://doi.org/10.1016/j.jmapro.2018.08.001.

[7] Xiong J, Li Y, Li R, Yin Z. Influences of process parameters on surface roughness of multi-layer single-pass thin-walled parts in GMAW-based additive manufacturing. J Mater Process Technol 2018;252:128–36. https://doi.org/10.1016/j.jmatprotec.2017.09.020.

[8] Lopes JG, Machado CM, Duarte VR, Rodrigues TA, Santos TG, Oliveira JP. Effect of milling parameters on HSLA steel parts produced by Wire and Arc Additive Manufacturing (WAAM). J Manuf Process 2020;59:739–49. https://doi.org/10.1016/j.jmapro.2020.10.007.

[9] Ley FH, Campbell SW, Galloway AM, McPherson NA. Effect of shielding gas parameters on weld metal thermal properties in gas metal arc welding. International Journal of Advanced Manufacturing Technology 2015;80:1213–21. https://doi.org/10.1007/s00170-015-7106-2.

[10] Xu F, Dhokia V, Colegrove P, McAndrew A, Williams S, Henstridge A, et al. Realisation of a multi-sensor framework for process monitoring of the wire arc additive manufacturing in

producing Ti-6Al-4V parts. Int J Comput Integr Manuf 2018;31:785–98. https://doi.org/10.1080/0951192X.2018.1466395.

[11] Tomar B, Shiva S, Nath T. A review on wire arc additive manufacturing: Processing parameters, defects, quality improvement and recent advances. Mater Today Commun 2022;31. https://doi.org/10.1016/j.mtcomm.2022.103739.

[12] Cunningham CR, Flynn JM, Shokrani A, Dhokia V, Newman ST. Invited review article: Strategies and processes for high quality wire arc additive manufacturing. Addit Manuf 2018;22:672–86. https://doi.org/10.1016/j.addma.2018.06.020.

[13] Cong B, Qi Z, Qi B, Sun H, Zhao G, Ding J. A comparative study of additively manufactured thin wall and block structure with Al-6.3%Cu alloy using cold metal transfer process. Applied Sciences (Switzerland) 2017;7. https://doi.org/10.3390/APP7030275.

[14] Machado L, Neto SC. Studying the Application of Additive Manufacturing to Large Parts. 2017.

[15] Duarte VR, Rodrigues TA, Schell N, Miranda RM, Oliveira JP, Santos TG. Hot forging wire and arc additive manufacturing (HF-WAAM). Addit Manuf 2020;35. https://doi.org/10.1016/j.addma.2020.101193.

[16] Sames WJ, List FA, Pannala S, Dehoff RR, Babu SS. The metallurgy and processing science of metal additive manufacturing. International Materials Reviews 2016;61:315–60. https://doi.org/10.1080/09506608.2015.1116649.

[17] TWI. What is hot cracking (solidification cracking). Https://WwwTwi-GlobalCom/Technical-Knowledge/Faqs/Faq-What-Is-Hot-Cracking-Solidification-Cracking 2017.

[18] Sun L, Jiang F, Huang R, Yuan D, Guo C, Wang J. Anisotropic mechanical properties and deformation behavior of low-carbon high-strength steel component fabricated by wire and arc additive manufacturing. Materials Science and Engineering: A 2020;787. https://doi.org/10.1016/j.msea.2020.139514.

[19] Gordon J V., Haden C V., Nied HF, Vinci RP, Harlow DG. Fatigue crack growth anisotropy, texture and residual stress in austenitic steel made by wire and arc additive manufacturing. Materials Science and Engineering: A 2018;724:431–8. https://doi.org/10.1016/j.msea.2018.03.075.

[20] Laghi V, Palermo M, Tonelli L, Gasparini G, Ceschini L, Trombetti T. Tensile properties and microstructural features of 304L austenitic stainless steel produced by wire-and-arc additive manufacturing. International Journal of Advanced Manufacturing Technology 2020;106:3693–705. https://doi.org/10.1007/s00170-019-04868-8.

[21] Singh S, Sharma SK, Rathod DW. A review on process planning strategies and challenges of WAAM. Mater Today Proc, vol. 47, Elsevier Ltd; 2020, p. 6564–75. https://doi.org/10.1016/j.matpr.2021.02.632.

[22] Ding D, Pan Z, Cuiuri D, Li H, Larkin N, Van Duin S. Automatic multi-direction slicing algorithms for wire based additive manufacturing. Robot Comput Integr Manuf 2016;37:139–50. https://doi.org/10.1016/j.rcim.2015.09.002.

[23] Yuan L, Pan Z, Polden J, Ding D, van Duin S, Li H. Integration of a multi-directional wire arc additive manufacturing system with an automated process planning algorithm. J Ind Inf Integr 2022;26. https://doi.org/10.1016/j.jii.2021.100265.

[24] Hu Z, Qin X, Shao T, Liu H. Understanding and overcoming of abnormity at start and end of the weld bead in additive manufacturing with GMAW. International Journal of Advanced Manufacturing Technology 2018;95:2357–68. https://doi.org/10.1007/s00170-017-1392-9.

[25] Wang Z, Zimmer-Chevret S, Léonard F, Abba G. Improvement strategy for the geometric accuracy of bead's beginning and end parts in wire-arc additive manufacturing (WAAM). International Journal of Advanced Manufacturing Technology 2022;118:2139–51. https://doi.org/10.1007/s00170-021-08037-8.

[26] Venturini G, Montevecchi F, Scippa A, Campatelli G. Optimization of WAAM Deposition Patterns for T-crossing Features. Procedia CIRP, vol. 55, Elsevier B.V.; 2016, p. 95–100. https://doi.org/10.1016/j.procir.2016.08.043.

[27] Ding D, Pan Z, Cuiuri D, Li H. A multi-bead overlapping model for robotic wire and arc additive manufacturing (WAAM). Robot Comput Integr Manuf 2015;31:101–10. https://doi.org/10.1016/j.rcim.2014.08.008.

[28] Pant H, Arora A, Gopakumar GS, Chadha U, Saeidi A, Patterson AE. Applications of wire arc additive manufacturing (WAAM) for aerospace component manufacturing. International Journal of Advanced Manufacturing Technology 2023;127:4995–5011. https://doi.org/10.1007/s00170-023-11623-7.

[29] STELIA Aerospace. STELIA Aerospace use WAAM build an airplane fuselage - 3D Printing Industry n.d.

[30] Titanium Tank. Waam3dcom 2020. https://www.waam3d.com/case-studies/titanium-tank (accessed September 26, 2024). 2020.

[31] ARA Nose Cone. Waam3dcom 2020. https://www.waam3d.com/case-studies/ara-nose-cone (accessed September 26, 2024). 2020.

[32] Li J, Cui Q, Pang C, Xu P, Luo W, Li J. Integrated vehicle chassis fabricated by wire and arc additive manufacturing: structure generation, printing radian optimisation, and performance prediction. Virtual Phys Prototyp 2024;19. https://doi.org/10.1080/17452759.2023.2301483.

[33] Josten A, Höfemann & M. Arc-welding based additive manufacturing for body reinforcement in automotive engineering n.d. https://doi.org/10.1007/s40194-020-00959-3/Published.

[34] Cortina M, Arrizubieta JI, Calleja A, Ukar E, Alberdi A. Case study to illustrate the potential of conformal cooling channels for hot stamping dies manufactured using hybrid process of laser metal deposition (LMD) and milling. Metals (Basel) 2018;8. https://doi.org/10.3390/met8020102.

[35] Alimov A, Sviridov A, Sydow B, Jensch F, Härtel S. Additive Manufacturing of Hot-Forming Dies Using Laser Powder Bed Fusion and Wire Arc Direct Energy Deposition Technologies. Metals (Basel) 2023;13. https://doi.org/10.3390/met13111842.

[36] Junker D, Hentschel O, Schramme R, Schmidt M, Merklein M. Performance of hot forging tools built by laser metal deposition of hot work tool steel X37CrMoV5-1. 2017.

[37] Ni M, Qin X, Ji F, Hu Z, Xiong X. Gradient Wire and Arc Additive Remanufacturing of 5CrNiMo Hot Forging Die: Microstructure, Mechanical Properties, and Applications. J Mater Eng Perform 2023. https://doi.org/10.1007/s11665-023-08095-x.

[38] Shen L, Zhou J, Ma X, Lu XZ, Tu JW, Shang X, et al. Microstructure and mechanical properties of hot forging die manufactured by bimetal-layer surfacing technology. J Mater Process Technol 2017;239:147–59. https://doi.org/10.1016/j.jmatprotec.2016.08.020.

[39] Zhang J, Xiao G, Peng J, Yu Y, Zhou J. Path Generation Strategy and Wire Arc Additive Manufacturing of Large Aviation Die with Complex Gradient Structure. Materials 2022;15. https://doi.org/10.3390/ma15176115.

[40] Dardaei Joghan H, Hölker-Jäger R, Komodromos A, Tekkaya AE. Hybrid Additive Manufacturing of Forming Tools. Automotive Innovation 2023;6:311–23. https://doi.org/10.1007/s42154-023-00239-y.

[41] Li R, Kim YS, Tho H Van, Yum YJ, Kim WJ, Yang SY. Additive manufacturing (AM) of piercing punches by the PBF method of metal 3D printing using mold steel powder materials. Journal of Mechanical Science and Technology 2019;33:809–17. https://doi.org/10.1007/s12206-019-0137-0.

[42] Home - Weld Wire. Weld Wire 2022. https://www.weldwire.net/ (accessed September 26, 2024). 2022.

[43] weldwire. ER70S-6 n.d. https://www.weldwire.net/weld_products/ww70s-6/ (accessed March 18, 2024).

[44] Bhadeshia HKDH, Honeycombe SR. 8 - The Heat Treatment of Steels: Hardenability. In: Bhadeshia HKDH, Honeycombe SR, editors. Steels (Third Edition). Third Edition, Oxford: Butterworth-Heinemann; 2006, p. 167–81. https://doi.org/https://doi.org/10.1016/B978-075068084-4/50010-8.

[45] ASTM. Standard Test Methods for Tension Testing of Metallic Materials [Metric] n.d.

[46] ASTM. Standard Test Methods for Vickers Hardness and Knoop Hardness of Metallic Materials 1 n.d. https://doi.org/10.1520/E0092-17.-17.

[47] Qi Z, Qi B, Cong B, Sun H, Zhao G, Ding J. Microstructure and mechanical properties of wire + arc additively manufactured 2024 aluminum alloy components: As-deposited and post heat-treated. J Manuf Process 2019;40:27–36. https://doi.org/10.1016/j.jmapro.2019.03.003.

[48] Arana M, Ukar E, Rodriguez I, Aguilar D, Álvarez P. Influence of deposition strategy and heat treatment on mechanical properties and microstructure of 2319 aluminium WAAM components. Mater Des 2022;221. https://doi.org/10.1016/j.matdes.2022.110974.

[49] Rodrigues TA, Escobar JD, Shen J, Duarte VR, Ribamar GG, Avila JA, et al. Effect of heat treatments on 316 stainless steel parts fabricated by wire and arc additive manufacturing: Microstructure and synchrotron X-ray diffraction analysis. Addit Manuf 2021;48. https://doi.org/10.1016/j.addma.2021.102428.

[50] Bermingham MJ, Nicastro L, Kent D, Chen Y, Dargusch MS. Optimising the mechanical properties of Ti-6Al-4V components produced by wire + arc additive manufacturing with post-process heat treatments. J Alloys Compd 2018;753:247–55. https://doi.org/10.1016/j.jallcom.2018.04.158.

[51] Kindermann RM, Roy MJ, Morana R, Prangnell PB. Process response of Inconel 718 to wire + arc additive manufacturing with cold metal transfer. Mater Des 2020;195. https://doi.org/10.1016/j.matdes.2020.109031.

# ANNEX

## ANNEX 1
## TABLE OF HEAT TREATMENTS

Table A.1 - Summary of heat treatments for DED-arc parts made of different materials

| Material | Wire feedstock | Process | Heat Treatment | Microstructural Effects | UTS [MPa] | Reference |
|---|---|---|---|---|---|---|
| Aluminium Alloy | ER2319 + ER5087 | GTAW | Heated from 30°C to 498°C by the rate of 300°C/h and kept for 90min, then quenched in cold water. Followed by Natural aging at room temperature for 48h. | Equiaxed non-dendrites and belt-like columnar non-dendrites (CND) | 458 | [47] |
| Aluminium Alloy | ER2319 | CMT based WAAM | Aging at 190 ºC temperature and 26h | Low anisotropy | 445 | [48] |
| Stainless steel | ER 316LSi | GMAW | Solution treated at 1050 ºC for 2h | Efficient dissolution of δ-ferrite dendrites and compositional redistribution into the austenitic matrix | - | [49] |
| Stainless Steel | ER 316LSi | GMAW | Solution treated at 1200 ºC for 1h | Efficient dissolution of δ-ferrite dendrites and compositional redistribution into the austenitic matrix | - | [49] |
| Titanium Alloy | Ti-6Al-4V | - | Stress relief at 753 ºC for 2 h | - | 872 | [50] |

| | | | | | | |
|---|---|---|---|---|---|---|
| Titanium Alloy | Ti-6Al-4V | - | Vacuum annealing at 1200 K for 2 h dwell with 5 K/min$^{-1}$ heating and cooling rate | - | 810 | [50] |
| Titanium Alloy | Ti-6Al-4V | - | Solution treated at 1240K for 1h, water quenched then aged at 868K for 2h and air cooled | - | 918 | [50] |
| Nickel Alloy | Inconel 718 | CMT based WAAM | Solution treated at 1040 °C for 1 h and aged at 790 ºC for 7h | Reducing micro segregation while presenting a higher dissolution of Laves phase with less formation of δ phase. | - | [51] |

# ANNEX 2
# NC-MILL G9F42050N
# CUTTING PARAMETERS

NC-Mill

G9F42 SERIES

## CARBIDE, 4 FLUTE SHORT **END MILL**



MG HM | 4 | 30° | PLAIN | X-Coating

Unit : mm

| EDP No. | Mill Diameter | Shank Diameter | Length of Cut | Overall Length |
|---|---|---|---|---|
| G9F42010N | 1.0 | 4 | 3 | 50 |
| G9F42020N | 2.0 | 4 | 6 | 50 |
| G9F42030N | 3.0 | 4 | 8 | 50 |
| G9F42040N | 4.0 | 4 | 11 | 50 |
| G9F42050N | 5.0 | 6 | 13 | 50 |
| G9F42060N | 6.0 | 6 | 16 | 50 |
| G9F42080N | 8.0 | 8 | 20 | 60 |
| G9F42100N | 10.0 | 10 | 25 | 75 |
| G9F42120N | 12.0 | 12 | 32 | 75 |
| G9F42140N | 14.0 | 14 | 32 | 75 |
| G9F42160N | 16.0 | 16 | 32 | 75 |
| G9F42200N | 20.0 | 20 | 32 | 100 |

| Mill Dia. Tolerance(mm) | Shank Dia. Tolerance |
|---|---|
| 0<br>- 0.030 | h6 |

## CUTTING CONDITIONS

| MATERIAL | CARBON STEELS ALLOY STEELS TOOL STEELS | | | | ALLOY STEELS PRE-HARDENED STEELS | | | | STAINLESS STEELS | | | | CAST IRON | | | |
|---|---|---|---|---|---|---|---|---|---|---|---|---|---|---|---|---|
| HARDNESS | ~ HRc30 | | | | HRc30 ~ HRc50 | | | | | | | | | | | |
| STRENGTH | ~ 1000N/mm² | | | | 1000 ~ 1500N/mm² | | | | | | | | | | | |
| DIAMETER | RPM | FEED | Vc | fz | RPM | FEED | Vc | fz | RPM | FEED | Vc | fz | RPM | FEED | Vc | fz |
| **1.0** | 19000 | 160 | 60 | 0.002 | 11050 | 90 | 35 | 0.002 | 9350 | 80 | 29 | 0.002 | 20200 | 670 | 63 | 0.008 |
| **2.0** | 10650 | 260 | 67 | 0.006 | 6950 | 155 | 44 | 0.006 | 5800 | 130 | 36 | 0.006 | 10100 | 690 | 63 | 0.017 |
| **3.0** | 8200 | 290 | 77 | 0.009 | 5150 | 185 | 49 | 0.009 | 4250 | 155 | 40 | 0.009 | 6550 | 690 | 62 | 0.026 |
| **4.0** | 6950 | 525 | 87 | 0.019 | 4250 | 325 | 53 | 0.019 | 3550 | 260 | 45 | 0.018 | 4950 | 690 | 62 | 0.035 |
| **5.0** | 5800 | 550 | 91 | 0.024 | 3450 | 330 | 54 | 0.024 | 2900 | 275 | 46 | 0.024 | 3950 | 690 | 62 | 0.044 |
| **6.0** | 5100 | 605 | 96 | 0.030 | 3100 | 380 | 58 | 0.031 | 2600 | 300 | 49 | 0.029 | 3200 | 830 | 60 | 0.065 |
| **8.0** | 3850 | 655 | 97 | 0.043 | 2300 | 350 | 58 | 0.038 | 1950 | 325 | 49 | 0.042 | 2400 | 880 | 60 | 0.092 |
| **10.0** | 2950 | 560 | 93 | 0.047 | 1850 | 275 | 58 | 0.037 | 1500 | 275 | 47 | 0.046 | 2000 | 930 | 63 | 0.116 |
| **12.0** | 2550 | 475 | 96 | 0.047 | 1550 | 230 | 58 | 0.037 | 1250 | 220 | 47 | 0.044 | 1550 | 970 | 58 | 0.156 |
| **14.0** | 2250 | 425 | 99 | 0.047 | 1400 | 210 | 62 | 0.038 | 1150 | 205 | 51 | 0.045 | 1400 | 1020 | 62 | 0.182 |
| **16.0** | 2000 | 380 | 101 | 0.048 | 1250 | 185 | 63 | 0.037 | 1050 | 185 | 53 | 0.044 | 1200 | 1050 | 60 | 0.219 |
| **20.0** | 1550 | 290 | 97 | 0.047 | 950 | 145 | 60 | 0.038 | 750 | 140 | 47 | 0.047 | 950 | 1120 | 60 | 0.295 |

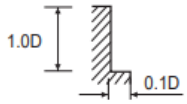


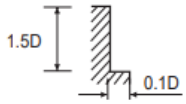


RPM = rev./min.
FEED = mm/min.
Vc = m/min.
fz = mm/t

# ANNEX 3
# NC-MILL G9F42050N
# CUTTING PARAMETERS

**Heavy Duty** Series

## 85510

Frese HEAVY DUTY a quattro taglienti
*Four flute HEAVY DUTY end mills*

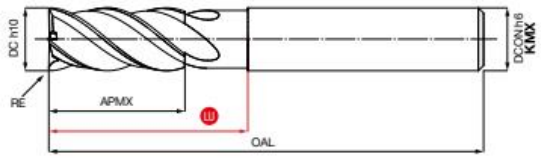


Gamma Raggi
*Radii Range*
**RE:** 0,2 - 0,3 - 0,5 - 1

Skin³ Coating | Quality UDP | H Execution | λ°s 40 Helix | Length

| Cod. Art. | DC h10 | LU | APMX | OAL | RE | DCON h6 | Z |
|---|---|---|---|---|---|---|---|
| 855100300 KMX | 3 | 15 | 11 | 60 | 0,2 | 6 | 4 |
| 855100400 KMX | 4 | 16 | 11 | 60 | 0,2 | 6 | 4 |
| 855100500 KMX | 5 | 18 | 11 | 60 | 0,2 | 6 | 4 |
| 855100600 KMX | 6 | 22 | 13 | 60 | 0,2 | 6 | 4 |
| 855100800 KMX | 8 | 30 | 19 | 72 | 0,3 | 8 | 4 |
| 855101000 KMX | 10 | 32 | 22 | 72 | 0,5 | 10 | 4 |
| 855101200 KMX | 12 | 38 | 26 | 83 | 0,5 | 12 | 4 |
| 855101400 KMX | 14 | 41 | 28 | 83 | 1 | 14 | 4 |
| 855101600 KMX | 16 | 42 | 32 | 92 | 1 | 16 | 4 |
| 855102000 KMX | 20 | 52 | 38 | 104 | 1 | 20 | 4 |
| 855102500 KMX | 25 | 63 | 45 | 125 | 1 | 25 | 4 |

Metodo convenzionale
*Conventional method*

Metodo trocoidale
*Trochoidal method*

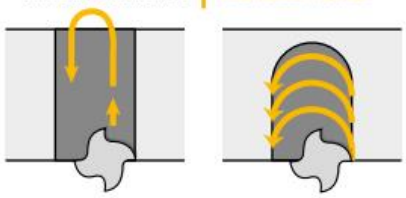

# Parametri di taglio/*Cutting parameters*

| Materiali *Materials* | | Contornatura *Shouldering* ap = 2ø \| ae = 0,5ø | Contornatura *Shouldering* ap = 2ø \| ae = 0,3ø | Contornatura *Shouldering* ap = 2ø \| ae = 0,15ø |
|---|---|---|---|---|
| | **Gruppo e descrizione** *Group and description* | **Vc (m/min.)** | **Vc (m/min.)** | **Vc (m/min.)** |
| Ghisa *Cast Iron* | ● Grigia e sferoidale *Grey and spheroidal* | 150 - 160 | 160 - 170 | 170 - 180 |
| Acciaio *Steel* | Basso contenuto di C *Low Carbon content* | 150 - 160 | 160 - 170 | 170 - 180 |
| | Medio contenuto di C *Medium Carbon content* | 150 - 160 | 160 - 170 | 170 - 180 |
| | ● Basso legato *Low alloy* | 140 - 150 | 150 - 160 | 160 - 170 |
| | Alto legato *High alloy* | 120 - 130 | 130 - 140 | 140 - 150 |
| | Acciaio da stampi e utensili *Tool and die Steel* | 110 - 120 | 120 - 130 | 130 -140 |
| Acciaio Inossidabile *Stainless Steel* | AISI 304 - 416 - 420 | – | 70 - 80 | 80 - 90 |
| | AISI 316 - 440 | – | 60 - 70 | 70 - 80 |
| | 17-4 PH 15-5 PH | – | 50 - 60 | 60 - 70 |
| | ◕ Leghe Cr - Co Cr - Co alloys | – | 40 - 50 | 40 - 50 |
| | Duplex F51 | – | 40 - 50 | 40 - 50 |
| | Super Duplex F55 | – | 25 - 30 | 40 - 50 |
| Acciai Temprati *Hardened Steel* | ● ≤ 54 HRC | – | – | 60 - 70 |
| | ◕ > 54 HRC | | | 40 - 50 |
| Superleghe resistenti al calore *Heat Resistant Super Alloys* | HRSA Hastelloy | – | – | 40 - 50 |
| | ◕ HRSA Inconel 625 | – | – | 40 - 50 |
| | HRSA Inconel 718 | – | – | 40 - 50 |
| | HRSA Nimonic | – | – | 40 - 50 |
| Ti | Titanio *Titanium* | – | – | 60 - 70 |
| | ◕ Leghe di Titanio *Titanium alloys* | – | – | 60 - 70 |

| DC | Avanzamento fz mm/tagliente \| *FEED mm/tooth* | | |
|---|---|---|---|
| 3 | 0,005 | 0,006 | 0,007 |
| 4 | 0,006 | 0,007 | 0,008 |
| 5 | 0,007 | 0,008 | 0,009 |
| 6 | 0,009 | 0,010 | 0,011 |
| 8 | 0,012 | 0,013 | 0,014 |
| 10 | 0,017 | 0,018 | 0,019 |
| 12 | 0,025 | 0,026 | 0,027 |
| 14 | 0,028 | 0,030 | 0,032 |
| 16 | 0,030 | 0,032 | 0,034 |
| 20 | 0,040 | 0,043 | 0,046 |
| 25 | 0,050 | 0,054 | 0,060 |

● consigliata/recommended ◕ accettabile/acceptable ○ non consigliata/not recommended

È consigliato l'utilizzo di un mandrino a forte serraggio e un'elevata rigidità della macchina utensile.
*We suggest the use of a tool holder with heavy duty clamping and elevated machine tool rigidity.*

# APPENDIX

## APPENDIX 1
## PRUSA SLICER SETTINGS FOR DED-ARC

**Print Settings**

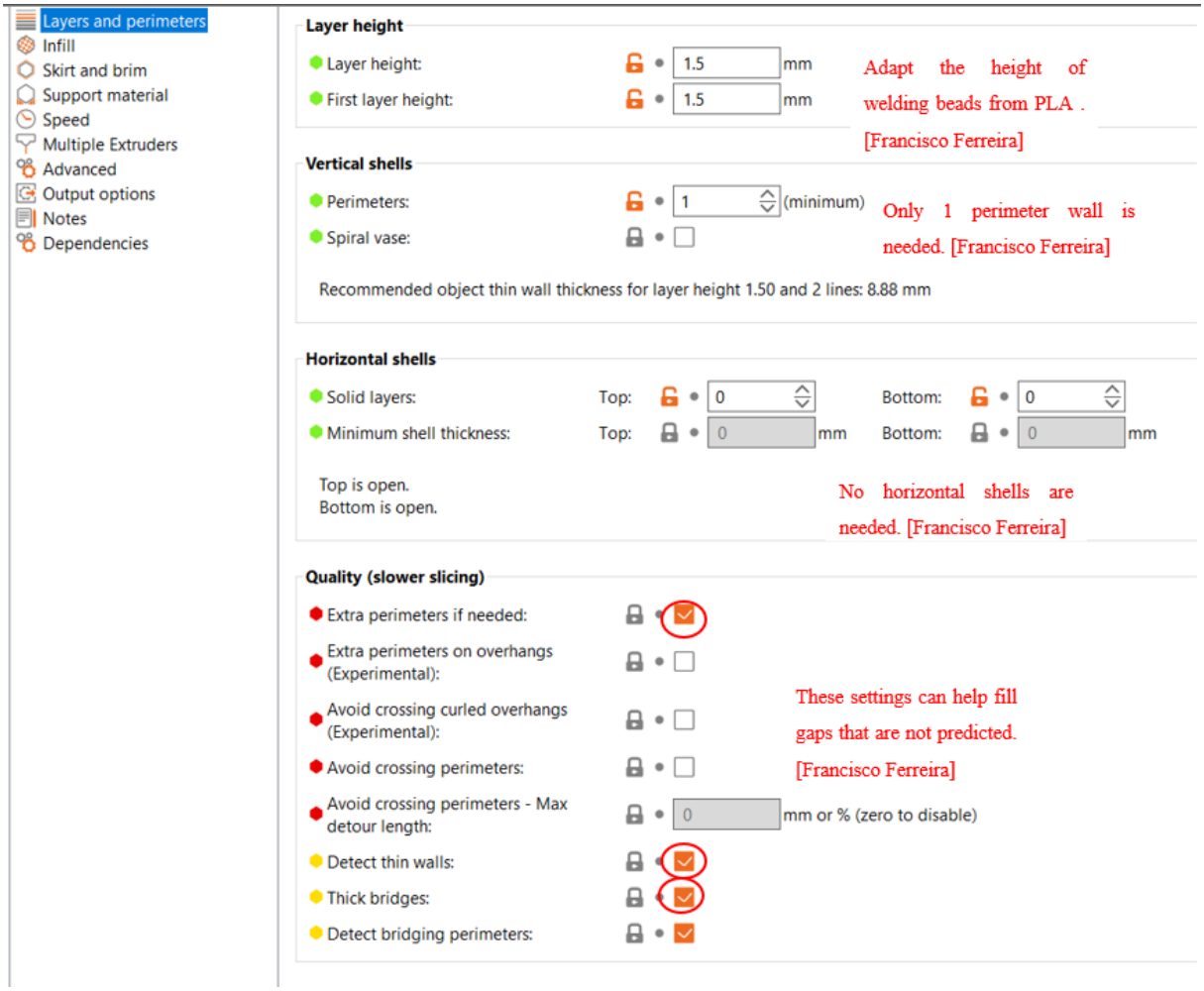

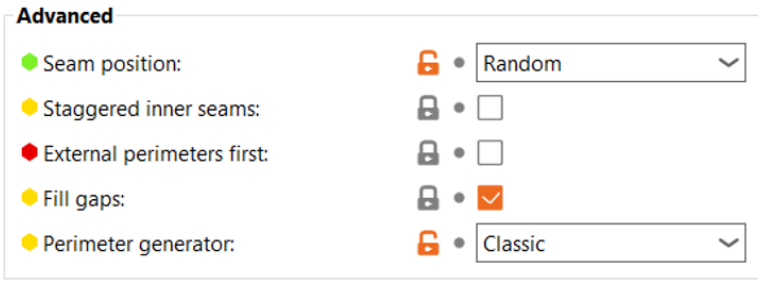


To make the beginning of the welding bead to start in a different point each time. [Francisco Ferreira]

To consider always the same width of the welding bead.

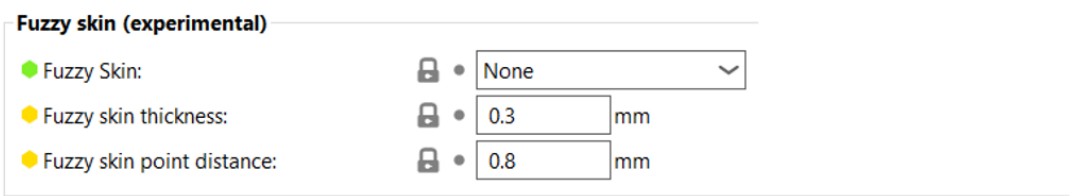


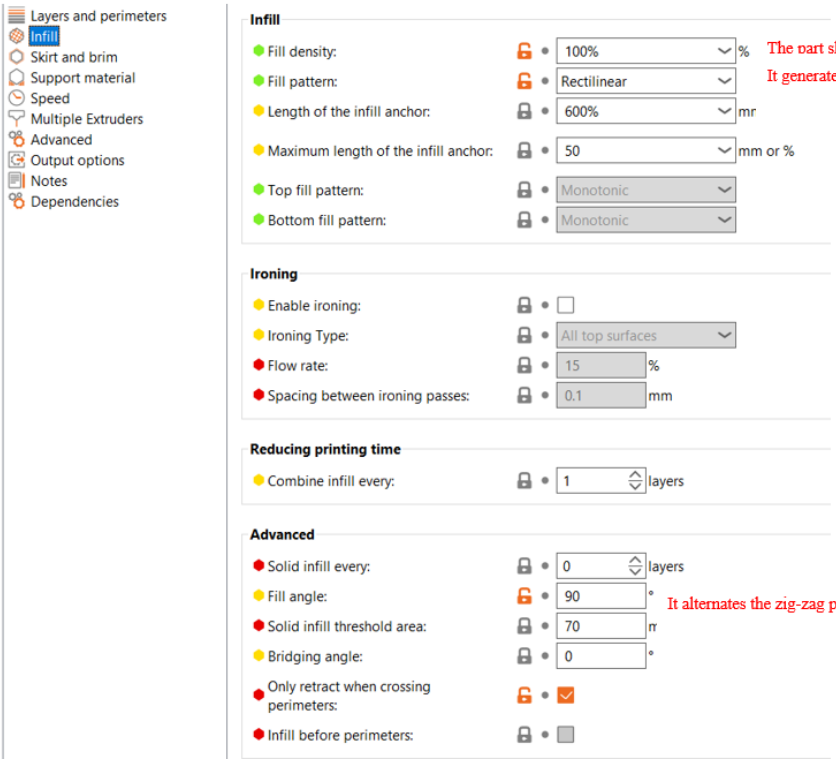


The part should be filled inside [Francisco Ferreira]

It generates a zig-zag strategy in the infill [Francisco Ferreira]

It alternates the zig-zag pattern from horizontal to vertical beads.

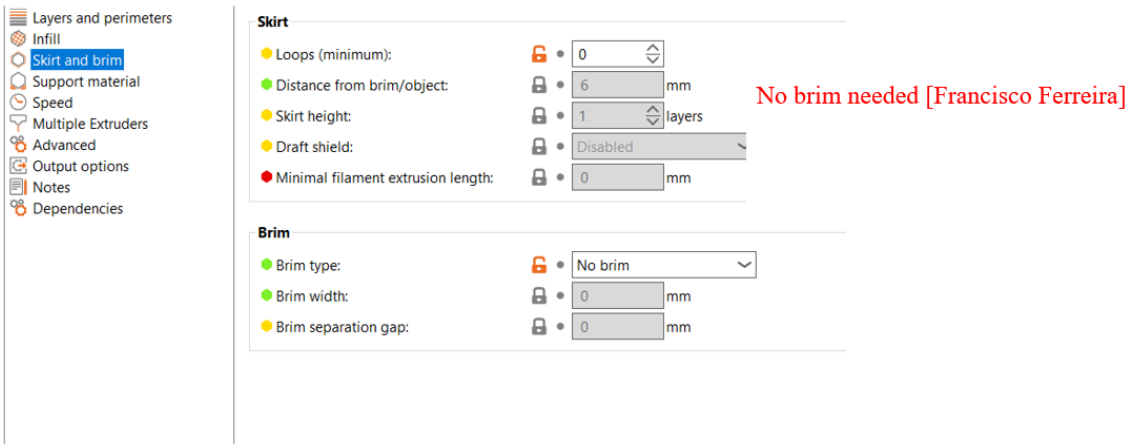
Layers and perimeters
Infill
Skirt and brim
Support material
Speed
Multiple Extruders
Advanced
Output options
Notes
Dependencies
Skirt
Loops (minimum): 0
Distance from brim/object: 6 mm
Skirt height: 1 layers
Draft shield: Disabled
Minimal filament extrusion length: 0 mm
Brim
Brim type: No brim
Brim width: 0 mm
Brim separation gap: 0 mm
No brim needed [Francisco Ferreira]

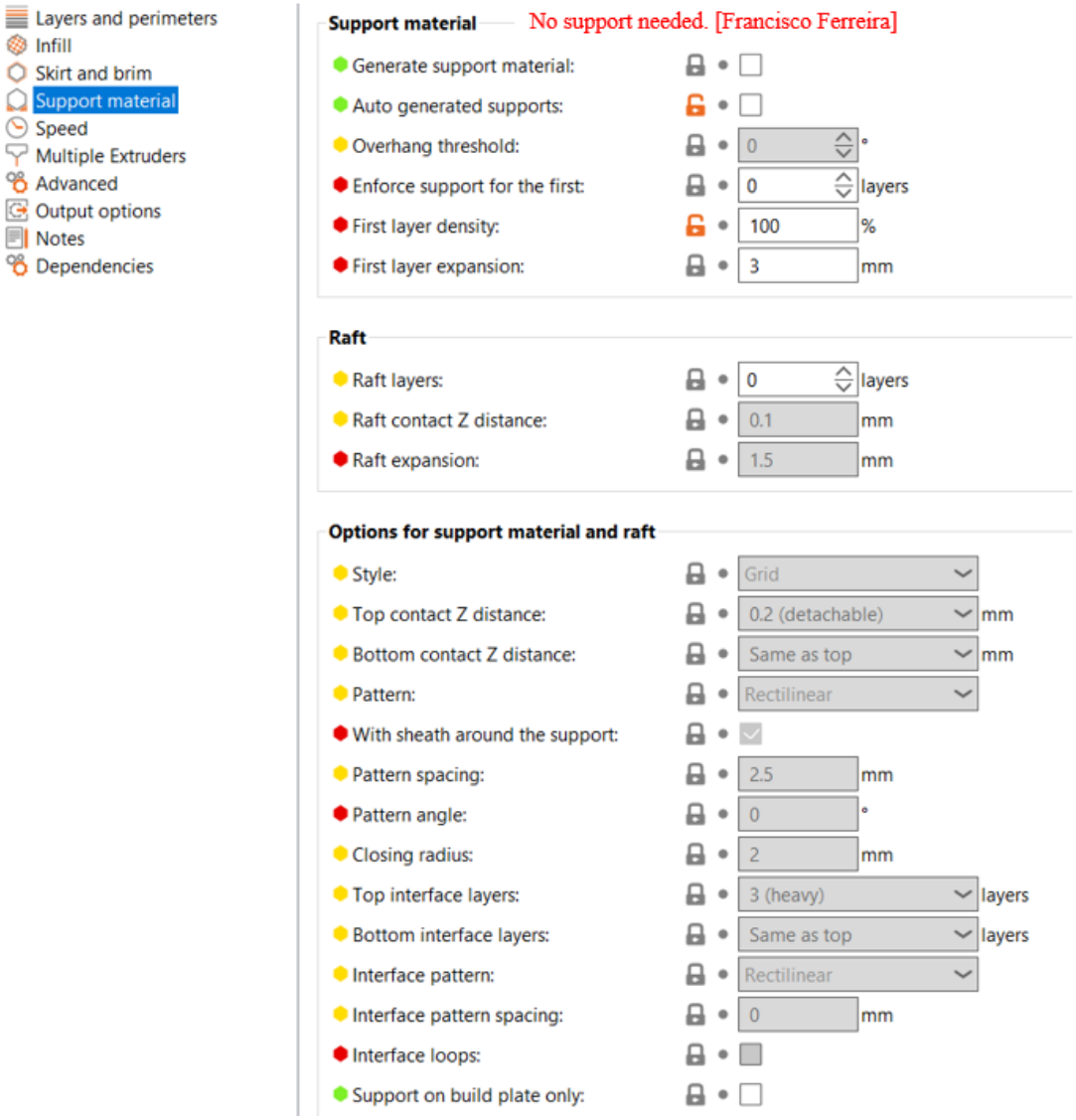
Layers and perimeters
Infill
Skirt and brim
Support material
Speed
Multiple Extruders
Advanced
Output options
Notes
Dependencies
Support material
No support needed. [Francisco Ferreira]
Generate support material:
Auto generated supports:
Overhang threshold: 0 °
Enforce support for the first: 0 layers
First layer density: 100 %
First layer expansion: 3 mm
Raft
Raft layers: 0 layers
Raft contact Z distance: 0.1 mm
Raft expansion: 1.5 mm
Options for support material and raft
Style: Grid
Top contact Z distance: 0.2 (detachable) mm
Bottom contact Z distance: Same as top mm
Pattern: Rectilinear
With sheath around the support:
Pattern spacing: 2.5 mm
Pattern angle: 0 °
Closing radius: 2 mm
Top interface layers: 3 (heavy) layers
Bottom interface layers: Same as top layers
Interface pattern: Rectilinear
Interface pattern spacing: 0 mm
Interface loops:
Support on build plate only:


Travel speed during welding = 400 mm / min = 6,666(6) mm / s

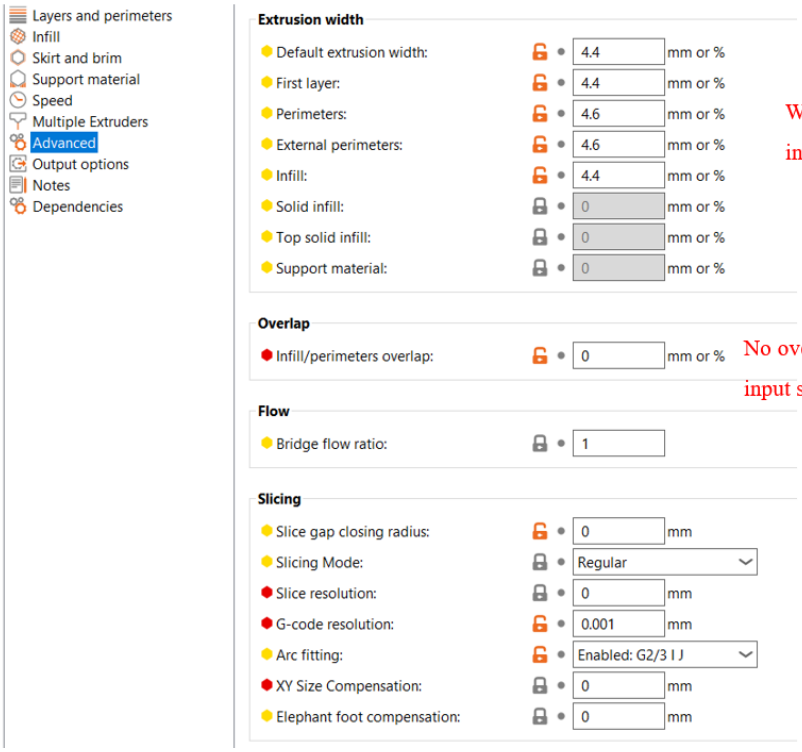


Welding bead width input values for infill and perimeter beads

No overlap was considered in the slicer input settings

## Printer settings


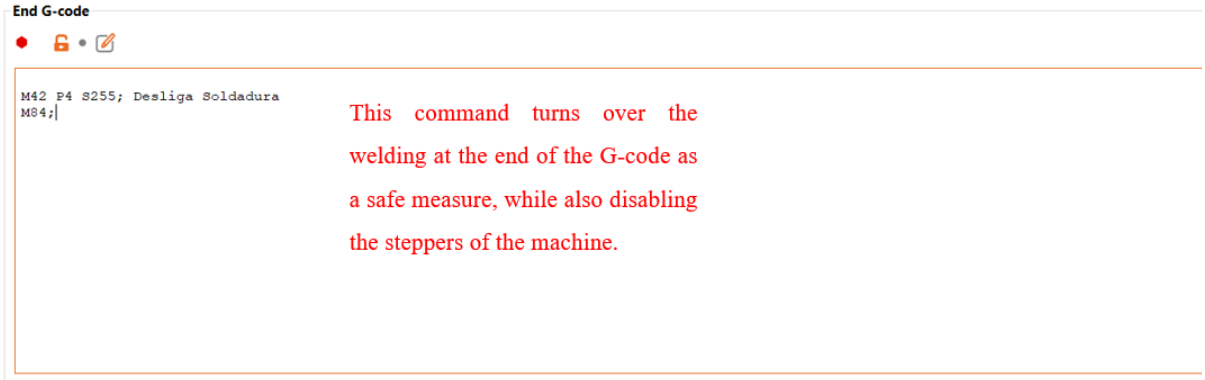


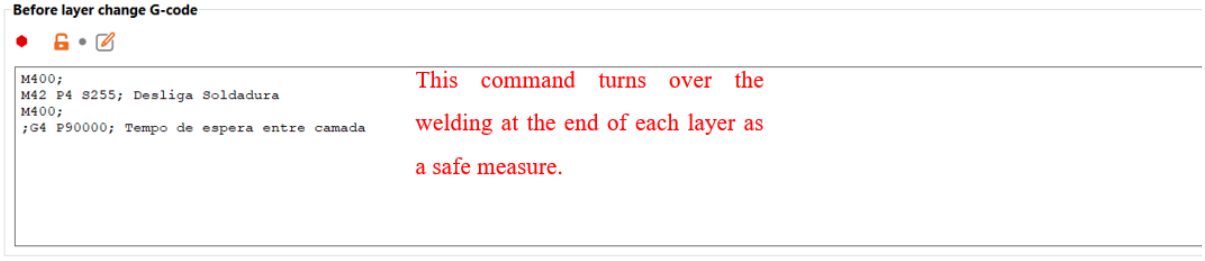


# APPENDIX 2
# PYTHON FILE TO SPLIT G-CODE

```
velocidade_avanço='400'
velocidade_chill='1800'
desvio_x=0
desvio=0.



file = open('g.txt','r')
read = file.readlines()
modified = []
count = 0
ligar = 0
layerx = []
inicios = []
linha=[]



#INSERE NO MODIFIED TODAS AS LINHAS DE CÓDIGO NECESSÁRIAS PARA O GNEW
for line in read:
   if line[0:4]=='G1 X' or line[0:4]=='G2 X' or line[0:4]=='G3 X':
      modified.append('M400\n')
      if line[-6] =='E':
         line = (line[0:-6]+'\n')
      if line[-7] =='E':
         line = (line[0:-7]+'\n')
      if line[-8] =='E':
         line = (line[0:-8]+'\n')
```

```
            if line[-9] =='E':
                line = (line[0:-9]+'\n')


            if line[-10] =='E':
                line = (line[0:-10]+'\n')


            if line[-11] =='E':
                line = (line[0:-11]+'\n')



        modified.append(line)


        if line == 'G1 F'+velocidade_avanço+'\n':
            inicios.append(len(modified))
            modified.extend(['M400;\n','M42 P4 S0; LIGA Soldadura\n','M400;\n'])
            #ligar = ligar +1
        if line[-6:] =="F"+velocidade_chill+"\n":
            modified.insert(-1,'M400;\n')
            modified.insert(-1,'M42 P4 S255; Desliga Soldadura\n')
            modified.insert(-1,'M400;\n')
            #count = count+1
        if line == 'M83 ; use relative distances for extrusion\n':                #TROCAR ENTRE M82
OU M83(DEFAULT)
            modified.pop(-1)
            modified.insert(-1,'M82 ; use absolute distances for extrusion\n')


    #CRIA O GNEW - NOVO GCODE COM OS COMANDOS DE LIGAR E DESLIGAR
SOLDADURA
```

```
gnew = open('gnew.txt','w')
for i in modified:
    if i[0:9]!="M42 P4 S0":         #TIRAR OS LIGAR SOLDADURA
        if i[-6:]=='F1800\n':
            gnew.write(i[0:-6]+'\n')        #TIRAR OS F1800
        else:
            gnew.write(i)
gnew.close()



for i in range(len(inicios)):
    #print(i)
    if i+1<len(inicios):
        layerx.append(modified[inicios[i]:inicios[i+1]])
    else:
        layerx.append(modified[inicios[i]:-1])


ncamadas=len(layerx)


for i in range(ncamadas):
    newlayer = open('layer'+str(i)+'.txt','w')
    newlayer.write(';layer'+str(i)+'\n\n')
    newlayer.write('G21 ; set units to millimeters\n')
    newlayer.write('G90 ; use absolute coordinates\n')
    newlayer.write('M82 ; use absolute distances for extrusion\n')
    newlayer.write('M42 P4 S255; Desliga Soldadura\n\n\n')
    newlayer.write('G1 F'+velocidade_avanço+'\n')

    if i==0:
        newlayer.write(read[21]) #adiciona as primeiras coordenadas que não estavam no código
        newlayer.write(read[22])
        newlayer.write('\n')
```

```
for j in range(len(layerx[i])):
    linha=layerx[i][j]
    finalx=len(linha)-2
    if linha[0:4]=='G1 X':

        for k in range(len(linha)):

            if linha[k]=='Y':
                finalx=k-1

        valorx=float(linha[4:finalx])
        valorx=valorx + desvio_x
        linha=linha[0:4] + str((round(valorx,2))) + linha[finalx:]

    newlayer.write(linha)
desvio_x=desvio_x+desvio
newlayer.close()
```

# APPENDIX 3
# G-CODES USED TO PRINT SAMPLE A

```
;layer0

G21 ; set units to millimeters
G90 ; use absolute coordinates
M82 ; use absolute distances for extrusion
M42 P4 S255; Desliga Soldadura


G1 F400
G1 X32.804 Y2.195 F1800
G1 Z1.8

 M400;
M42 P4 S0; LIGA Soldadura
M400;
M400
G1 X48.9 Y2.195
M400
G1 X48.9 Y59.805
M400
G1 X13.1 Y59.805
M400
G1 X13.1 Y2.195
M400
G1 X32.05 Y2.195
M400
M400;
M42 P4 S255; Desliga Soldadura
M400;
G1 X32.05 Y2.195 F1800
```

```
M400
G1 X44.99 Y57.707
;TYPE:Internal infill
G1 F400

;layer1

G21 ; set units to millimeters
G90 ; use absolute coordinates
M82 ; use absolute distances for extrusion
M42 P4 S255; Desliga Soldadura


G1 F400
M400;
M42 P4 S0; LIGA Soldadura
M400;
M400
G1 X44.99 Y6.009
M400
G1 X41.0 Y6.009
M400
G1 X41.0 Y55.991
M400
G1 X37.0 Y55.991
M400
G1 X37.0 Y6.009
M400
G1 X33.0 Y6.009
M400
G1 X33.0 Y55.991
M400
G1 X29.0 Y55.991
M400
G1 X29.0 Y6.009
```

```
M400
G1 X25.0 Y6.009
M400
G1 X25.0 Y55.991
M400
G1 X21.0 Y55.991
M400
G1 X21.0 Y6.009
M400
G1 X17.01 Y6.009
M400
G1 X17.01 Y57.707
;LAYER_CHANGE
;Z:3.6
;HEIGHT:1.8
M400;
M42 P4 S255; Desliga Soldadura
M400;
;G4 P90000; Tempo de espera entre camada

M400;
M42 P4 S255; Desliga Soldadura
M400;
G1 Z3.6 F1800
M400;

M400
G1 X48.24 Y2.295
G1 Z3.6
;TYPE:External perimeter
;WIDTH:4.4
G1 F400

;layer2
```

G21 ; set units to millimeters
G90 ; use absolute coordinates
M82 ; use absolute distances for extrusion
M42 P4 S255; Desliga Soldadura

G1 F400
M400;
M42 P4 S0; LIGA Soldadura
M400;
M400
G1 X48.8 Y2.295
M400
G1 X48.8 Y59.705
M400
G1 X13.2 Y59.705
M400
G1 X13.2 Y2.295
M400
G1 X47.49 Y2.295
M400
M400;
M42 P4 S255; Desliga Soldadura
M400;
G1 X47.49 Y2.295 F1800
M400
G1 X15.4 Y6.209
;TYPE:Internal infill
;WIDTH:4.2
G1 F400

;layer3

G21 ; set units to millimeters
G90 ; use absolute coordinates

```
M82 ; use absolute distances for extrusion
M42 P4 S255; Desliga Soldadura


G1 F400
M400;
M42 P4 S0; LIGA Soldadura
M400;
M400
G1 X44.89 Y6.209
M400
G1 X44.89 Y10.023
M400
G1 X17.11 Y10.023
M400
G1 X17.11 Y13.837
M400
G1 X44.89 Y13.837
M400
G1 X44.89 Y17.651
M400
G1 X17.11 Y17.651
M400
G1 X17.11 Y21.465
M400
G1 X44.89 Y21.465
M400
G1 X44.89 Y25.279
M400
G1 X17.11 Y25.279
M400
G1 X17.11 Y29.093
M400
G1 X44.89 Y29.093
M400
```

```
G1 X44.89 Y32.907
M400
G1 X17.11 Y32.907
M400
G1 X17.11 Y36.721
M400
G1 X44.89 Y36.721
M400
G1 X44.89 Y40.535
M400
G1 X17.11 Y40.535
M400
G1 X17.11 Y44.349
M400
G1 X44.89 Y44.349
M400
G1 X44.89 Y48.163
M400
G1 X17.11 Y48.163
M400
G1 X17.11 Y51.977
M400
G1 X44.89 Y51.977
M400
G1 X44.89 Y55.791
M400
G1 X15.4 Y55.791
;LAYER_CHANGE
;Z:5.4
;HEIGHT:1.8
M400;
M42 P4 S255; Desliga Soldadura
M400;
;G4 P90000; Tempo de espera entre camada
```

```
M400;
M42 P4 S255; Desliga Soldadura
M400;
G1 Z5.4 F1800
M400;

M400
G1 X21.91 Y59.705
G1 Z5.4
;TYPE:External perimeter
;WIDTH:4.4
G1 F400


;layer4

G21 ; set units to millimeters
G90 ; use absolute coordinates
M82 ; use absolute distances for extrusion
M42 P4 S255; Desliga Soldadura


G1 F400
M400;
M42 P4 S0; LIGA Soldadura
M400;
M400
G1 X13.2 Y59.705
M400
G1 X13.2 Y2.295
M400
G1 X48.8 Y2.295
M400
G1 X48.8 Y59.705
M400
```

G1 X22.66 Y59.705
M400
M400;
M42 P4 S255; Desliga Soldadura
M400;
G1 X22.66 Y59.705 F1800
M400
G1 X17.18 Y57.507
;TYPE:Internal infill
;WIDTH:4.2
G1 F400

;layer5

G21 ; set units to millimeters
G90 ; use absolute coordinates
M82 ; use absolute distances for extrusion
M42 P4 S255; Desliga Soldadura

G1 F400
M400;
M42 P4 S0; LIGA Soldadura
M400;
M400
G1 X17.18 Y6.209
M400
G1 X21.13 Y6.209
M400
G1 X21.13 Y55.791
M400
G1 X25.08 Y55.791
M400
G1 X25.08 Y6.209
M400

G1 X29.03 Y6.209
M400
G1 X29.03 Y55.791
M400
G1 X32.97 Y55.791
M400
G1 X32.97 Y6.209
M400
G1 X36.92 Y6.209
M400
G1 X36.92 Y55.791
M400
G1 X40.87 Y55.791
M400
G1 X40.87 Y6.209
M400
G1 X44.82 Y6.209
M400
G1 X44.82 Y57.507
;LAYER_CHANGE
;Z:7.2
;HEIGHT:1.8
M400;
M42 P4 S255; Desliga Soldadura
M400;
;G4 P90000; Tempo de espera entre camada

M400;
M42 P4 S255; Desliga Soldadura
M400;
G1 Z7.2 F1800
M400;

M400
G1 X41.17 Y59.705

G1 Z7.2
;TYPE:External perimeter
;WIDTH:4.4
G1 F400

;layer6

G21 ; set units to millimeters
G90 ; use absolute coordinates
M82 ; use absolute distances for extrusion
M42 P4 S255; Desliga Soldadura

G1 F400
M400;
M42 P4 S0; LIGA Soldadura
M400;
M400
G1 X13.2 Y59.705
M400
G1 X13.2 Y2.295
M400
G1 X48.8 Y2.295
M400
G1 X48.8 Y59.705
M400
G1 X41.92 Y59.705
M400
M400;
M42 P4 S255; Desliga Soldadura
M400;
G1 X41.92 Y59.705 F1800
M400
G1 X15.4 Y55.791

```
;TYPE:Internal infill
;WIDTH:4.2
G1 F400


;layer7

G21 ; set units to millimeters
G90 ; use absolute coordinates
M82 ; use absolute distances for extrusion
M42 P4 S255; Desliga Soldadura


G1 F400
M400;
M42 P4 S0; LIGA Soldadura
M400;
M400
G1 X44.89 Y55.791
M400
G1 X44.89 Y51.977
M400
G1 X17.11 Y51.977
M400
G1 X17.11 Y48.163
M400
G1 X44.89 Y48.163
M400
G1 X44.89 Y44.349
M400
G1 X17.11 Y44.349
M400
G1 X17.11 Y40.535
M400
G1 X44.89 Y40.535
```

M400
G1 X44.89 Y36.721
M400
G1 X17.11 Y36.721
M400
G1 X17.11 Y32.907
M400
G1 X44.89 Y32.907
M400
G1 X44.89 Y29.093
M400
G1 X17.11 Y29.093
M400
G1 X17.11 Y25.279
M400
G1 X44.89 Y25.279
M400
G1 X44.89 Y21.465
M400
G1 X17.11 Y21.465
M400
G1 X17.11 Y17.651
M400
G1 X44.89 Y17.651
M400
G1 X44.89 Y13.837
M400
G1 X17.11 Y13.837
M400
G1 X17.11 Y10.023
M400
G1 X44.89 Y10.023
M400
G1 X44.89 Y6.209
M400

```
G1 X15.4 Y6.209
;LAYER_CHANGE
;Z:9
;HEIGHT:1.8
M400;
M42 P4 S255; Desliga Soldadura
M400;
;G4 P90000; Tempo de espera entre camada

M400;
M42 P4 S255; Desliga Soldadura
M400;
G1 Z9 F1800
M400;

M400
G1 X23.74 Y2.295
G1 Z9
;TYPE:External perimeter
;WIDTH:4.4
G1 F400


;layer8

G21 ; set units to millimeters
G90 ; use absolute coordinates
M82 ; use absolute distances for extrusion
M42 P4 S255; Desliga Soldadura


G1 F400
M400;
M42 P4 S0; LIGA Soldadura
M400;
```

M400
G1 X48.8 Y2.295
M400
G1 X48.8 Y59.705
M400
G1 X13.2 Y59.705
M400
G1 X13.2 Y2.295
M400
G1 X22.99 Y2.295
M400
M400;
M42 P4 S255; Desliga Soldadura
M400;
G1 X22.99 Y2.295 F1800
M400
G1 X17.18 Y57.507
;TYPE:Internal infill
;WIDTH:4.2
G1 F400

;layer9

G21 ; set units to millimeters
G90 ; use absolute coordinates
M82 ; use absolute distances for extrusion
M42 P4 S255; Desliga Soldadura

G1 F400
M400;
M42 P4 S0; LIGA Soldadura
M400;
M400

G1 X17.18 Y6.209
M400
G1 X21.13 Y6.209
M400
G1 X21.13 Y55.791
M400
G1 X25.08 Y55.791
M400
G1 X25.08 Y6.209
M400
G1 X29.03 Y6.209
M400
G1 X29.03 Y55.791
M400
G1 X32.97 Y55.791
M400
G1 X32.97 Y6.209
M400
G1 X36.92 Y6.209
M400
G1 X36.92 Y55.791
M400
G1 X40.87 Y55.791
M400
G1 X40.87 Y6.209
M400
G1 X44.82 Y6.209
M400
G1 X44.82 Y57.507
;LAYER_CHANGE
;Z:10.8
;HEIGHT:1.8
M400;
M42 P4 S255; Desliga Soldadura
M400;

```
;G4 P90000; Tempo de espera entre camada

M400;
M42 P4 S255; Desliga Soldadura
M400;
G1 Z10.8 F1800
M400;

M400
G1 X41.53 Y59.705
G1 Z10.8
;TYPE:External perimeter
;WIDTH:4.4
G1 F400


;layer10

G21 ; set units to millimeters
G90 ; use absolute coordinates
M82 ; use absolute distances for extrusion
M42 P4 S255; Desliga Soldadura


G1 F400
M400;
M42 P4 S0; LIGA Soldadura
M400;
M400
G1 X13.2 Y59.705
M400
G1 X13.2 Y2.295
M400
G1 X48.8 Y2.295
M400
```

```
G1 X48.8 Y59.705
M400
G1 X42.28 Y59.705
M400
M400;
M42 P4 S255; Desliga Soldadura
M400;
G1 X42.28 Y59.705 F1800
M400
G1 X15.4 Y55.791
;TYPE:Internal infill
;WIDTH:4.2
G1 F400

;layer11

G21 ; set units to millimeters
G90 ; use absolute coordinates
M82 ; use absolute distances for extrusion
M42 P4 S255; Desliga Soldadura


G1 F400
M400;
M42 P4 S0; LIGA Soldadura
M400;
M400
G1 X44.89 Y55.791
M400
G1 X44.89 Y51.977
M400
G1 X17.11 Y51.977
M400
G1 X17.11 Y48.163
M400
```

G1 X44.89 Y48.163
M400
G1 X44.89 Y44.349
M400
G1 X17.11 Y44.349
M400
G1 X17.11 Y40.535
M400
G1 X44.89 Y40.535
M400
G1 X44.89 Y36.721
M400
G1 X17.11 Y36.721
M400
G1 X17.11 Y32.907
M400
G1 X44.89 Y32.907
M400
G1 X44.89 Y29.093
M400
G1 X17.11 Y29.093
M400
G1 X17.11 Y25.279
M400
G1 X44.89 Y25.279
M400
G1 X44.89 Y21.465
M400
G1 X17.11 Y21.465
M400
G1 X17.11 Y17.651
M400
G1 X44.89 Y17.651
M400
G1 X44.89 Y13.837

```
M400
G1 X17.11 Y13.837
M400
G1 X17.11 Y10.023
M400
G1 X44.89 Y10.023
M400
G1 X44.89 Y6.209
M400
G1 X15.4 Y6.209
;LAYER_CHANGE
;Z:12.6
;HEIGHT:1.8
M400;
M42 P4 S255; Desliga Soldadura
M400;
;G4 P90000; Tempo de espera entre camada

M400;
M42 P4 S255; Desliga Soldadura
M400;
G1 Z12.6 F1800
M400;

M400
G1 X13.2 Y36.72
G1 Z12.6
;TYPE:External perimeter
;WIDTH:4.4
G1 F400


;layer12

G21 ; set units to millimeters
```

G90 ; use absolute coordinates
M82 ; use absolute distances for extrusion
M42 P4 S255; Desliga Soldadura

G1 F400
M400;
M42 P4 S0; LIGA Soldadura
M400;
M400
G1 X13.2 Y2.295
M400
G1 X48.8 Y2.295
M400
G1 X48.8 Y59.705
M400
G1 X13.2 Y59.705
M400
G1 X13.2 Y37.47
M400
M400;
M42 P4 S255; Desliga Soldadura
M400;
G1 X13.2 Y37.47 F1800
M400
G1 X17.18 Y57.507
;TYPE:Internal infill
;WIDTH:4.2
G1 F400

;layer13

G21 ; set units to millimeters
G90 ; use absolute coordinates

M82 ; use absolute distances for extrusion
M42 P4 S255; Desliga Soldadura

G1 F400
M400;
M42 P4 S0; LIGA Soldadura
M400;
M400
G1 X17.18 Y6.209
M400
G1 X21.13 Y6.209
M400
G1 X21.13 Y55.791
M400
G1 X25.08 Y55.791
M400
G1 X25.08 Y6.209
M400
G1 X29.03 Y6.209
M400
G1 X29.03 Y55.791
M400
G1 X32.97 Y55.791
M400
G1 X32.97 Y6.209
M400
G1 X36.92 Y6.209
M400
G1 X36.92 Y55.791
M400
G1 X40.87 Y55.791
M400
G1 X40.87 Y6.209
M400

```
G1 X44.82 Y6.209
M400
G1 X44.82 Y57.507
;LAYER_CHANGE
;Z:14.4
;HEIGHT:1.8
M400;
M42 P4 S255; Desliga Soldadura
M400;
;G4 P90000; Tempo de espera entre camada

M400;
M42 P4 S255; Desliga Soldadura
M400;
G1 Z14.4 F1800
M400;

M400
G1 X48.8 Y37.906
G1 Z14.4
;TYPE:External perimeter
;WIDTH:4.4
G1 F400


;layer14

G21 ; set units to millimeters
G90 ; use absolute coordinates
M82 ; use absolute distances for extrusion
M42 P4 S255; Desliga Soldadura


G1 F400
M400;
```

M42 P4 S0; LIGA Soldadura
M400;
M400
G1 X48.8 Y59.705
M400
G1 X13.2 Y59.705
M400
G1 X13.2 Y2.295
M400
G1 X48.8 Y2.295
M400
G1 X48.8 Y37.156
M400
M400;
M42 P4 S255; Desliga Soldadura
M400;
G1 X48.8 Y37.156 F1800
M400
G1 X15.4 Y55.791
;TYPE:Internal infill
;WIDTH:4.2
G1 F400

;layer15

G21 ; set units to millimeters
G90 ; use absolute coordinates
M82 ; use absolute distances for extrusion
M42 P4 S255; Desliga Soldadura

G1 F400
M400;
M42 P4 S0; LIGA Soldadura

M400;
M400
G1 X44.89 Y55.791
M400
G1 X44.89 Y51.977
M400
G1 X17.11 Y51.977
M400
G1 X17.11 Y48.163
M400
G1 X44.89 Y48.163
M400
G1 X44.89 Y44.349
M400
G1 X17.11 Y44.349
M400
G1 X17.11 Y40.535
M400
G1 X44.89 Y40.535
M400
G1 X44.89 Y36.721
M400
G1 X17.11 Y36.721
M400
G1 X17.11 Y32.907
M400
G1 X44.89 Y32.907
M400
G1 X44.89 Y29.093
M400
G1 X17.11 Y29.093
M400
G1 X17.11 Y25.279
M400
G1 X44.89 Y25.279

```
M400
G1 X44.89 Y21.465
M400
G1 X17.11 Y21.465
M400
G1 X17.11 Y17.651
M400
G1 X44.89 Y17.651
M400
G1 X44.89 Y13.837
M400
G1 X17.11 Y13.837
M400
G1 X17.11 Y10.023
M400
G1 X44.89 Y10.023
M400
G1 X44.89 Y6.209
M400
G1 X15.4 Y6.209
;LAYER_CHANGE
;Z:16.2
;HEIGHT:1.8
M400;
M42 P4 S255; Desliga Soldadura
M400;
;G4 P90000; Tempo de espera entre camada

M400;
M42 P4 S255; Desliga Soldadura
M400;
G1 Z16.2 F1800
M400;

M400
```

G1 X48.8 Y11.02
G1 Z16.2
;TYPE:External perimeter
;WIDTH:4.4
G1 F400

;layer16

G21 ; set units to millimeters
G90 ; use absolute coordinates
M82 ; use absolute distances for extrusion
M42 P4 S255; Desliga Soldadura

G1 F400
M400;
M42 P4 S0; LIGA Soldadura
M400;
M400
G1 X48.8 Y59.705
M400
G1 X13.2 Y59.705
M400
G1 X13.2 Y2.295
M400
G1 X48.8 Y2.295
M400
G1 X48.8 Y10.27
M400
M400;
M42 P4 S255; Desliga Soldadura
M400;
G1 X44.82 Y57.507 F1800
;TYPE:Internal infill
;WIDTH:4.2

G1 F400

;layer17

G21 ; set units to millimeters
G90 ; use absolute coordinates
M82 ; use absolute distances for extrusion
M42 P4 S255; Desliga Soldadura

G1 F400
M400;
M42 P4 S0; LIGA Soldadura
M400;
M400
G1 X44.82 Y6.209
M400
G1 X40.87 Y6.209
M400
G1 X40.87 Y55.791
M400
G1 X36.92 Y55.791
M400
G1 X36.92 Y6.209
M400
G1 X32.97 Y6.209
M400
G1 X32.97 Y55.791
M400
G1 X29.03 Y55.791
M400
G1 X29.03 Y6.209
M400
G1 X25.08 Y6.209

```
M400
G1 X25.08 Y55.791
M400
G1 X21.13 Y55.791
M400
G1 X21.13 Y6.209
M400
G1 X17.18 Y6.209
M400
G1 X17.18 Y57.507
;LAYER_CHANGE
;Z:18
;HEIGHT:1.8
M400;
M42 P4 S255; Desliga Soldadura
M400;
;G4 P90000; Tempo de espera entre camada

M400;
M42 P4 S255; Desliga Soldadura
M400;
G1 Z18 F1800
M400;

M400
G1 X48.8 Y3.027
G1 Z18
;TYPE:External perimeter
;WIDTH:4.4
G1 F400

;layer18

G21 ; set units to millimeters
G90 ; use absolute coordinates
```

M82 ; use absolute distances for extrusion
M42 P4 S255; Desliga Soldadura

G1 F400
M400;
M42 P4 S0; LIGA Soldadura
M400;
M400
G1 X48.8 Y59.705
M400
G1 X13.2 Y59.705
M400
G1 X13.2 Y2.295
M400
G1 X48.78 Y2.295
M400
M400;
M42 P4 S255; Desliga Soldadura
M400;
G1 X15.4 Y6.209 F1800
;TYPE:Internal infill
;WIDTH:4.2
G1 F400

;layer19

G21 ; set units to millimeters
G90 ; use absolute coordinates
M82 ; use absolute distances for extrusion
M42 P4 S255; Desliga Soldadura

G1 F400
M400;

M42 P4 S0; LIGA Soldadura

M400;

M400

G1 X44.89 Y6.209

M400

G1 X44.89 Y10.023

M400

G1 X17.11 Y10.023

M400

G1 X17.11 Y13.837

M400

G1 X44.89 Y13.837

M400

G1 X44.89 Y17.651

M400

G1 X17.11 Y17.651

M400

G1 X17.11 Y21.465

M400

G1 X44.89 Y21.465

M400

G1 X44.89 Y25.279

M400

G1 X17.11 Y25.279

M400

G1 X17.11 Y29.093

M400

G1 X44.89 Y29.093

M400

G1 X44.89 Y32.907

M400

G1 X17.11 Y32.907

M400

G1 X17.11 Y36.721

M400

```
G1 X44.89 Y36.721
M400
G1 X44.89 Y40.535
M400
G1 X17.11 Y40.535
M400
G1 X17.11 Y44.349
M400
G1 X44.89 Y44.349
M400
G1 X44.89 Y48.163
M400
G1 X17.11 Y48.163
M400
G1 X17.11 Y51.977
M400
G1 X44.89 Y51.977
M400
G1 X44.89 Y55.791
M400
G1 X15.4 Y55.791
;LAYER_CHANGE
;Z:19.8
;HEIGHT:1.8
M400;
M42 P4 S255; Desliga Soldadura
M400;
;G4 P90000; Tempo de espera entre camada

M400;
M42 P4 S255; Desliga Soldadura
M400;
G1 Z19.8 F1800
M400;
```

```
M400
G1 X31.36 Y59.705
G1 Z19.8
;TYPE:External perimeter
;WIDTH:4.4
G1 F400

;layer20

G21 ; set units to millimeters
G90 ; use absolute coordinates
M82 ; use absolute distances for extrusion
M42 P4 S255; Desliga Soldadura


G1 F400
M400;
M42 P4 S0; LIGA Soldadura
M400;
M400
G1 X13.2 Y59.705
M400
G1 X13.2 Y2.295
M400
G1 X48.8 Y2.295
M400
G1 X48.8 Y59.705
M400
G1 X32.11 Y59.705
M400
M400;
M42 P4 S255; Desliga Soldadura
M400;
G1 X32.11 Y59.705 F1800
M400
```

G1 X44.82 Y57.507
;TYPE:Internal infill
;WIDTH:4.2
G1 F400

;layer21

G21 ; set units to millimeters
G90 ; use absolute coordinates
M82 ; use absolute distances for extrusion
M42 P4 S255; Desliga Soldadura

G1 F400
M400;
M42 P4 S0; LIGA Soldadura
M400;
M400
G1 X44.82 Y6.209
M400
G1 X40.87 Y6.209
M400
G1 X40.87 Y55.791
M400
G1 X36.92 Y55.791
M400
G1 X36.92 Y6.209
M400
G1 X32.97 Y6.209
M400
G1 X32.97 Y55.791
M400
G1 X29.03 Y55.791
M400
G1 X29.03 Y6.209

M400
G1 X25.08 Y6.209
M400
G1 X25.08 Y55.791
M400
G1 X21.13 Y55.791
M400
G1 X21.13 Y6.209
M400
G1 X17.18 Y6.209
M400
G1 X17.18 Y57.507
;LAYER_CHANGE
;Z:21.6
;HEIGHT:1.8
M400;
M42 P4 S255; Desliga Soldadura
M400;
;G4 P90000; Tempo de espera entre camada

M400;
M42 P4 S255; Desliga Soldadura
M400;
G1 Z21.6 F1800
M400;

M400
G1 X43.99 Y59.705
G1 Z21.6
;TYPE:External perimeter
;WIDTH:4.4
G1 F400

;layer22

G21 ; set units to millimeters
G90 ; use absolute coordinates
M82 ; use absolute distances for extrusion
M42 P4 S255; Desliga Soldadura

G1 F400
M400;
M42 P4 S0; LIGA Soldadura
M400;
M400
G1 X13.2 Y59.705
M400
G1 X13.2 Y2.295
M400
G1 X48.8 Y2.295
M400
G1 X48.8 Y59.705
M400
G1 X44.74 Y59.705
M400
M400;
M42 P4 S255; Desliga Soldadura
M400;
G1 X15.4 Y55.791 F1800
;TYPE:Internal infill
;WIDTH:4.2
G1 F400

;layer23

G21 ; set units to millimeters
G90 ; use absolute coordinates
M82 ; use absolute distances for extrusion

M42 P4 S255; Desliga Soldadura

G1 F400
M400;
M42 P4 S0; LIGA Soldadura
M400;
M400
G1 X44.89 Y55.791
M400
G1 X44.89 Y51.977
M400
G1 X17.11 Y51.977
M400
G1 X17.11 Y48.163
M400
G1 X44.89 Y48.163
M400
G1 X44.89 Y44.349
M400
G1 X17.11 Y44.349
M400
G1 X17.11 Y40.535
M400
G1 X44.89 Y40.535
M400
G1 X44.89 Y36.721
M400
G1 X17.11 Y36.721
M400
G1 X17.11 Y32.907
M400
G1 X44.89 Y32.907
M400
G1 X44.89 Y29.093

M400
G1 X17.11 Y29.093
M400
G1 X17.11 Y25.279
M400
G1 X44.89 Y25.279
M400
G1 X44.89 Y21.465
M400
G1 X17.11 Y21.465
M400
G1 X17.11 Y17.651
M400
G1 X44.89 Y17.651
M400
G1 X44.89 Y13.837
M400
G1 X17.11 Y13.837
M400
G1 X17.11 Y10.023
M400
G1 X44.89 Y10.023
M400
G1 X44.89 Y6.209
M400
G1 X15.4 Y6.209
;LAYER_CHANGE
;Z:23.4
;HEIGHT:1.8
M400;
M42 P4 S255; Desliga Soldadura
M400;
;G4 P90000; Tempo de espera entre camada

M400;

M42 P4 S255; Desliga Soldadura
M400;
G1 Z23.4 F1800
M400;

M400
G1 X48.8 Y51.712
G1 Z23.4
;TYPE:External perimeter
;WIDTH:4.4
G1 F400

;layer24

G21 ; set units to millimeters
G90 ; use absolute coordinates
M82 ; use absolute distances for extrusion
M42 P4 S255; Desliga Soldadura

G1 F400
M400;
M42 P4 S0; LIGA Soldadura
M400;
M400
G1 X48.8 Y59.705
M400
G1 X13.2 Y59.705
M400
G1 X13.2 Y2.295
M400
G1 X48.8 Y2.295
M400
G1 X48.8 Y50.962

M400
M400;
M42 P4 S255; Desliga Soldadura
M400;
G1 X44.82 Y57.507 F1800
;TYPE:Internal infill
;WIDTH:4.2
G1 F400

;layer25

G21 ; set units to millimeters
G90 ; use absolute coordinates
M82 ; use absolute distances for extrusion
M42 P4 S255; Desliga Soldadura

G1 F400
M400;
M42 P4 S0; LIGA Soldadura
M400;
M400
G1 X44.82 Y6.209
M400
G1 X40.87 Y6.209
M400
G1 X40.87 Y55.791
M400
G1 X36.92 Y55.791
M400
G1 X36.92 Y6.209
M400
G1 X32.97 Y6.209
M400
G1 X32.97 Y55.791

M400
G1 X29.03 Y55.791
M400
G1 X29.03 Y6.209
M400
G1 X25.08 Y6.209
M400
G1 X25.08 Y55.791
M400
G1 X21.13 Y55.791
M400
G1 X21.13 Y6.209
M400
G1 X17.18 Y6.209
M400
G1 X17.18 Y57.507
;LAYER_CHANGE
;Z:25.2
;HEIGHT:1.8
M400;
M42 P4 S255; Desliga Soldadura
M400;
;G4 P90000; Tempo de espera entre camada

M400;
M42 P4 S255; Desliga Soldadura
M400;
G1 Z25.2 F1800
M400;

M400
G1 X38.63 Y2.295
G1 Z25.2
;TYPE:External perimeter
;WIDTH:4.4

G1 F400

;layer26

G21 ; set units to millimeters
G90 ; use absolute coordinates
M82 ; use absolute distances for extrusion
M42 P4 S255; Desliga Soldadura

G1 F400
M400;
M42 P4 S0; LIGA Soldadura
M400;
M400
G1 X48.8 Y2.295
M400
G1 X48.8 Y59.705
M400
G1 X13.2 Y59.705
M400
G1 X13.2 Y2.295
M400
G1 X37.88 Y2.295
M400
M400;
M42 P4 S255; Desliga Soldadura
M400;
G1 X37.88 Y2.295 F1800
M400
G1 X15.4 Y6.209
;TYPE:Internal infill
;WIDTH:4.2
G1 F400

;layer27

G21 ; set units to millimeters
G90 ; use absolute coordinates
M82 ; use absolute distances for extrusion
M42 P4 S255; Desliga Soldadura

G1 F400
M400;
M42 P4 S0; LIGA Soldadura
M400;
M400
G1 X44.89 Y6.209
M400
G1 X44.89 Y10.023
M400
G1 X17.11 Y10.023
M400
G1 X17.11 Y13.837
M400
G1 X44.89 Y13.837
M400
G1 X44.89 Y17.651
M400
G1 X17.11 Y17.651
M400
G1 X17.11 Y21.465
M400
G1 X44.89 Y21.465
M400
G1 X44.89 Y25.279
M400
G1 X17.11 Y25.279
M400

G1 X17.11 Y29.093
M400
G1 X44.89 Y29.093
M400
G1 X44.89 Y32.907
M400
G1 X17.11 Y32.907
M400
G1 X17.11 Y36.721
M400
G1 X44.89 Y36.721
M400
G1 X44.89 Y40.535
M400
G1 X17.11 Y40.535
M400
G1 X17.11 Y44.349
M400
G1 X44.89 Y44.349
M400
G1 X44.89 Y48.163
M400
G1 X17.11 Y48.163
M400
G1 X17.11 Y51.977
M400
G1 X44.89 Y51.977
M400
G1 X44.89 Y55.791
M400
G1 X15.4 Y55.791
;LAYER_CHANGE
;Z:27
;HEIGHT:1.8
M400;

```
M42 P4 S255; Desliga Soldadura
M400;
;G4 P90000; Tempo de espera entre camada

M400;
M42 P4 S255; Desliga Soldadura
M400;
G1 Z27 F1800
M400;

M400
G1 X48.8 Y34.999
G1 Z27
;TYPE:External perimeter
;WIDTH:4.4
G1 F400

;layer28

G21 ; set units to millimeters
G90 ; use absolute coordinates
M82 ; use absolute distances for extrusion
M42 P4 S255; Desliga Soldadura


G1 F400
M400;
M42 P4 S0; LIGA Soldadura
M400;
M400
G1 X48.8 Y59.705
M400
G1 X13.2 Y59.705
M400
G1 X13.2 Y2.295
```

M400
G1 X48.8 Y2.295
M400
G1 X48.8 Y34.249
M400
M400;
M42 P4 S255; Desliga Soldadura
M400;
G1 X48.8 Y34.249 F1800
M400
G1 X44.82 Y57.507
;TYPE:Internal infill
;WIDTH:4.2
G1 F400

;layer29

G21 ; set units to millimeters
G90 ; use absolute coordinates
M82 ; use absolute distances for extrusion
M42 P4 S255; Desliga Soldadura

G1 F400
M400;
M42 P4 S0; LIGA Soldadura
M400;
M400
G1 X44.82 Y6.209
M400
G1 X40.87 Y6.209
M400
G1 X40.87 Y55.791
M400

```
G1 X36.92 Y55.791
M400
G1 X36.92 Y6.209
M400
G1 X32.97 Y6.209
M400
G1 X32.97 Y55.791
M400
G1 X29.03 Y55.791
M400
G1 X29.03 Y6.209
M400
G1 X25.08 Y6.209
M400
G1 X25.08 Y55.791
M400
G1 X21.13 Y55.791
M400
G1 X21.13 Y6.209
M400
G1 X17.18 Y6.209
M400
G1 X17.18 Y57.507
;LAYER_CHANGE
;Z:28.8
;HEIGHT:1.8
M400;
M42 P4 S255; Desliga Soldadura
M400;
;G4 P90000; Tempo de espera entre camada

M400;
M42 P4 S255; Desliga Soldadura
M400;
G1 Z28.8 F1800
```

```
M400;

M400
G1 X48.8 Y40.812
G1 Z28.8
;TYPE:External perimeter
;WIDTH:4.4
G1 F400
;layer30

G21 ; set units to millimeters
G90 ; use absolute coordinates
M82 ; use absolute distances for extrusion
M42 P4 S255; Desliga Soldadura


G1 F400
M400;
M42 P4 S0; LIGA Soldadura
M400;
M400
G1 X48.8 Y59.705
M400
G1 X13.2 Y59.705
M400
G1 X13.2 Y2.295
M400
G1 X48.8 Y2.295
M400
G1 X48.8 Y40.062
M400
M400;
M42 P4 S255; Desliga Soldadura
M400;
G1 X48.8 Y40.062 F1800
```

M400
G1 X15.4 Y55.791
;TYPE:Internal infill
;WIDTH:4.2
G1 F400

;layer31

G21 ; set units to millimeters
G90 ; use absolute coordinates
M82 ; use absolute distances for extrusion
M42 P4 S255; Desliga Soldadura

G1 F400
M400;
M42 P4 S0; LIGA Soldadura
M400;
M400
G1 X44.89 Y55.791
M400
G1 X44.89 Y51.977
M400
G1 X17.11 Y51.977
M400
G1 X17.11 Y48.163
M400
G1 X44.89 Y48.163
M400
G1 X44.89 Y44.349
M400
G1 X17.11 Y44.349
M400
G1 X17.11 Y40.535
M400

G1 X44.89 Y40.535
M400
G1 X44.89 Y36.721
M400
G1 X17.11 Y36.721
M400
G1 X17.11 Y32.907
M400
G1 X44.89 Y32.907
M400
G1 X44.89 Y29.093
M400
G1 X17.11 Y29.093
M400
G1 X17.11 Y25.279
M400
G1 X44.89 Y25.279
M400
G1 X44.89 Y21.465
M400
G1 X17.11 Y21.465
M400
G1 X17.11 Y17.651
M400
G1 X44.89 Y17.651
M400
G1 X44.89 Y13.837
M400
G1 X17.11 Y13.837
M400
G1 X17.11 Y10.023
M400
G1 X44.89 Y10.023
M400
G1 X44.89 Y6.209

```
M400
G1 X15.4 Y6.209
;LAYER_CHANGE
;Z:30.6
;HEIGHT:1.8
M400;
M42 P4 S255; Desliga Soldadura
M400;
;G4 P90000; Tempo de espera entre camada

M400;
M42 P4 S255; Desliga Soldadura
M400;
G1 Z30.6 F1800
M400;

M400
G1 X35.54 Y59.705
G1 Z30.6
;TYPE:External perimeter
;WIDTH:4.4
G1 F400

;layer32

G21 ; set units to millimeters
G90 ; use absolute coordinates
M82 ; use absolute distances for extrusion
M42 P4 S255; Desliga Soldadura


G1 F400
M400;
M42 P4 S0; LIGA Soldadura
M400;
```

M400
G1 X13.2 Y59.705
M400
G1 X13.2 Y2.295
M400
G1 X48.8 Y2.295
M400
G1 X48.8 Y59.705
M400
G1 X36.29 Y59.705
M400
M400;
M42 P4 S255; Desliga Soldadura
M400;
G1 X36.29 Y59.705 F1800
M400
G1 X44.82 Y57.507
;TYPE:Internal infill
;WIDTH:4.2
G1 F400

;layer33

G21 ; set units to millimeters
G90 ; use absolute coordinates
M82 ; use absolute distances for extrusion
M42 P4 S255; Desliga Soldadura

G1 F400
M400;
M42 P4 S0; LIGA Soldadura
M400;
M400
G1 X44.82 Y6.209

M400
G1 X40.87 Y6.209
M400
G1 X40.87 Y55.791
M400
G1 X36.92 Y55.791
M400
G1 X36.92 Y6.209
M400
G1 X32.97 Y6.209
M400
G1 X32.97 Y55.791
M400
G1 X29.03 Y55.791
M400
G1 X29.03 Y6.209
M400
G1 X25.08 Y6.209
M400
G1 X25.08 Y55.791
M400
G1 X21.13 Y55.791
M400
G1 X21.13 Y6.209
M400
G1 X17.18 Y6.209
M400
G1 X17.18 Y57.507
;LAYER_CHANGE
;Z:32.4
;HEIGHT:1.8
M400;
M42 P4 S255; Desliga Soldadura
M400;
;G4 P90000; Tempo de espera entre camada

```
M400;
M42 P4 S255; Desliga Soldadura
M400;
G1 Z32.4 F1800
M400;

M400
G1 X13.2 Y4.475
G1 Z32.4
;TYPE:External perimeter
;WIDTH:4.4
G1 F400

;layer34

G21 ; set units to millimeters
G90 ; use absolute coordinates
M82 ; use absolute distances for extrusion
M42 P4 S255; Desliga Soldadura


G1 F400
M400;
M42 P4 S0; LIGA Soldadura
M400;
M400
G1 X13.2 Y2.295
M400
G1 X48.8 Y2.295
M400
G1 X48.8 Y59.705
M400
G1 X13.2 Y59.705
M400
```

G1 X13.2 Y5.225
M400
M400;
M42 P4 S255; Desliga Soldadura
M400;
G1 X15.4 Y6.209 F1800
;TYPE:Internal infill
;WIDTH:4.2
G1 F400

;layer35

G21 ; set units to millimeters
G90 ; use absolute coordinates
M82 ; use absolute distances for extrusion
M42 P4 S255; Desliga Soldadura

G1 F400
M400;
M42 P4 S0; LIGA Soldadura
M400;
M400
G1 X44.89 Y6.209
M400
G1 X44.89 Y10.023
M400
G1 X17.11 Y10.023
M400
G1 X17.11 Y13.837
M400
G1 X44.89 Y13.837
M400
G1 X44.89 Y17.651

M400
G1 X17.11 Y17.651
M400
G1 X17.11 Y21.465
M400
G1 X44.89 Y21.465
M400
G1 X44.89 Y25.279
M400
G1 X17.11 Y25.279
M400
G1 X17.11 Y29.093
M400
G1 X44.89 Y29.093
M400
G1 X44.89 Y32.907
M400
G1 X17.11 Y32.907
M400
G1 X17.11 Y36.721
M400
G1 X44.89 Y36.721
M400
G1 X44.89 Y40.535
M400
G1 X17.11 Y40.535
M400
G1 X17.11 Y44.349
M400
G1 X44.89 Y44.349
M400
G1 X44.89 Y48.163
M400
G1 X17.11 Y48.163
M400

```
G1 X17.11 Y51.977
M400
G1 X44.89 Y51.977
M400
G1 X44.89 Y55.791
M400
G1 X15.4 Y55.791
;LAYER_CHANGE
;Z:34.2
;HEIGHT:1.8
M400;
M42 P4 S255; Desliga Soldadura
M400;
;G4 P90000; Tempo de espera entre camada

M400;
M42 P4 S255; Desliga Soldadura
M400;
G1 Z34.2 F1800
M400;

M400
G1 X40.81 Y2.295
G1 Z34.2
;TYPE:External perimeter
;WIDTH:4.4
G1 F400

;layer36

G21 ; set units to millimeters
G90 ; use absolute coordinates
M82 ; use absolute distances for extrusion
M42 P4 S255; Desliga Soldadura
```

G1 F400
M400;
M42 P4 S0; LIGA Soldadura
M400;
M400
G1 X48.8 Y2.295
M400
G1 X48.8 Y59.705
M400
G1 X13.2 Y59.705
M400
G1 X13.2 Y2.295
M400
G1 X40.06 Y2.295
M400
M400;
M42 P4 S255; Desliga Soldadura
M400;
G1 X40.06 Y2.295 F1800
M400
G1 X44.82 Y57.507
;TYPE:Internal infill
;WIDTH:4.2
G1 F400

;layer37

G21 ; set units to millimeters
G90 ; use absolute coordinates
M82 ; use absolute distances for extrusion
M42 P4 S255; Desliga Soldadura

G1 F400

M400;
M42 P4 S0; LIGA Soldadura
M400;
M400
G1 X44.82 Y6.209
M400
G1 X40.87 Y6.209
M400
G1 X40.87 Y55.791
M400
G1 X36.92 Y55.791
M400
G1 X36.92 Y6.209
M400
G1 X32.97 Y6.209
M400
G1 X32.97 Y55.791
M400
G1 X29.03 Y55.791
M400
G1 X29.03 Y6.209
M400
G1 X25.08 Y6.209
M400
G1 X25.08 Y55.791
M400
G1 X21.13 Y55.791
M400
G1 X21.13 Y6.209
M400
G1 X17.18 Y6.209
M400
G1 X17.18 Y57.507
;LAYER_CHANGE
;Z:36

```
;HEIGHT:1.8
M400;
M42 P4 S255; Desliga Soldadura
M400;
;G4 P90000; Tempo de espera entre camada

M400;
M42 P4 S255; Desliga Soldadura
M400;
G1 Z36 F1800
M400;

M400
G1 X17.87 Y59.705
G1 Z36
;TYPE:External perimeter
;WIDTH:4.4
G1 F400

;layer38

G21 ; set units to millimeters
G90 ; use absolute coordinates
M82 ; use absolute distances for extrusion
M42 P4 S255; Desliga Soldadura


G1 F400
M400;
M42 P4 S0; LIGA Soldadura
M400;
M400
G1 X13.2 Y59.705
M400
G1 X13.2 Y2.295
```

M400
G1 X48.8 Y2.295
M400
G1 X48.8 Y52.122
M400
G1 X48.8 Y59.705
M400
G1 X18.62 Y59.705
M400
M400;
M42 P4 S255; Desliga Soldadura
M400;
G1 X15.4 Y55.791 F1800
;TYPE:Internal infill
;WIDTH:4.2
G1 F400

;layer39

G21 ; set units to millimeters
G90 ; use absolute coordinates
M82 ; use absolute distances for extrusion
M42 P4 S255; Desliga Soldadura

G1 F400
M400;
M42 P4 S0; LIGA Soldadura
M400;
M400
G1 X44.89 Y55.791
M400
G1 X44.89 Y51.977
M400

G1 X17.11 Y51.977
M400
G1 X17.11 Y48.163
M400
G1 X44.89 Y48.163
M400
G1 X44.89 Y44.349
M400
G1 X17.11 Y44.349
M400
G1 X17.11 Y40.535
M400
G1 X44.89 Y40.535
M400
G1 X44.89 Y36.721
M400
G1 X17.11 Y36.721
M400
G1 X17.11 Y32.907
M400
G1 X44.89 Y32.907
M400
G1 X44.89 Y29.093
M400
G1 X17.11 Y29.093
M400
G1 X17.11 Y25.279
M400
G1 X44.89 Y25.279
M400
G1 X44.89 Y21.465
M400
G1 X17.11 Y21.465
M400
G1 X17.11 Y17.651

```
M400
G1 X44.89 Y17.651
M400
G1 X44.89 Y13.837
M400
G1 X17.11 Y13.837
M400
G1 X17.11 Y10.023
M400
G1 X44.89 Y10.023
M400
G1 X44.89 Y6.209
M400
G1 X15.4 Y6.209
;LAYER_CHANGE
;Z:37.8
;HEIGHT:1.8
M400;
M42 P4 S255; Desliga Soldadura
M400;
;G4 P90000; Tempo de espera entre camada

M400;
M42 P4 S255; Desliga Soldadura
M400;
G1 Z37.8 F1800
M400;

M400
G1 X48.8 Y37.179
G1 Z37.8
;TYPE:External perimeter
;WIDTH:4.4
G1 F400
```

;layer40

G21 ; set units to millimeters
G90 ; use absolute coordinates
M82 ; use absolute distances for extrusion
M42 P4 S255; Desliga Soldadura

G1 F400
M400;
M42 P4 S0; LIGA Soldadura
M400;
M400
G1 X48.8 Y59.705
M400
G1 X13.2 Y59.705
M400
G1 X13.2 Y2.295
M400
G1 X48.8 Y2.295
M400
G1 X48.8 Y36.429
M400
M400;
M42 P4 S255; Desliga Soldadura
M400;
G1 X48.8 Y36.429 F1800
M400
G1 X44.82 Y57.507
;TYPE:Internal infill
;WIDTH:4.2
G1 F400

;layer41

G21 ; set units to millimeters
G90 ; use absolute coordinates
M82 ; use absolute distances for extrusion
M42 P4 S255; Desliga Soldadura

G1 F400
M400;
M42 P4 S0; LIGA Soldadura
M400;
M400
G1 X44.82 Y6.209
M400
G1 X40.87 Y6.209
M400
G1 X40.87 Y55.791
M400
G1 X36.92 Y55.791
M400
G1 X36.92 Y6.209
M400
G1 X32.97 Y6.209
M400
G1 X32.97 Y55.791
M400
G1 X29.03 Y55.791
M400
G1 X29.03 Y6.209
M400
G1 X25.08 Y6.209
M400
G1 X25.08 Y55.791
M400
G1 X21.13 Y55.791

M400
G1 X21.13 Y6.209
M400
G1 X17.18 Y6.209
M400
G1 X17.18 Y57.507
;LAYER_CHANGE
;Z:39.6
;HEIGHT:1.8
M400;
M42 P4 S255; Desliga Soldadura
M400;
;G4 P90000; Tempo de espera entre camada

M400;
M42 P4 S255; Desliga Soldadura
M400;
G1 Z39.6 F1800
M400;

M400
G1 X48.8 Y6.842
G1 Z39.6
;TYPE:External perimeter
;WIDTH:4.4
G1 F400

;layer42

G21 ; set units to millimeters
G90 ; use absolute coordinates
M82 ; use absolute distances for extrusion
M42 P4 S255; Desliga Soldadura

G1 F400
M400;
M42 P4 S0; LIGA Soldadura
M400;
M400
G1 X48.8 Y59.705
M400
G1 X13.2 Y59.705
M400
G1 X13.2 Y2.295
M400
G1 X48.8 Y2.295
M400
G1 X48.8 Y6.092
M400
M400;
M42 P4 S255; Desliga Soldadura
M400;
G1 X48.8 Y6.092 F1800
M400
G1 X15.4 Y6.209
;TYPE:Internal infill
;WIDTH:4.2
G1 F400

;layer43

G21 ; set units to millimeters
G90 ; use absolute coordinates
M82 ; use absolute distances for extrusion
M42 P4 S255; Desliga Soldadura

G1 F400
M400;
M42 P4 S0; LIGA Soldadura
M400;
M400
G1 X44.89 Y6.209
M400
G1 X44.89 Y10.023
M400
G1 X17.11 Y10.023
M400
G1 X17.11 Y13.837
M400
G1 X44.89 Y13.837
M400
G1 X44.89 Y17.651
M400
G1 X17.11 Y17.651
M400
G1 X17.11 Y21.465
M400
G1 X44.89 Y21.465
M400
G1 X44.89 Y25.279
M400
G1 X17.11 Y25.279
M400
G1 X17.11 Y29.093
M400
G1 X44.89 Y29.093
M400
G1 X44.89 Y32.907
M400
G1 X17.11 Y32.907
M400

```
G1 X17.11 Y36.721
M400
G1 X44.89 Y36.721
M400
G1 X44.89 Y40.535
M400
G1 X17.11 Y40.535
M400
G1 X17.11 Y44.349
M400
G1 X44.89 Y44.349
M400
G1 X44.89 Y48.163
M400
G1 X17.11 Y48.163
M400
G1 X17.11 Y51.977
M400
G1 X44.89 Y51.977
M400
G1 X44.89 Y55.791
M400
G1 X15.4 Y55.791
;LAYER_CHANGE
;Z:41.4
;HEIGHT:1.8
M400;
M42 P4 S255; Desliga Soldadura
M400;
;G4 P90000; Tempo de espera entre camada

M400;
M42 P4 S255; Desliga Soldadura
M400;
G1 Z41.4 F1800
```

M400;

M400
G1 X29.19 Y2.295
G1 Z41.4
;TYPE:External perimeter
;WIDTH:4.4
G1 F400
;layer44

G21 ; set units to millimeters
G90 ; use absolute coordinates
M82 ; use absolute distances for extrusion
M42 P4 S255; Desliga Soldadura

G1 F400
M400;
M42 P4 S0; LIGA Soldadura
M400;
M400
G1 X48.8 Y2.295
M400
G1 X48.8 Y59.705
M400
G1 X13.2 Y59.705
M400
G1 X13.2 Y2.295
M400
G1 X28.44 Y2.295
M400
M400;
M42 P4 S255; Desliga Soldadura
M400;
G1 X17.18 Y57.507 F1800

```
;TYPE:Internal infill
;WIDTH:4.2
G1 F400
;layer45

G21 ; set units to millimeters
G90 ; use absolute coordinates
M82 ; use absolute distances for extrusion
M42 P4 S255; Desliga Soldadura


G1 F400
M400;
M42 P4 S0; LIGA Soldadura
M400;
M400
G1 X17.18 Y6.209
M400
G1 X21.13 Y6.209
M400
G1 X21.13 Y55.791
M400
G1 X25.08 Y55.791
M400
G1 X25.08 Y6.209
M400
G1 X29.03 Y6.209
M400
G1 X29.03 Y55.791
M400
G1 X32.97 Y55.791
M400
G1 X32.97 Y6.209
M400
G1 X36.92 Y6.209
```

M400
G1 X36.92 Y55.791
M400
G1 X40.87 Y55.791
M400
G1 X40.87 Y6.209
M400
G1 X44.82 Y6.209
M400
G1 X44.82 Y57.507
M107dds

# APPENDIX 4
# TECHNICAL DRAWING OF THE TENSILE SPECIMEN

| | | | | |
|---|---|---|---|---|
| Proj. | 27/06/2024 | João Figueiredo | F.C.T.-U.N.L.<br>*Master's Thesis* | *João Figueiredo* |
| Des. | 27/06/2024 | João Figueiredo | | |
| Copiou | | | | |
| Visto | | | | |

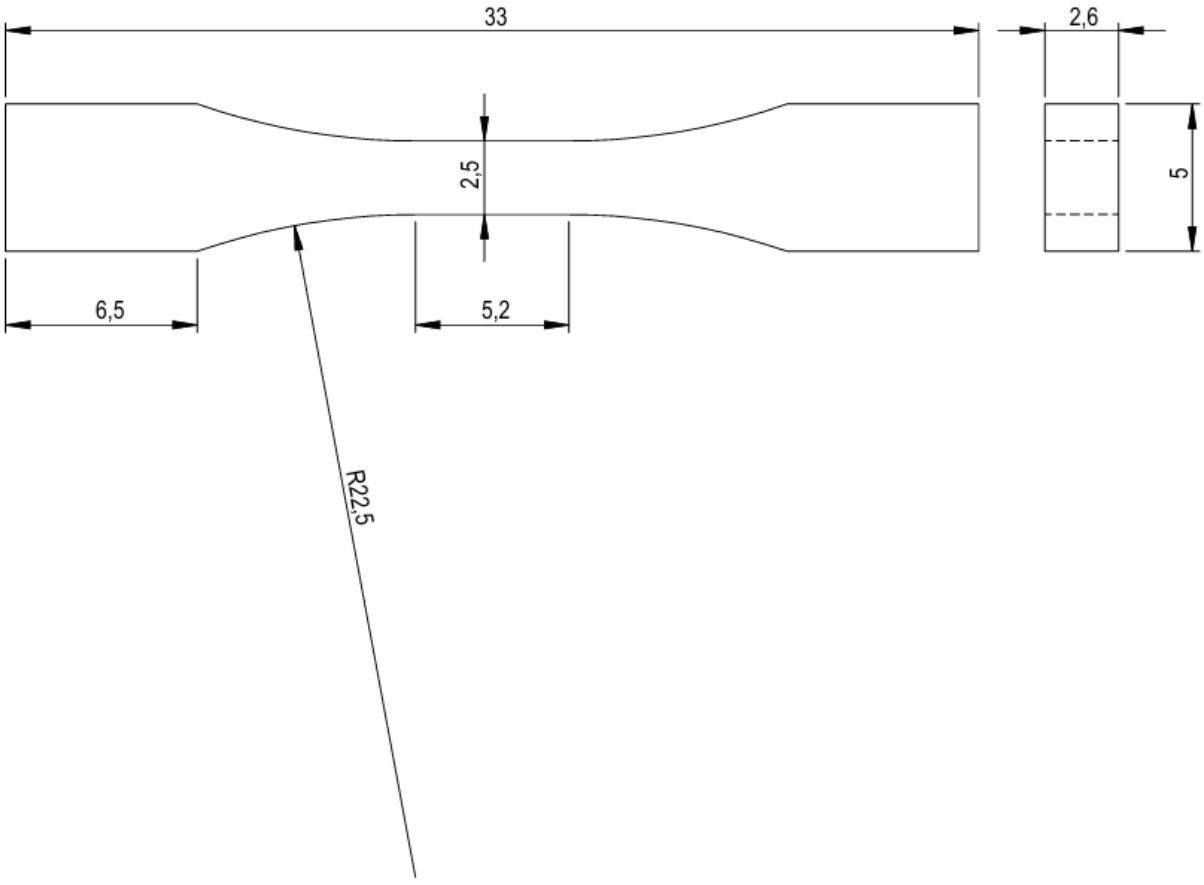


| | | | |
|---|---|---|---|
| Observações: | 4:1<br>Tolerân.<br>NP265<br>Médio | *Tensile specimen adapted from ASTM E8 standard* | 1 |

# APPENDIX 5
# TECHNICAL DRAWING OF THE PART AFTER ITS RE-DESIGN AND ASSEMBLY

| | | | | |
|---|---|---|---|---|
| Proj. | 21/09/24 | João Figueiredo | F.C.T.-U.N.L.<br>*Master's Thesis* | *João Figueiredo* |
| Des. | 21/09/24 | João Figueiredo | | |
| Copiou | | | | |
| Visto | | | | |

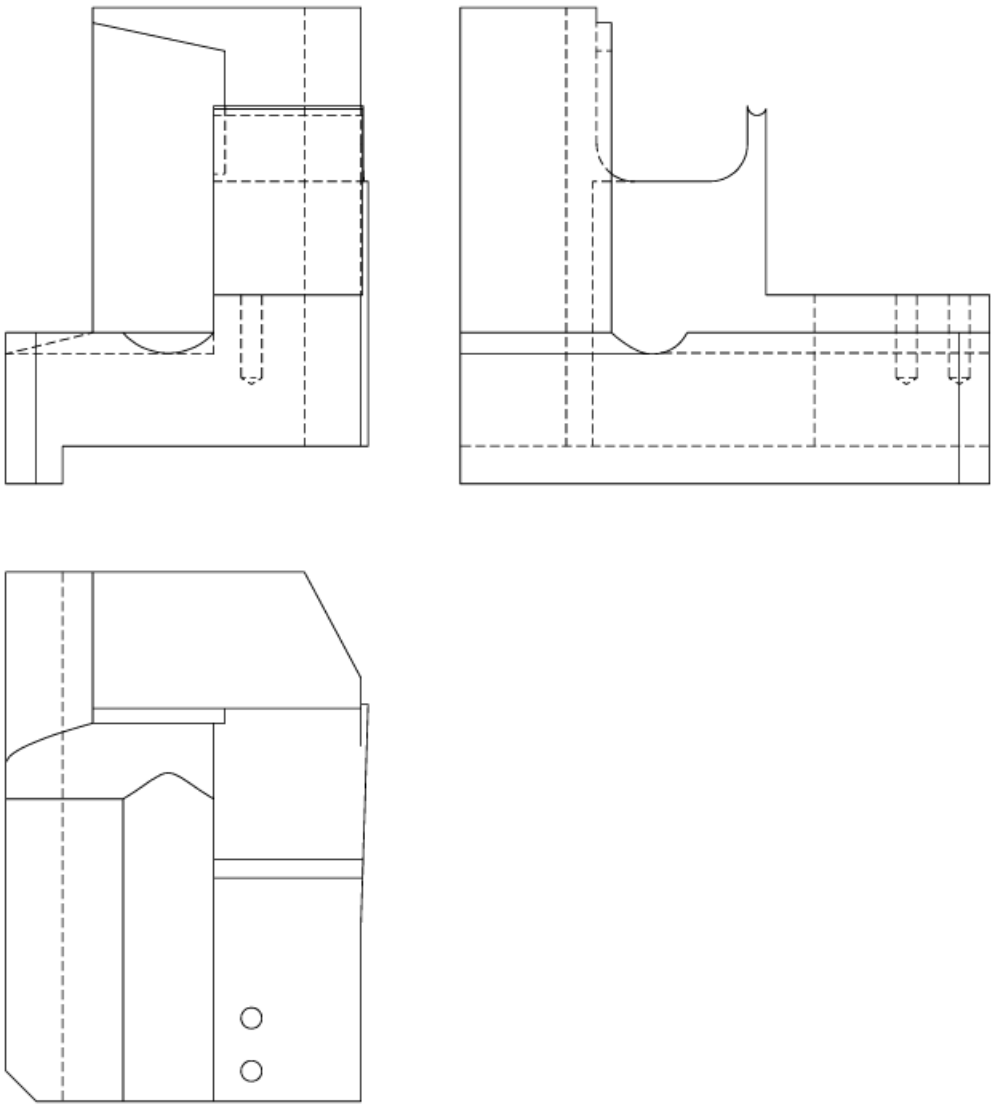

| | | | |
|---|---|---|---|
| Observações: | 1:2<br>Tolerân.<br>NP 265<br>Médio | *Part 1* | 2 |

| | | | | |
|---|---|---|---|---|
| Proj. | 21/09/2024 | João Figueiredo | F.C.T.-U.N.L.<br>*Master's Thesis* | *João Figueiredo* |
| Des. | 21/09/2024 | João Figueiredo | | |
| Copiou | | | | |
| Visto | | | | |

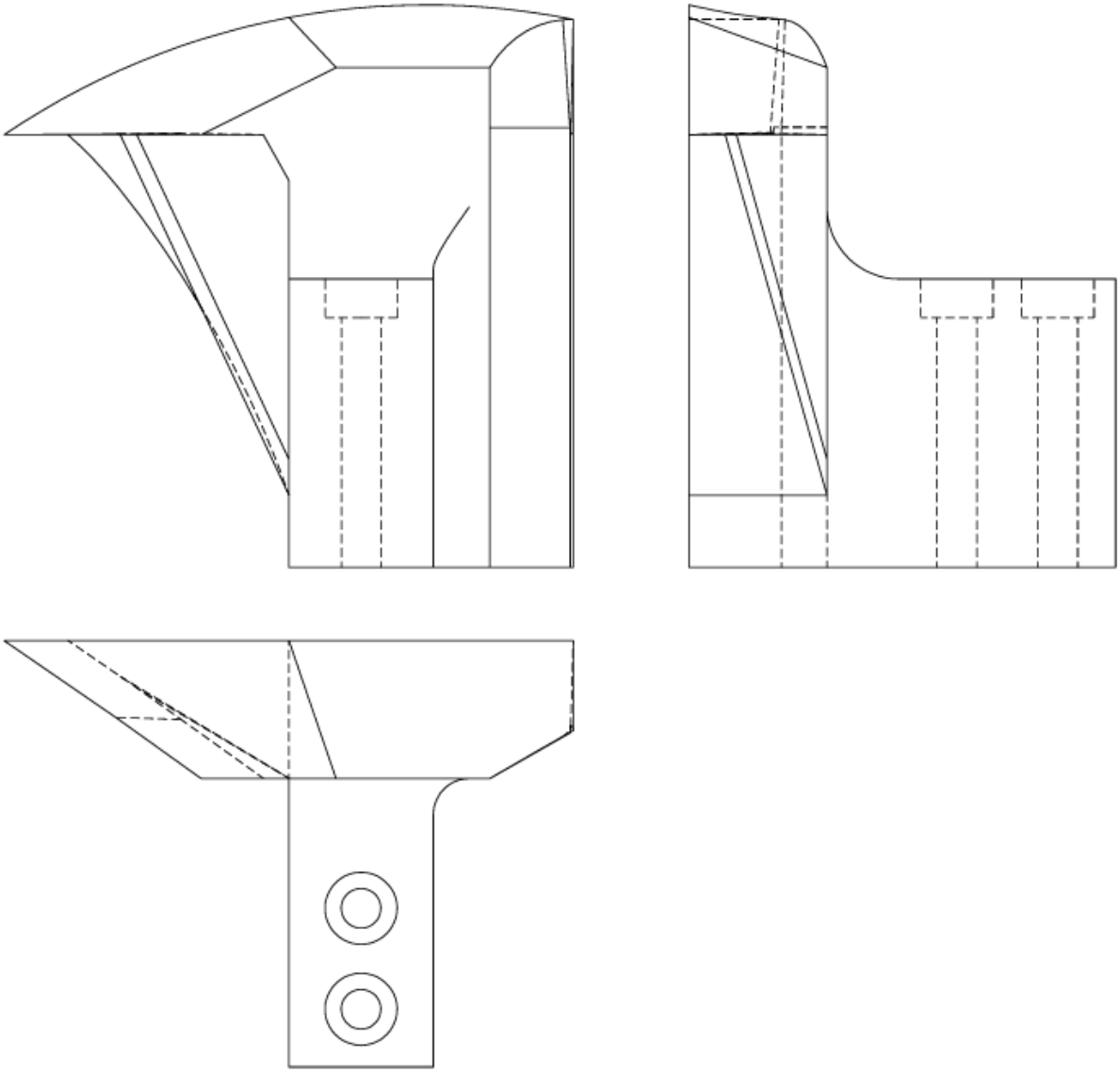

| | | | |
|---|---|---|---|
| Observações: | 1:1<br>Tolerân.<br>NP 265<br>Médio | *Part 2* | *3* |

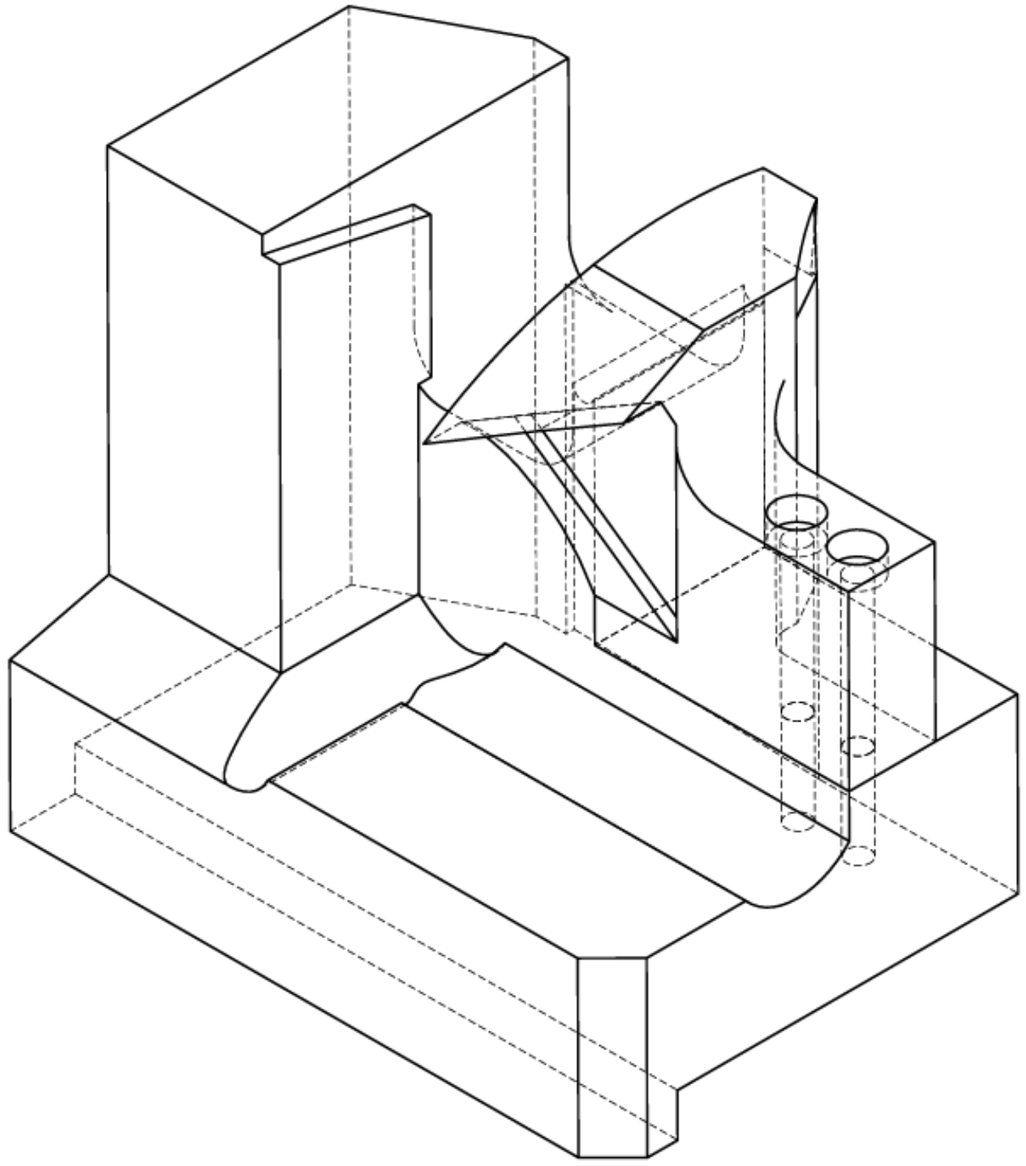

ISOMETRIC VIEW
SCALE 1:1

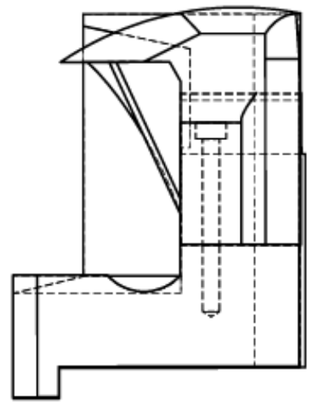

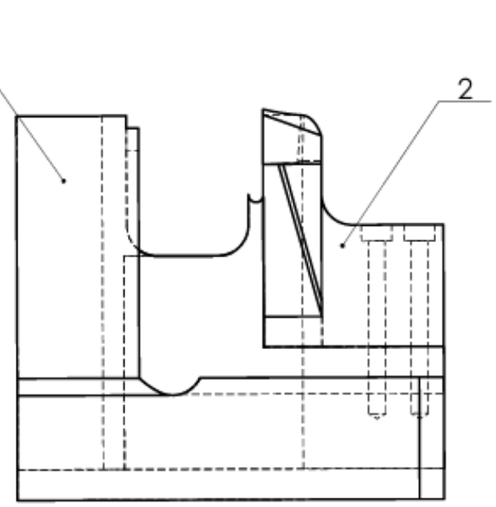


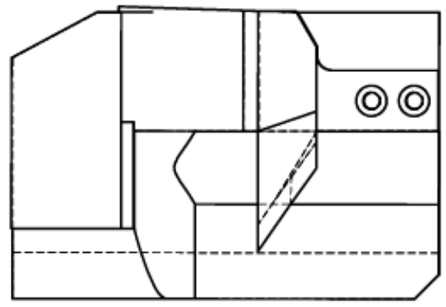

| | | | | | | | |
|---|---|---|---|---|---|---|---|
| 1 | Part 2 | | ER70S-6 | 3 | | A | |
| 1 | Part 1 | | ER70S-6 | 2 | | A | |
| Nº | DESIGNAÇÃO | Nº DA NORMA Nº DO DESENHO | MATERIAL | Nº REF. | PRODUTO SEMI ACABADO Nº DO MOLDE Nº DA MATRIZ | PESO | OBSERVAÇÕES |

| | | | |
|---|---|---|---|
| PROJ. | 21/09/2024 | FCT FACULDADE DE CIÊNCIAS E TECNOLOGIA UNIVERSIDADE NOVA DE LISBOA | João Figueiredo MIEMc |
| DES. | 21/09/2024 | DEMI 2023-2024 | |
| ESCALA 1:2 | | ASSEMBLY | 5 |
| TOLERÂN. NP-265 MÉDIO | | | |

# APPENDIX 6
# UNIAXIAL TENSILE TEST RESULTS

Table A. 2 - Strength and ductility results from uniaxial tensile testing.

| Specimen Identification | UTS [MPa] | Elongation to fracture [%] |
|---|---|---|
| A1 | - | 23.9 |
| A2 | - | 24.7 |
| A3 | 495 | 21.9 |
| A4 | 493 | 25.1 |
| | | |
| B1 | 496 | 25.8 |
| B2 | 492 | 22.7 |
| B3 | 495 | 26.3 |
| B4 | 497 | 26.8 |
| | | |
| C1 | 500 | 24.9 |
| C2 | 493 | 22.8 |
| C3 | 492 | 23.0 |
| C4 | 498 | 21.8 |
| | | |
| D1 | 496 | 23.3 |
| D2 | 489 | 25.7 |

| | | |
|---|---|---|
| D3 | 489 | 23.3 |
| D4 | 491 | - |

Table A. 3 - Strength and ductility average results from uniaxial tensile testing.

| Specimen Identification | UTS [MPa] | Elongation to fracture [%] |
|---|---|---|
| Average A | 494 | 23.9 |
| Average B | 495 | 25.4 |
| Average C | 496 | 23.1 |
| Average D | 491 | 24.1 |
| Combined average | 494 | 24.1 |

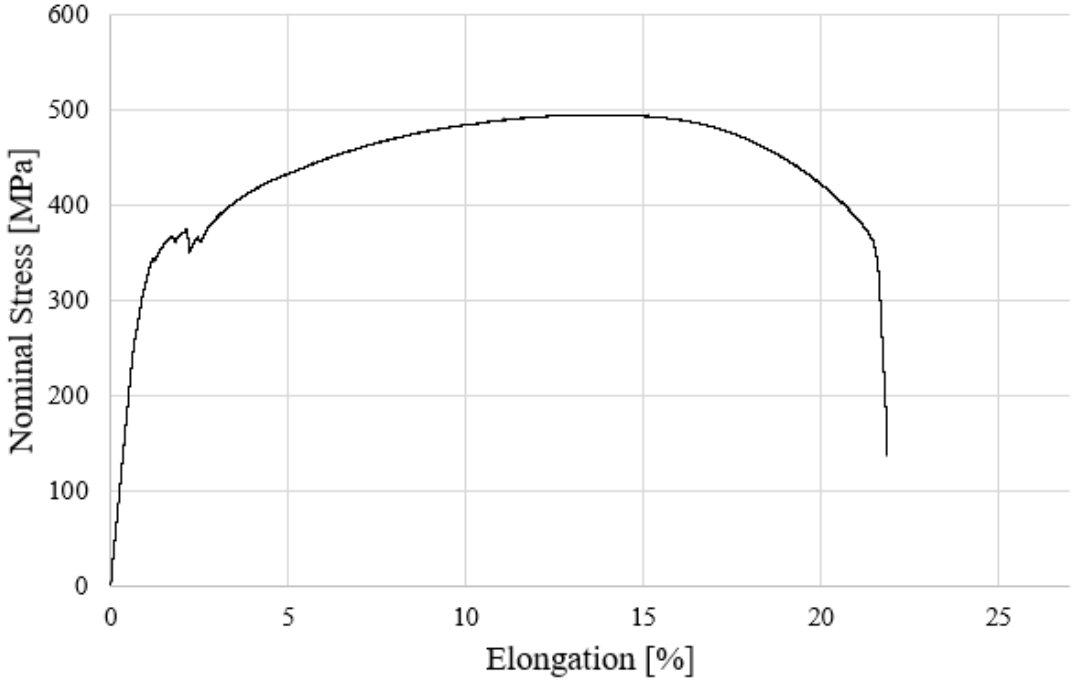


Figure A. 1 - Uniaxial tensile tests graph A3

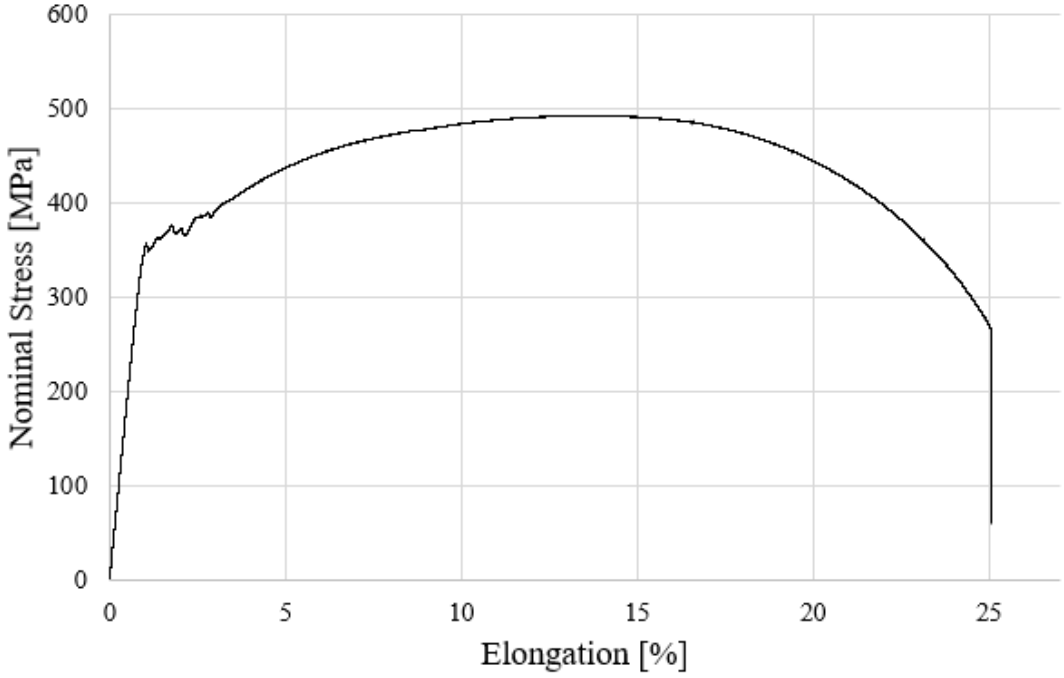


Figure A. 2 - Uniaxial tensile tests graph A4

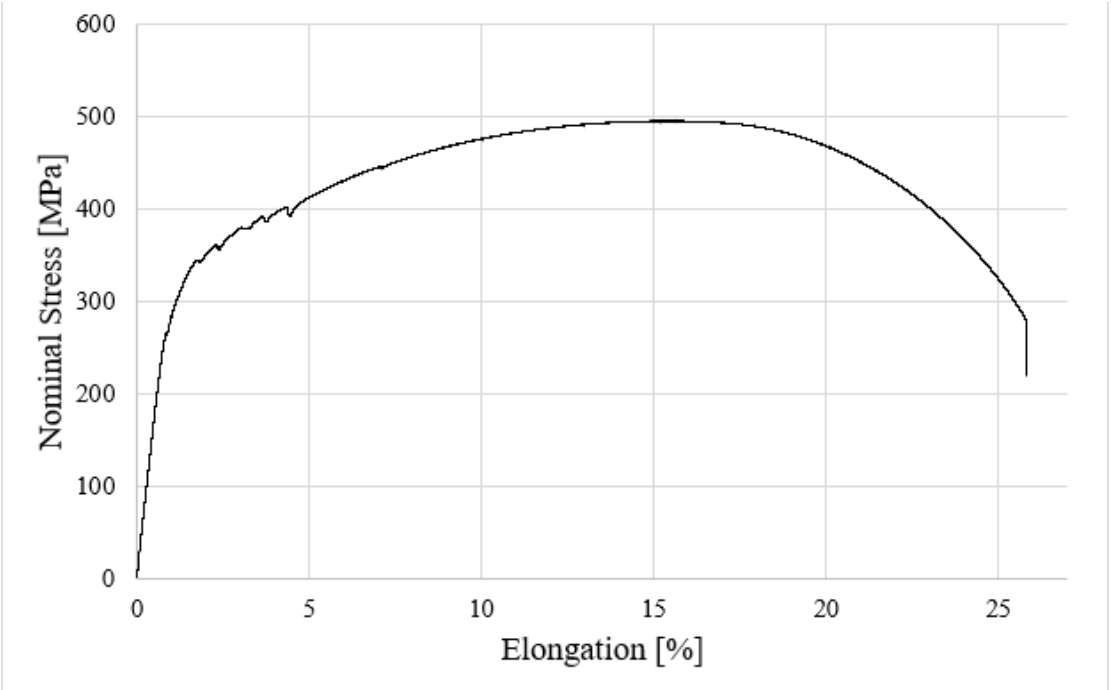


Figure A. 3 - Uniaxial tensile tests graph B1.

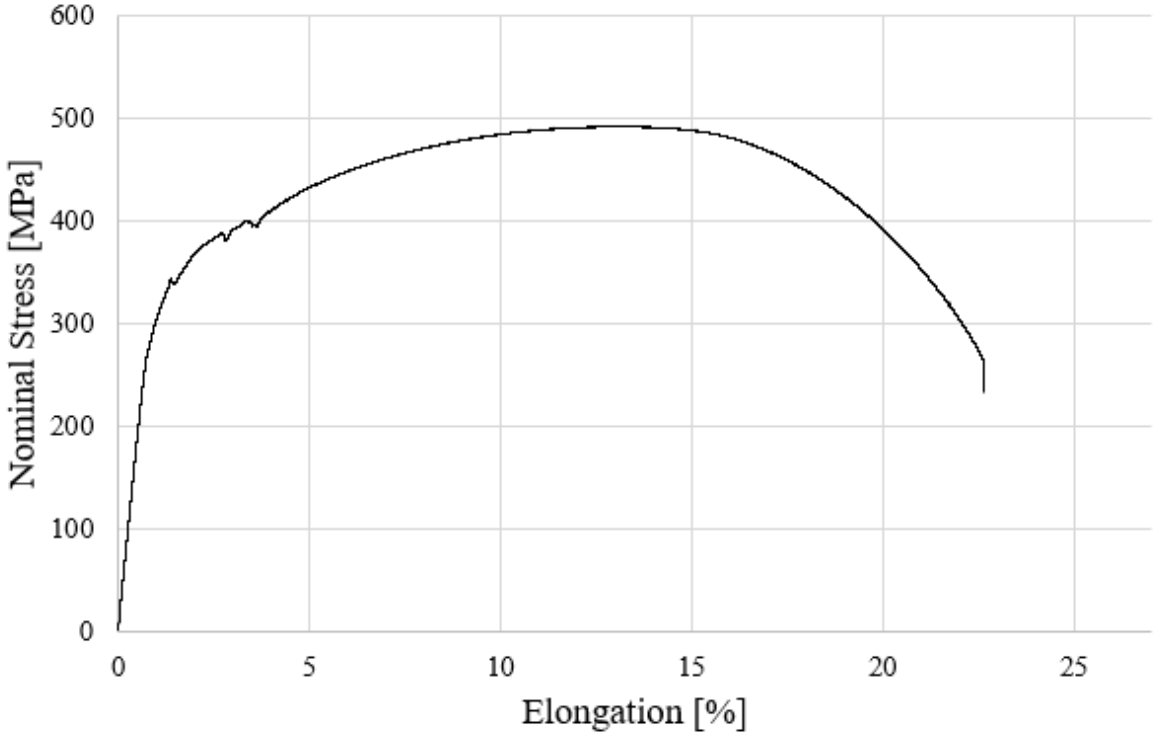


Figure A. 4 - Uniaxial tensile tests graph B2.

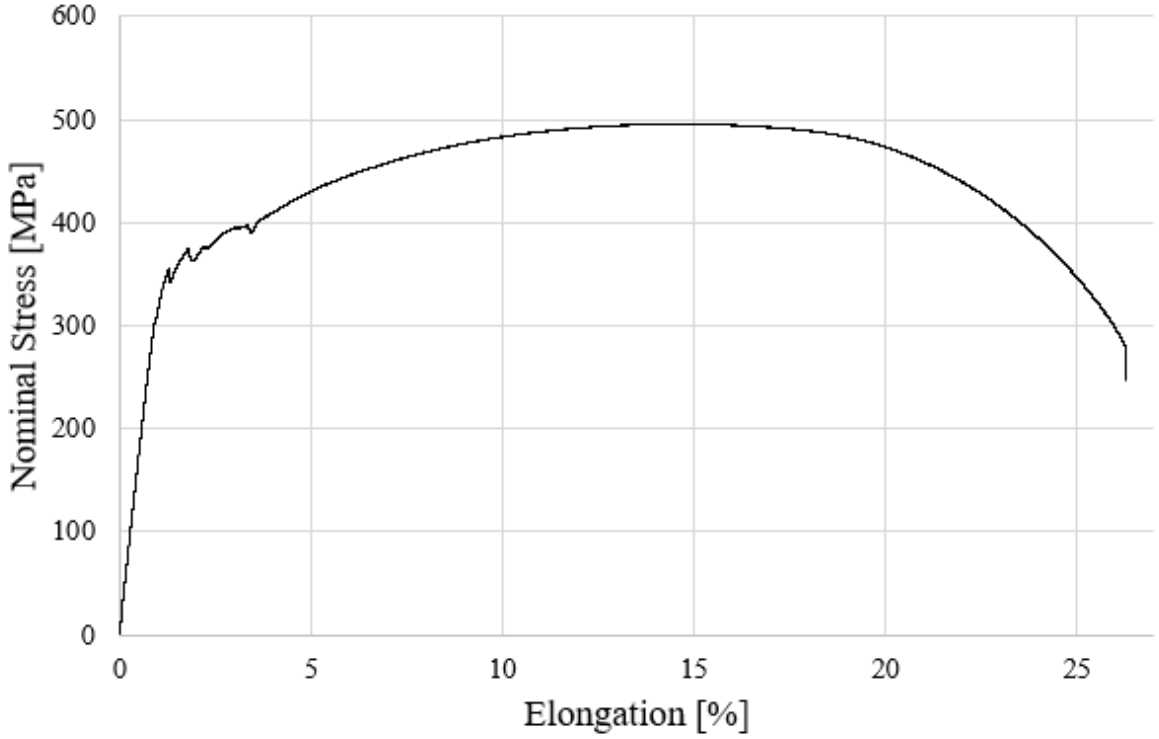


Figure A. 5 - Uniaxial tensile tests graph B3.

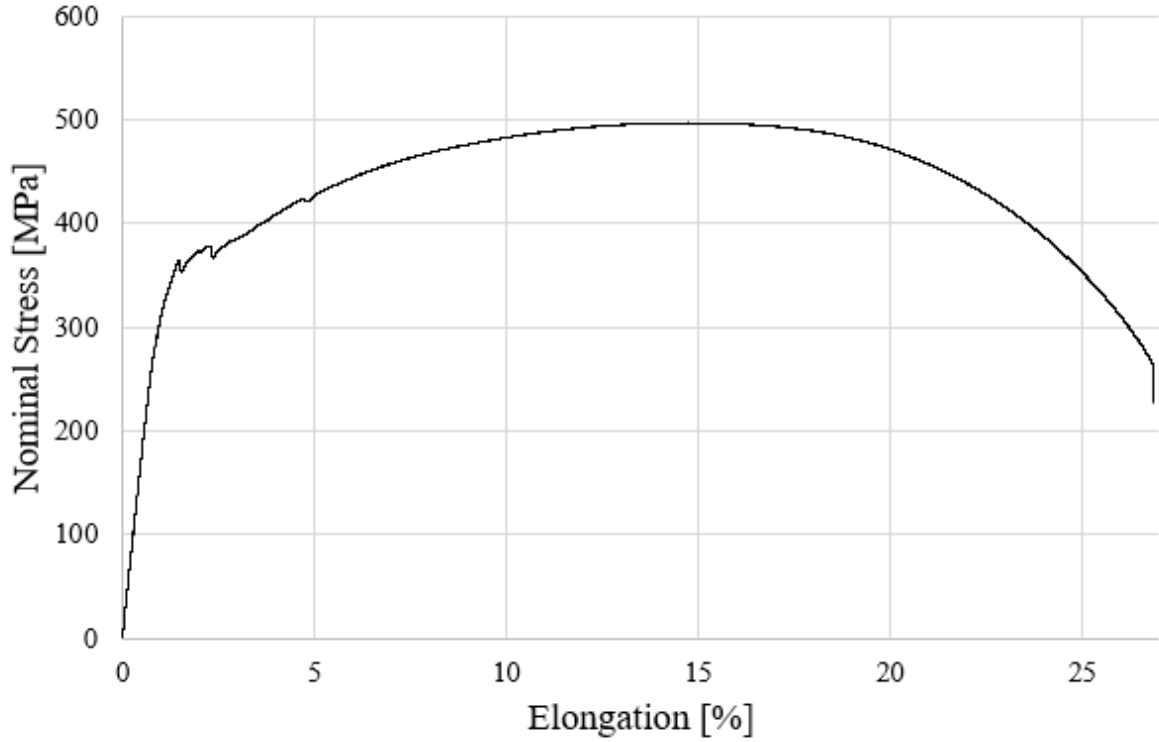


Figure A. 6 - Uniaxial tensile tests graph B4.

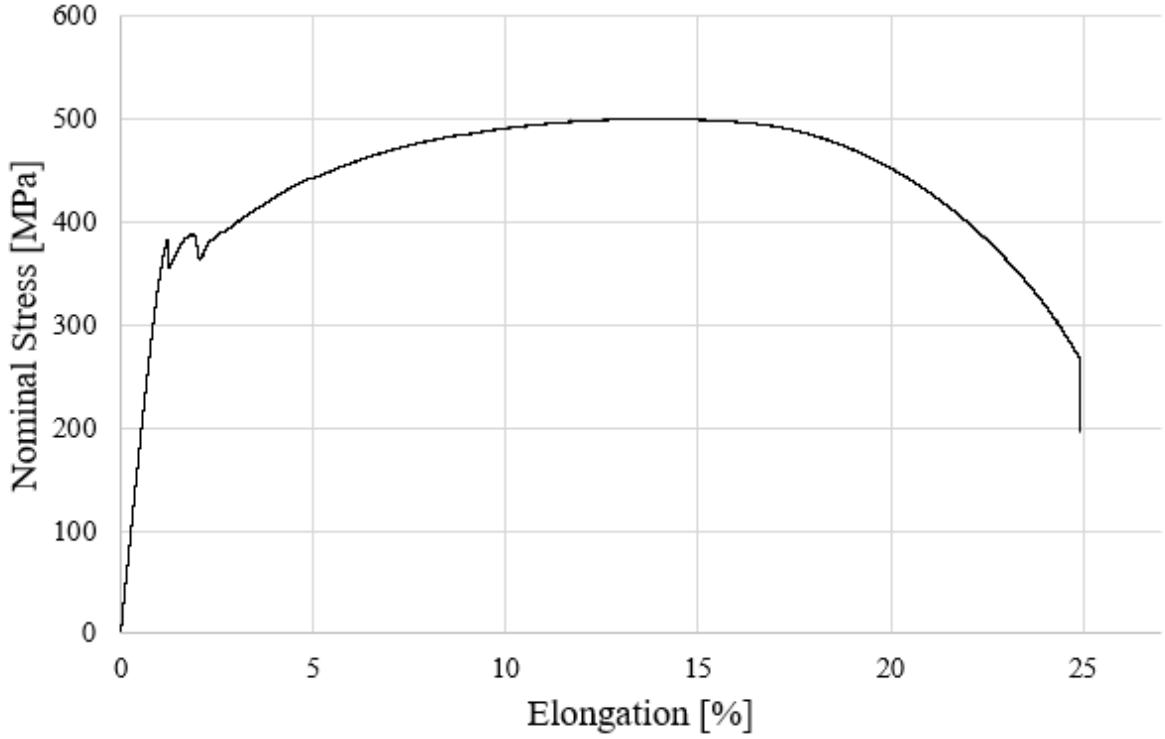


Figure A. 7 - Uniaxial tensile test graph C1

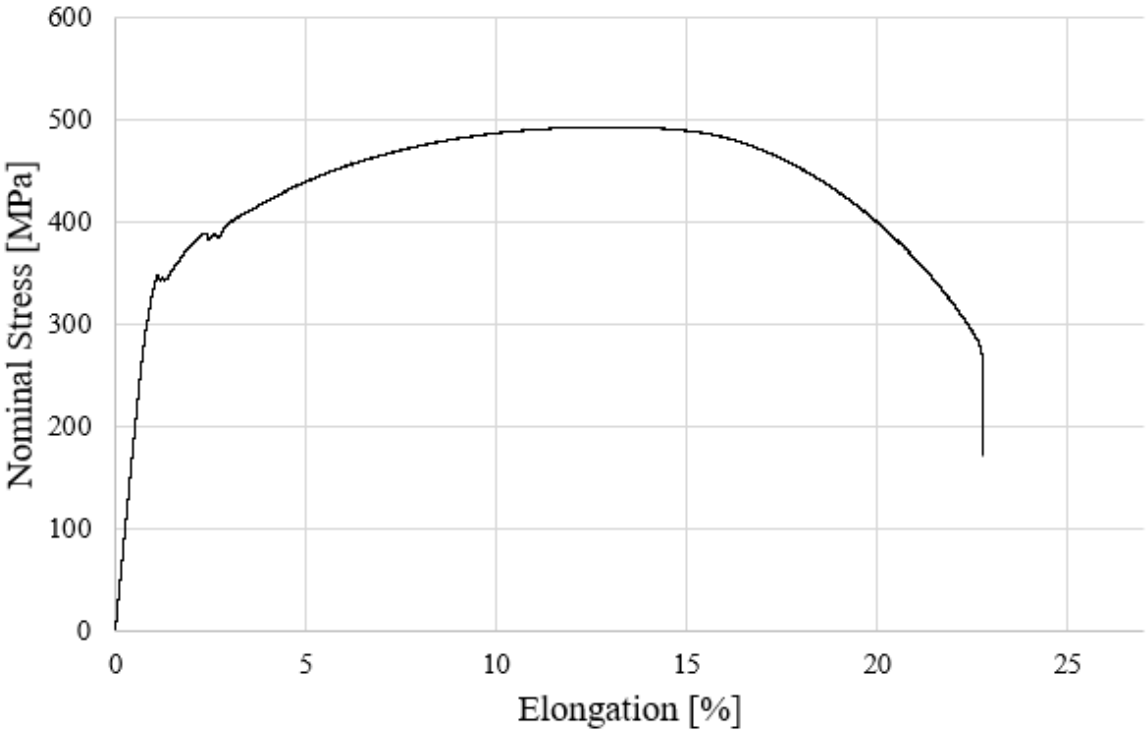


Figure A. 8 - Uniaxial tensile test graph C2.

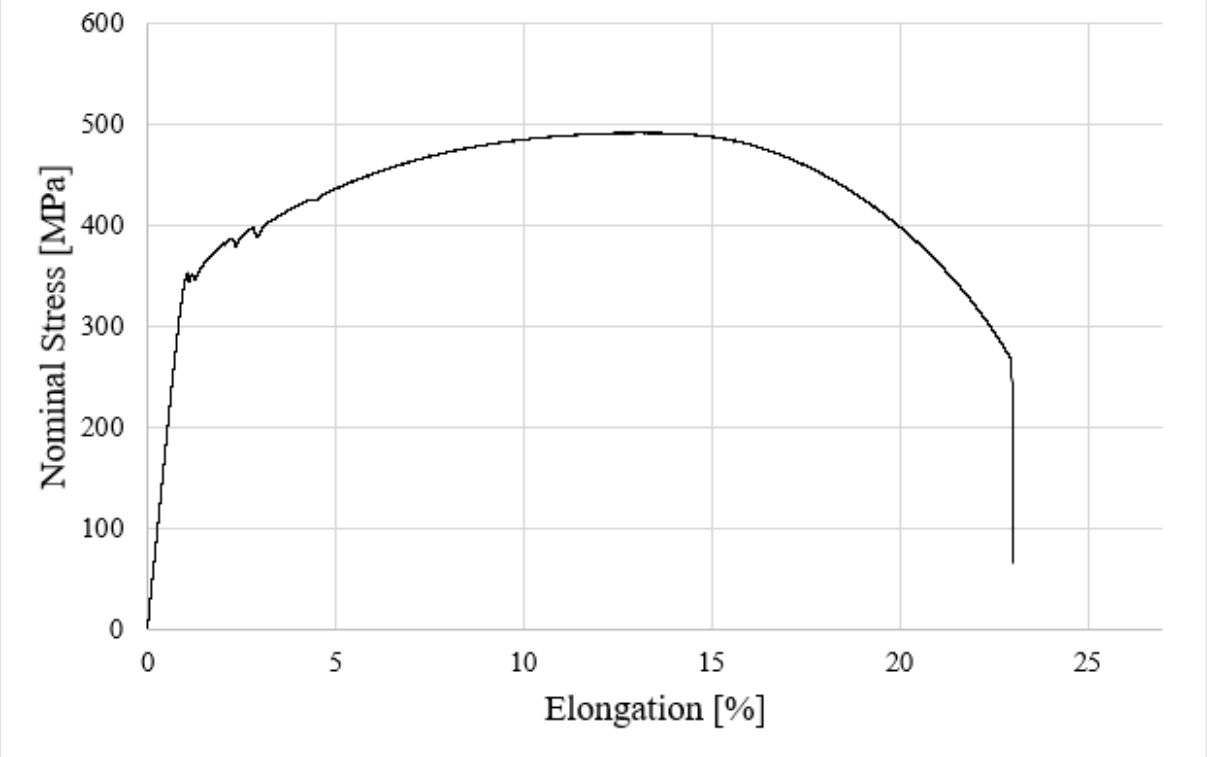


Figure A. 9 - Uniaxial tensile test graph C3.

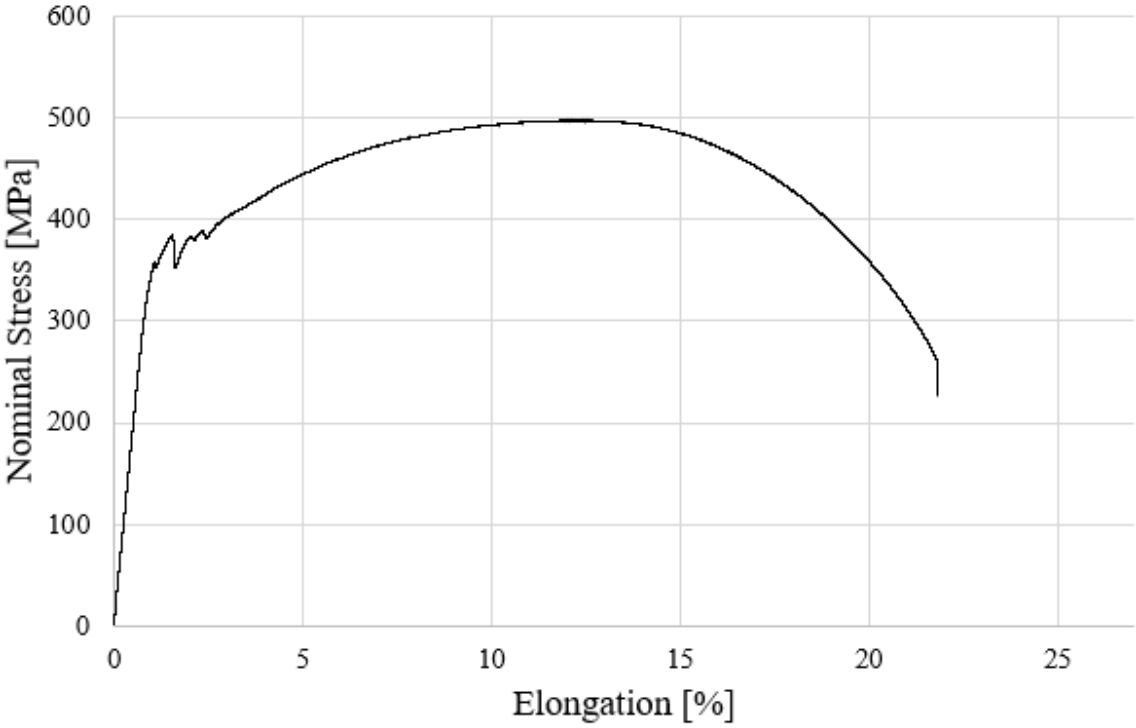


Figure A. 10 - Uniaxial tensile test graph C4.

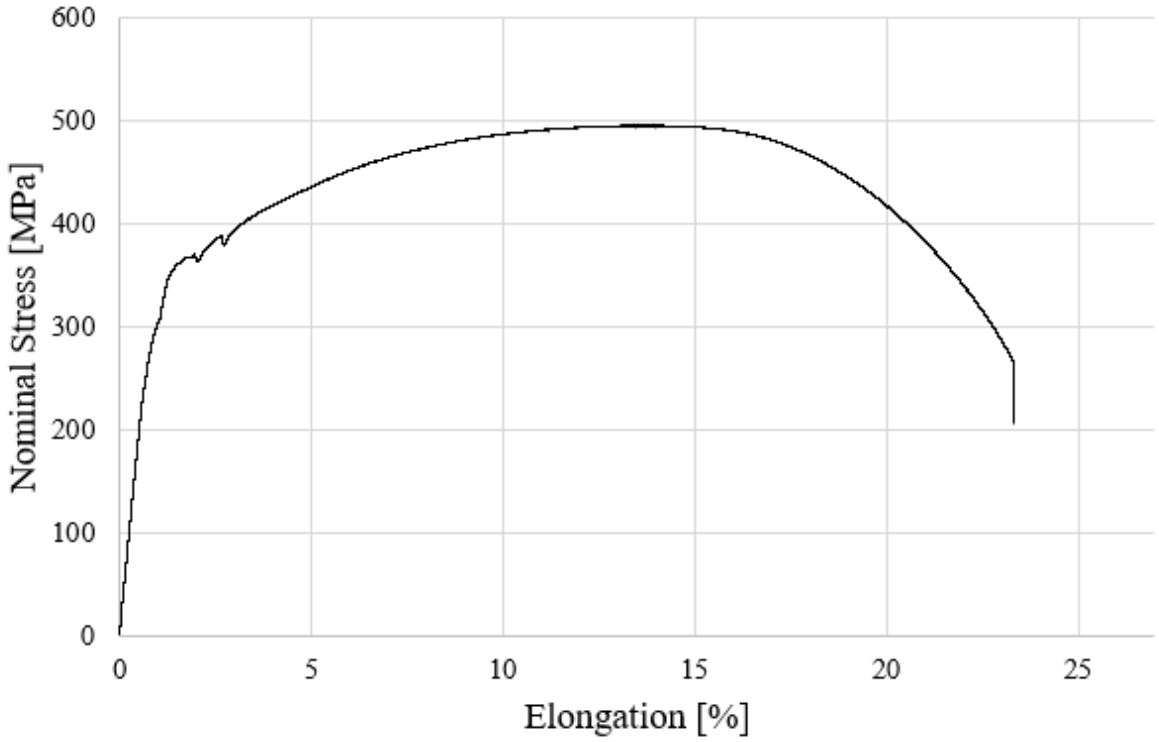


Figure A. 11 - Uniaxial tensile test graph D1.

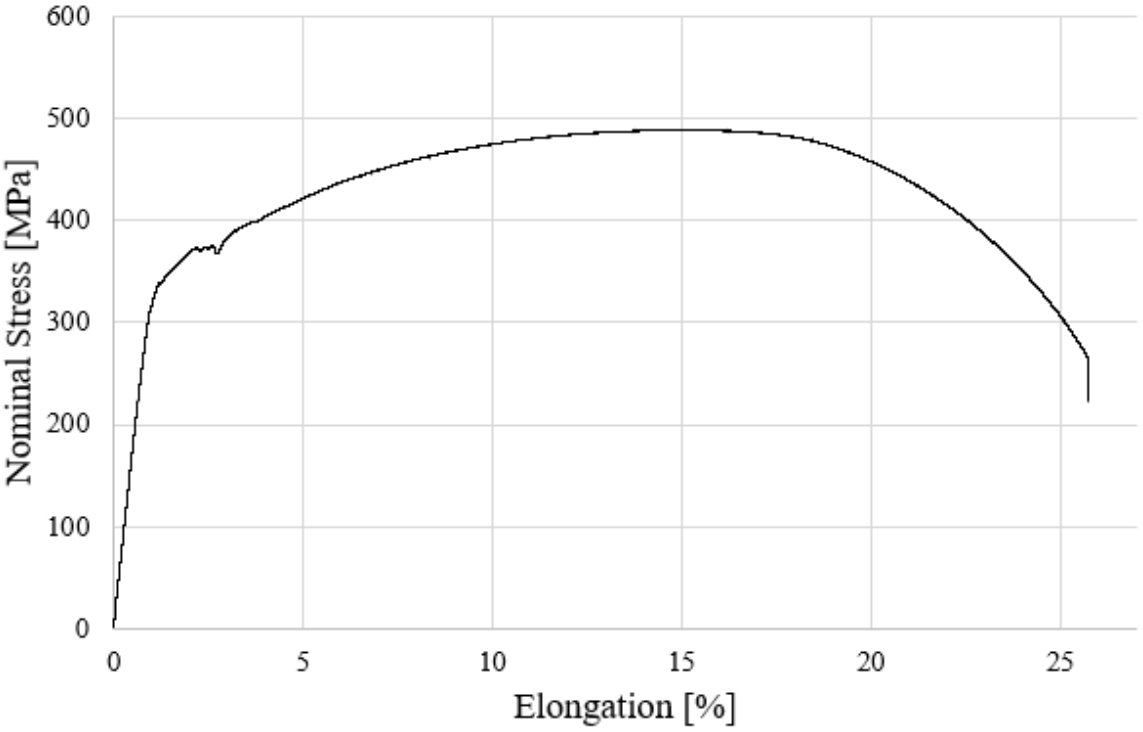

Figure A. 12 - Uniaxial tensile test graph D2.

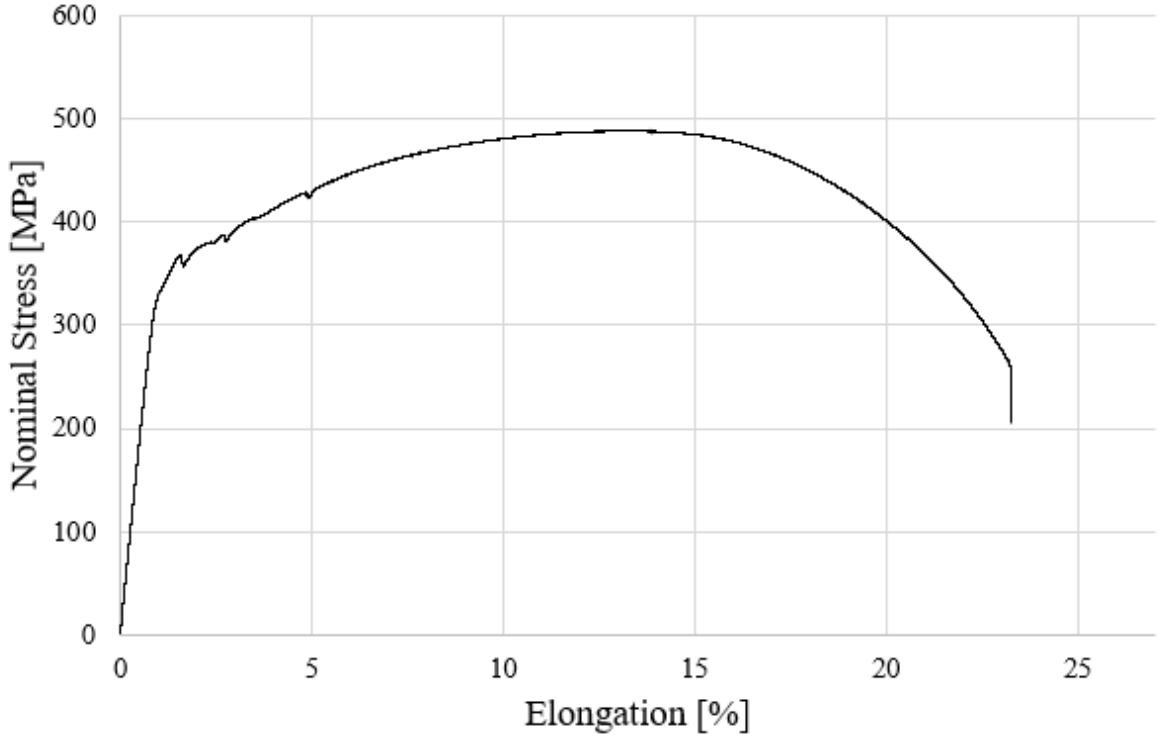


Figure A. 13 - Uniaxial tensile test graph D3.

# APPENDIX 7
# MICROHARDNESS TEST RESULTS

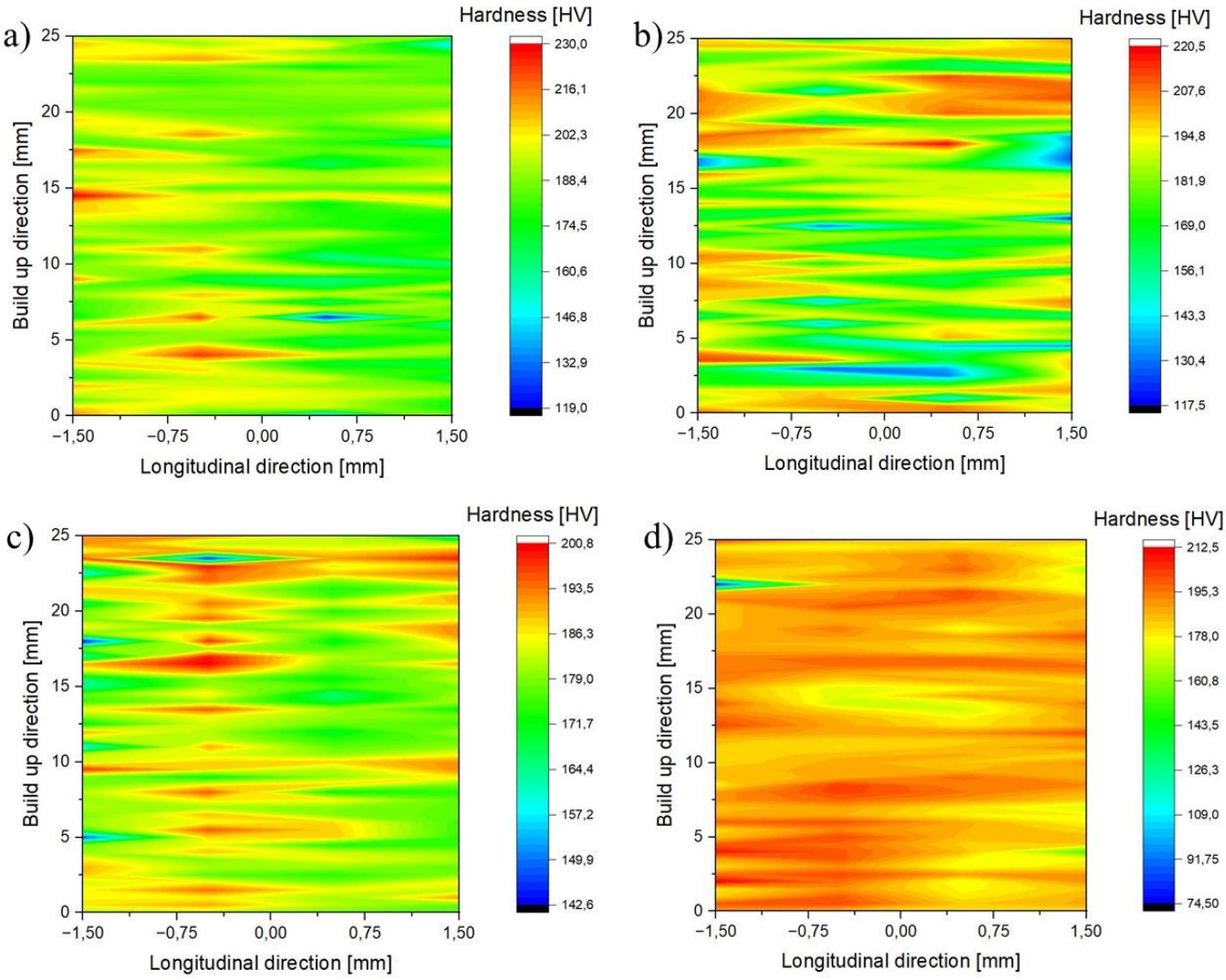


Figure A. 14 - Microhardness results of samples: a) A; b) B; c) C; d) D.